Aalto University
School of Chemical
Engineering

Jani Fellman

PRINTED CIRCUIT BOARD (PCB) SCRAP MELTING AND MIXING WITH MOLTEN FAYALITE SLAG

Master´s Programme in Chemical, Biochemical and Materials Engineering
Major in Sustainable Metals Processing

Master's thesis for the degree of Master of Science in Technology submitted for inspection, Porvoo, September 10th, 2018.

Supervisor	Professor Ari Jokilaakso
Instructors	M.Sc. Lassi Klemettinen
	M.Sc. Miikka Marjakoski

Aalto-yliopisto
Kemian tekniikan
korkeakoulu

Aalto-yliopisto, PL 11000, 00076 AALTO
www.aalto.fi
Diplomityön tiivistelmä

Tekijä	Jani Kristian Daniel Fellman
Työn nimi	Piirikorttiromun sulaminen ja sekoittuminen sulaan fajaliittikuonaan.
Koulutusohjelma	Kemian, biokemian ja materiaalitekniikan maisteriohjelma
Pääaine	Kestävä metallien prosessointi
Työn valvoja	Ari Jokilaakso
Työn ohjaaja(t)/Työn tarkastaja(t)	Lassi Klemettinen & Miikka Marjakoski
Päivämäärä 10.09.2018	**Sivumäärä** 62+33 **Kieli** Englanti

Tiivistelmä

Sähköeletroniikkaromun (SER) määrä on kasvanut viime vuosikymmeninä merkittävästi ja nopeasti. Kun lisäksi huomioidaan metallien raaka-aineiden laadun heikkeneminen, metalliteollisuuden kannalta on hyödyllistä tutkia uusia raaka-aine lähteitä sekä tapoja valmistaa metalleja. Piirikorttiromu on SER:n osa, mikä sisältää merkittävän määrän kuparia sekä arvometalleja verrattuna malmiperäisiin raaka-aineisiin. Piirikorttiromua voidaan käsitellä pyrometallurgisin keinoin mitä tapahtuu jo jonkin verran teollisuudessa, kuten liekkisulatuksessa.

Tässä työssä tutkittiin piirikorttiromun käyttäytymistä sulan kuonan pinnalla laboratoriomittakaavan uunissa. Tutkimusmenetelmänä käytetiin kirjallisuustutkimusta sekä kokeellista tutkimusta. Työn kirjallisuusosuus kuvaa piirikorttiromun yleisen koostumuksen ja viime vuosikymmeninä tapahtuneet muutokset, sekä teoreettisen tarkastelun piirikorttiromun sulamisesta ajan suhteen. Piirikorttiromu koostuu metalli-, keraami- sekä muovifraktioista. Kokeellisessa osuudessa tutkittiin piirikorttien sekä synteettisten Cu-Ni-Al seospalojen käyttäytymistä. Kokeissa käytettiin pystysuuntaista putkiuunia, joka oli 1350 °C lämpötilassa ja inertissä kaasuatmosfäärissä. Tutkittavat näytteet pudotettiin sulaa fajaliittikuonaa sisältäviin, kartiomaisiin upokkaisiin. Näin tuotetut näytteet tutkittiin optisesti ja koostumuksellisesti käyttämällä pyyhkäisyelektronimikroskooppia (SEM) sekä röntgenanalysaattoria (EDS).

Tulokset näyttivät, että piirikorttiromu sulaa kuonan pinnalla 2-5 minuutissa ja muodostaa metalliseospisaroita, jotka sisälsivät kuparia, lyijyä, tinaa, nikkeliä, kultaa sekä hopeaa. Pisaroiden todettiin laskeutuvan upokkaan pohjalle. Piirikortin keraamisen osuus sekoittui kuonaan. Muoviosuus pyrolysoitui ja muodostui kiinteää, mustaa sakkaa tai öljyä.

Tulokset lisäävät ymmärrystä piirikorttiromun sulamisesta, sekä tämän romufraktion käytöstä sulatusuuneissa. Tämä ei kuitenkaan riitä muodostamaan kokonaiskuvaa eri piirikorttiromusta löytyvien aineiden vaikutuksesta pyrometallurgisissa prosesseissa, joten lisätutkimus on tarpeellista.

Avainsanat Piirkorttiromu, Sulaminen, SER, Kupari, Arvometallit, Pyrometallurgia

Aalto University
School of Chemical
Engineering

Aalto University, P.O. BOX 11000, 00076 AALTO
www.aalto.fi

Abstract of master's thesis

Author	Jani Kristian Daniel Fellman
Title of thesis	Printed Circuit Board (PCB) Scrap Melting and Mixing with Molten Fayalite Slag
Degree Programme	Master´s Programme in Chemical, Biochemical and Materials Engineering
Major	Sustainable Metals Processing
Thesis supervisor	Ari Jokilaakso
Thesis advisor(s) / Thesis examiner(s)	Lassi Klemettinen & Miikka Marjakoski
Date 10.09.2018	**Number of pages** 62+33 **Language** English

Abstract

The amount of waste electrical and electronic equipment (WEEE) in the world has grown rapidly during recent decades. This paired with the decrease in grade of primary sources for metals emphasizes the industry to study new sources for metals. Waste printed circuit boards (WPCB) are a part of WEEE, that has higher concentration of copper and precious metals when compared to primary ore sources. PCB material can be processed using pyrometallurgy and is already done in some processes, such as copper flash smelting.

In this thesis the behavior of printed circuit board scrap was studied when it was dropped on top of molten slag. The subject was studied by using literature sources and experiments. The theoretical part defines the general composition of PCB's, changes in this composition during recent decades and the theoretical melting behavior of PCB's as a function of time. The PCB's comprise of metal, ceramic and polymer fractions. Experimental part studied the melting behavior of PCB pieces and synthetic Cu-Ni-Al alloys using a vertical tube furnace at 1350°C and under inert atmosphere. The sample pieces were dropped into molten fayalite slag containing crucibles. The produced samples were analyzed optically and compositionally using scanning electron microscope (SEM) and X-ray energy dispersive spectrometry (EDS).

The results of experimental study showed that the PCB pieces melted between 2-5 minutes and formed metal alloy droplets containing Cu, Pb, Sn, Ni, Au and Ag. The droplets descended towards the bottom of the crucible. The ceramic fraction mixed with slag and the polymer fraction of the PCB's pyrolysed and formed solid, charred residue or oil.

The results give an understanding in melting behavior of PCB's and their use in smelting furnaces. Although, more research is needed to fully understand how the different elements affect the process as the amount of PCB in feed increases.

Keywords PCB, Melting behavior, WEEE, Cu, Precious metals, Pyrometallurgy

Foreword

This work was funded by with Boliden Harjavalta and Aalto University, supervised by prof. Ari Jokilaakso.
This thesis was not easy from the day one to the final months of editing and receiving comments. But here it is. First, I would like to thank my supervisor Ari Jokilaakso for patience and very quick replies and commenting on all the different questions/problems I encountered or made up during my work. My instructor Lassi Klemettinen was crucial during the experimental part, which was borderline chaotic at first. In addition, he gave very detailed comments, which I think improved my work significantly. My other instructor Miikka Marjakoski gave professional comments on behalf of Boliden Harjavalta, which on their part improved my work as well.
Overall thanks go to all who worked in metallurgy and thermodynamics department during spring and summer of 2018. And finally, I would like to thank my significant other Tiitu, who patiently motivated and supported me through all the 8 months filled with frustration and challenges.

Jani Fellman
Porvoo, 10.9.2018

Aalto University
School of Chemical
Engineering

Aalto University, P.O. BOX 11000, 00076 AALTO
www.aalto.fi

Abstract of master's thesis

"Research is what I´m doing when I don´t know what I´m doing"

- Wernher von Braun

Table of Contents

List of abbreviations and variables

FS = Flash Smelting

FSF = Flash Smelting Furnace

PCB = Printed Circuit Board

WEEE = Waste Electrical and Electronic equipment

LCM = Lumped Capacitance Method

FR = Fire Retardant

CPU = Central Processing unit

BGA = Ball Grid Array

LGA = Land Grid Array

PGA = Pin Grid Array

PCI = Peripheral Component Interconnect

DIMM = Dual Inline Memory Module

RAM = Random Access Memory

PBDD/F = PolyBrominated Dibenzo Dioxins/Furans

PCDD = PolyChlorinated Dibenzo Dioxins/Furans

α = Thermal diffusivity [m^2/s]

$\frac{dT}{dt}$ = Change of temperature over time t

ρ = Density [kg/m^3]

A = Area of an object [m^2]

C = Lumped Thermal Capacitance of the object material

c = Heat Capacity [$(kgm^2)/(Ks^2)$]

h = Heat transfer coefficient [$W/(m^2K)$]

l_k = Characteristic Measurement of an object (V/A) [m]

k = Thermal conductivity [W/(mK)]

R = Convective Thermal Resistance

T = Temperature [°K]

V = Volume [V]

Bi = Biot's number

Fo = Fouriers number

1. Introduction

Recent advancements in electronic and electrical technologies have caused a rapid growth in the amount of Waste Electrical and Electronic equipment (WEEE) scrap in the last two decades. This has forced researchers to find ways to utilize the continuously growing amount of waste and recover the valuables within. The two major contributors to continuous growth are the increasing availability of computers, laptops, phones and other personal electronics to larger population and the decreasing useful life cycle expectancy of these applications.[1,2]

The purpose of current work is to analyze the behavior of a piece of printed circuit board (PCB) when it drops on top of the surface of molten slag in a copper flash smelter. This thesis aims to first analyze the thermal behavior theoretically through a literature survey. A secondary goal is to gather information about PCB composition and the possible changes in this composition during recent decades.

The literature review consists of three parts. First, the Flash Smelting technology (FS) is introduced. Second, the composition of WEEE is presented and how this composition has changed over the recent two decades. Finally, the thermal behavior of printed circuit boards is theoretically inspected. After the literature review, the behavior of WEEE samples is investigated experimentally by dropping small pieces on top of molten slag. The experimental section presents the setup used and results obtained. The purpose of this part is to assess the melting behavior as a function of time using experimental analysis. The idea is to find out if or when the PCB structure will melt. Furthermore, if the melting happens, where the resulting phases and elements are located and in what form.

This thesis expands the work done previously by P. I. Guntoro [3], which briefly studied the behavior of WEEE in a matte – slag system. The motivation for this thesis is to find out whether it is beneficial to insert WEEE scrap into the settler of a Flash Smelter furnace or not. Reaction conditions and behavior in the reaction shaft has been inspected in previous work with numerical methods and simulations [4-7], but this thesis aims at finding out the behavior of unreacted WEEE scrap when it is placed on top of slag.

Part I: Literature Review

2. Flash Smelting furnace

This chapter describes the Flash Smelting (FS) and provides an overview of the technology and what it is utilized for. Furthermore, the importance of slag in FS is discussed and what the slag is comprised of.

Flash smelting is a widely used technology in producing primary copper. FS utilizes Cu-Fe-S concentrates, chalchopyrite mineral, silica flux and recycled materials to produce molten matte and slag. The necessary heat for melting the concentrate is nearly self-generated in the reaction shaft by blowing oxygen enriched air into dried Cu-Fe-S concentrate. This causes the sulfide mineral particles in the concentrate to react rapidly with O_2 content of the blast, causing controlled oxidation of iron and sulfur. This reaction releases a large amount of heat which results in melting of the solid feed. The temperature inside the furnace is controlled at approximately 1250 °C. [8]

The FS process is continuous and practically auto-thermal, provided that sufficient oxygen enrichment is used. The FS process produces three major products: molten Cu-Fe-S matte with ~65 % Cu concentration (1); molten iron-silicate slag containing 1-2 wt-% Cu (2) and hot, dust-laden off gas rich in SO_2 (3). [8]

Figures 1 and 2 show a schematic view of an Outotec flash furnace. A flash smelting furnace is typically a U-shaped reactor, which consist of a reaction shaft, a bottom settler and an uptake shaft. Concentrate is fed into the reaction shaft, where the feed forms a steady suspension with the process air and descends towards the bottom settler. The feed melts in the reaction shaft and produces molten matte, slag and off-gas. The molten material settles below in settler part and the dust containing process off-gas continues through the uptake shaft to a heat recovery boiler. The slag and matte are tapped out of the furnace through separate tap holes and the dust collected from an electrostatic precipitator is recycled back to the process. [8]

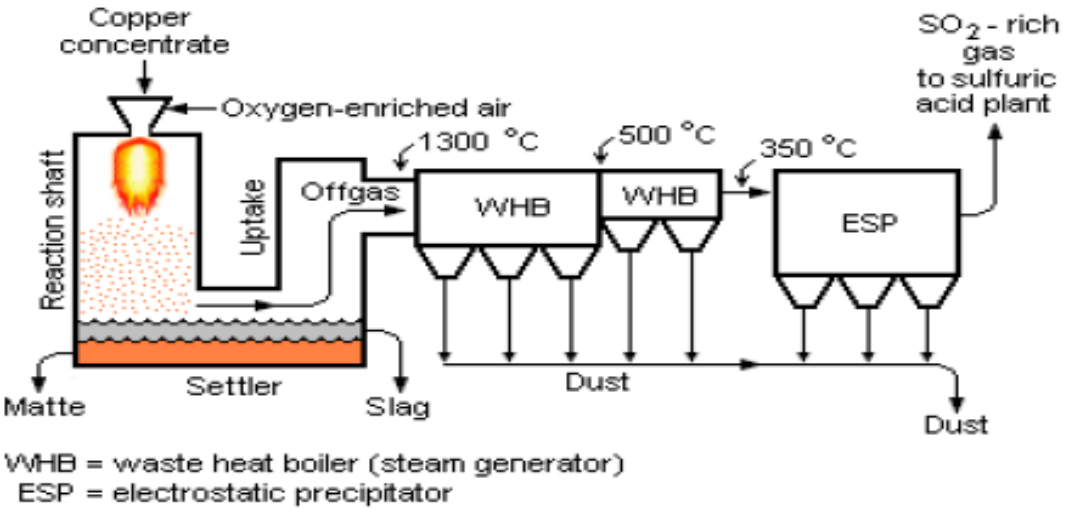

Figure 1. A schematic view of the FS process [9]

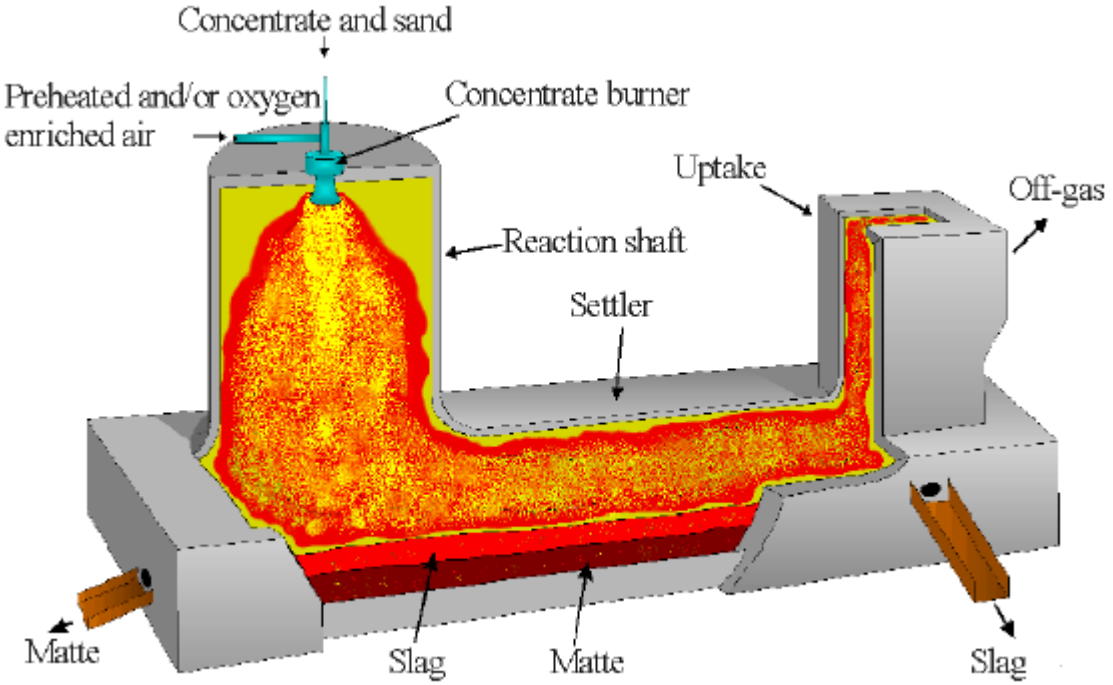

Figure 2. An illustration of the Flash Smelting furnace [7]

In any process that produces molten metal or matte, the more easily oxidized impurities from the feed material and gangue separate into a phase called slag, which floats on top of the molten matte. Since many of these oxides have inherently high melting points, fluxing agents need to be added to the process to form a liquid, which can absorb the impurities. When both the metal and the slag are in liquid form, the separation is easily

achieved by gravity. The molten metal or matte, having higher density, settles to the bottom and the less dense slag floats on top. [10]

The most important parameters for the used slag are melting temperature and viscosity. Melting temperature needs to be nearly the same for the slag and metal to avoid wasting energy in heating the reaction temperature needlessly high. The viscosity needs to be low for the slag to flow easily out of the furnace. As stated above, these parameters are achieved by charging different fluxing agents into the furnace. The most traditional fluxes in copper smelting are silica (SiO_2) and lime (CaO). [10]

Slags with high concentration of SiO_2 have poor fluidity due to the tendency of silica to polymerize. In addition, aluminum oxide likes to join silica in forming polymers. SiO_2 dissolves according to the ionic reaction (1):

$$SiO_2 + 2O^{2-} \rightarrow SiO_4{}^{4-} \quad (1)$$

The arrangement of Si and O is tetrahedral. Any number of these units can join with $AlO_3{}^{3-}$ to form long chains. This causes the slag to be viscous since long Si-Al-O chains cannot move past one another. [10]

These long chains can be broken by adding basic oxides such as CaO, FeO or others. These dissolve to form single ions, following reaction (2):

$$CaO \rightarrow Ca^{2+} + O^{2-} \quad (2)$$

Ca^{2+} neutralizes the open ends in SiO_2 tetrahedron structure, thus breaking the long chains and enabling the smaller units to move more freely in the slag. [10]

The historical slag system in copper smelting is FeO-Fe_2O_3-SiO_2 slag in an acidic refractory system. This system was formed by adding silica to the iron containing melt to form a slag with the oxidized iron. [10]

The properties of FeO - Fe_2O_3 - SiO_2 system vary as a relation of FeO and Fe_2O_3 concentrations. This translates as the oxygen potential, according to reaction (3):

$$Fe_2O_3(slag) = 2FeO(slag) + \frac{1}{2}O_2 \quad (3)$$

The formation and properties of fayalite slag were important to understand in the experiments done in this thesis.

3. Waste printed circuit board

The composition of Waste Printed Circuit Boards (often referenced with acronym WPCB) varies significantly depending on the application, structure or supplier. Overall, PCB waste has a dual nature, as it contains toxic and hazardous materials, but also many profitable metals (~30 wt-%). These metals include base metals (Cu, Zn, Ni, Pb, Sn), precious metals (Ag, Au, Pd) and minor traces of rare earth elements. [1]

Current practices of WEEE recycling include mechanical, pyrometallurgical, hydrometallurgical and biometallurgical technologies.[2,11] WPCB's and other scrap can be fed into different process stages depending on the metal content of the scrap and the process used. Considerable additions of WEEE into processes that are optimized for primary ores may cause significant changes in the process chemistry and therefore alter the behavior of different elements and lead to issues in process operation.

3.1 Printed circuit boards composition

Printed circuit boards contain lines and pads that connect separate points together. A PCB enables both power and signals to transmit between equipment and/or components.[12] All PCB's are typically composed of three parts: a non-conductive substrate or laminate, conducting substrate printed on top of or inside the laminate and components attached to the top layers of the board. [1] Figures 3-8 show different structures of printed circuit boards with increasing degree of complexity. Depending on the application, a PCB can be relatively simple (simple household appliances) or very complex (computer components, motherboards, smartphones). [12] Depending on the structure and alignment, PCB's are classified as single-sided, double-sided or multilayered.

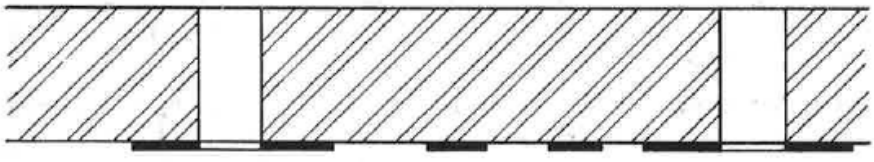

Figure 3. Single sided board [12]

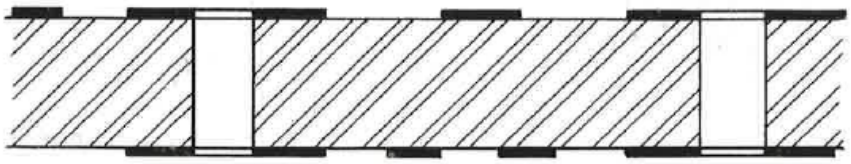

Figure 4. Double sided, non-through-plated board [12]

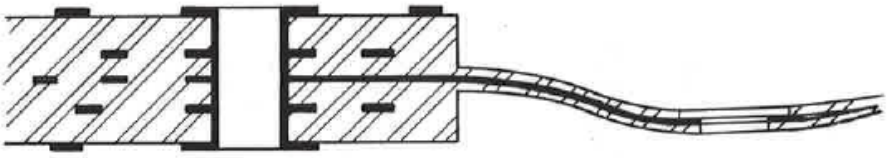

Figure 5. Five-layer rigid with single tail [12]

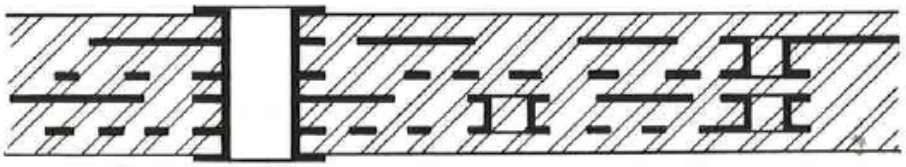

Figure 6. Six layer buried via-hole board [12]

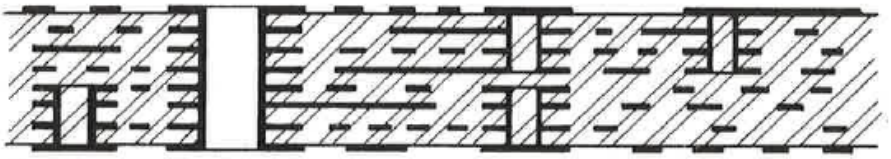

Figure 7. Double multilayer board [12]

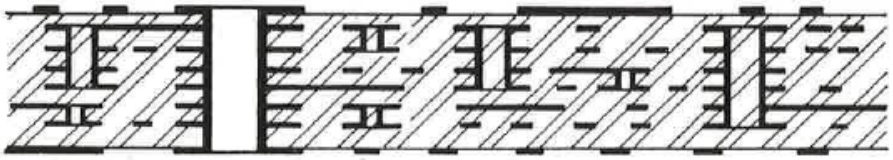

Figure 8. Eight-layer sequential multilayer board [12]

The inner structure is comprised of a non-conductive substrate or laminate layer, conductive circuit on top or inside the substrate layer, solder mask and a silkscreen. On top of the board, there are several different types of components attached, with varying compositions and purposes. The electronic components are attached to the surface of the board by a solder, which has a metallic composition and makes electrical connections possible. In addition, the solder functions as a mechanically strong adhesive.[13,14]

Commonly, the conductive circuits are made of copper. The conductive tracks are drawn in the board by covering copper with etch resistant layer. Etching resistant elements can contain nickel, tin, tin-lead, silver or gold. After etching, the board is covered by a solder mask to protect the formed tracks. The solder mask is a thin layer of polymer, which gives the board its typical green color (other colors are possible).[13,14]

The substrate part is made of several types of substances, but the most commonly used is FR4 (Fire Retardant). FR4 consists of epoxy resin reinforced with glass fiber and brominated flame retardants. In addition to FR4, another popular material for substrate is FR2, which is made of phenolic resin reinforced with paper and brominated fire retardants. [15]

Figure 9 shows a SEM picture of a PCB cross-section. This figure clearly shows a fiberglass core (referred as (1) in the figure), a copper sheet laminate (referred as (2)) and epoxy resin cover (referred as (3)). The fiberglass matrix forms a woven structure, which consists of aluminum, silicon and calcium. [16]

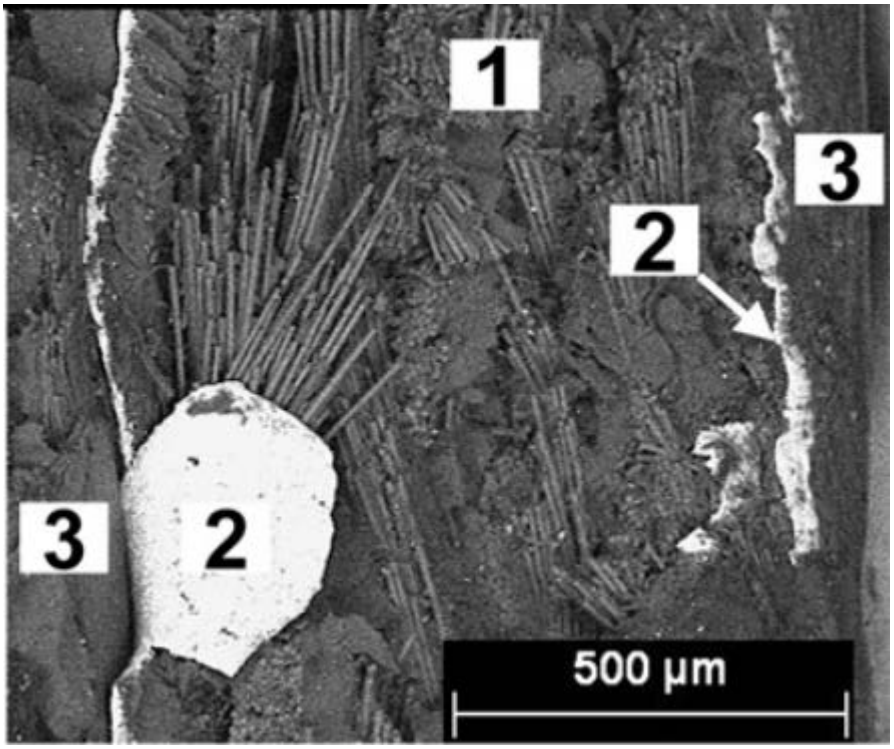

Figure 9, A SEM picture of a PCB board, showing a fiberglass core (1), a copper sheet laminate (2) and epoxy resin cover (3) [16]

3.2 Chemical composition of PCB´s

In economical aspect, the most valuable metals in PCB scrap are copper and precious metals (gold, silver and palladium). In addition, printed circuit boards contain rare earth elements. These elements could also be of economic interest, provided there is a process efficient enough for their extraction. [16] The non-metallic fraction consists of cured thermosetting resins, glass fiber (cellulose paper), ceramics, brominated flame retardants and other additives. [17]

Tables 1-2 show the precious and base metal concentrations in PCB's. The data was collected from multiple sources between years 1997 and 2018. From tables 1 and 2, it can be observed that the composition of PCB's varies significantly. The variation in composition depends on the manufacturer, application purpose and perhaps from different classification methods and processing technologies used to treat the e-scrap.

Table 1. Precious metals content of PCB's in ppm

Au	Ag	Pd	Pt	Reference
110	280			18
350				19
80	1000			20
420	1240			21
1000	2000	50		22
350	1300	250	4,6	23
570	3301	294	30	24
250	1000	110		25
250	1000	100		26
80	3300			17
230	600	100		27
200	450	220		28
830	830			29
200	900			30
80	2000			31
300	500	100		16
1000	2000	50		32
372	570			33
80	3300			34
	210			35
24	57	15		36
60	60	10		37

30	40			[38]
3	10			[39]
7	106	5		[37]
	130	50		[37]
1	40	1		[37]
330.0	**984.1**	**96.8**	**17.3**	**Average**

Table 2. Base metals content of PCB's in wt-%

Cu	Fe	Al	Sn	Pb	Ni	Zn	Sb	Reference
10	12	7		1.2	0.85	1.6		[18]
22	3.6		2.6	1.55	0.32			[19]
26.8	5.3	4.7	1		0.47	1.5	0.06	[20]
15.6	1.4		3.24	1.35	0.28	0.16		[21]
20	8	2	4	2	2	1	0.4	[22]
17.85	2	4.78	5.28	4.19	1.63	2.17		[23]
23.47	1.22	1.33	1.54	0.99	2.35	1.51		[24]
20	7	5	2.9	1.5	1			[25]
16	5	5	3	2	1			[26]
20	8	2	4	2	2	1	0.04	[17]
10	9	6	2	2	1			[27]
15	5		6	3	2			[28]
24	8		4	5	3			[29]
18	7	5						[30]
18.1	5.6	7.3	1.9	1	0.5			[40]
27	5	2			0.5			[31]
16	3				2			[16]
20	8	2	4	2	2	1	0.4	[32]
25	3.7	4.98	1.17	3	0.88	1.46		[33]
26.8	5.3	4.7	1		0.47	1.5	0.06	[34]
34	10.57		3.39	1.87	2.6	5.92		[35]
20	1.3		1.8	2.3		0.27		[36]
14.3	4.5			2.2	1.1			[37]
27	2		3	3		0.5		[38]
10.32	16.84		1.44	0.64		1.63		[39]
40.8	0.28		1.6	1.36	0.39	0.41		[37]
8.02						2.21		[37]
33.87	1.03		0.15	4.96	0.13	0.94		[37]
20.8	**5.5**	**4.3**	**2.7**	**2.2**	**1.2**	**1.5**	**0.2**	**Average**

The graphs in figures 10 and 11 below show the data trends from tables 1-2 as composition over time. The graphs show clearly that the composition varies greatly for copper and silver compositions. Observing the base metal concentration trendlines, the

concentrations of copper and lead has increased, while tin and aluminum has decreased. The concentrations of all precious metals with significant amount of data (gold, silver and palladium) have decreased, especially the concentration of silver.

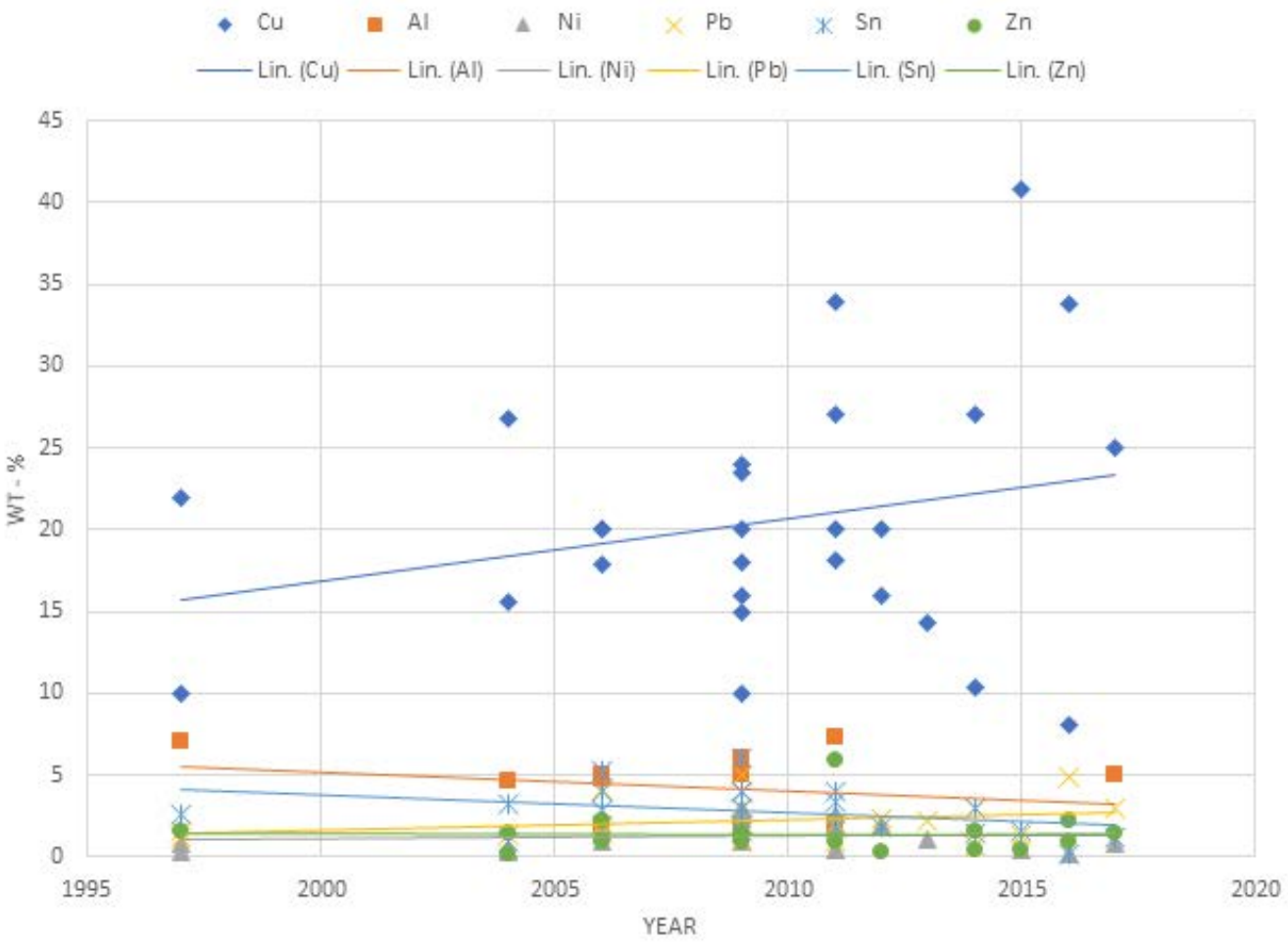

Figure 10. Base metals composition data and change in composition over time

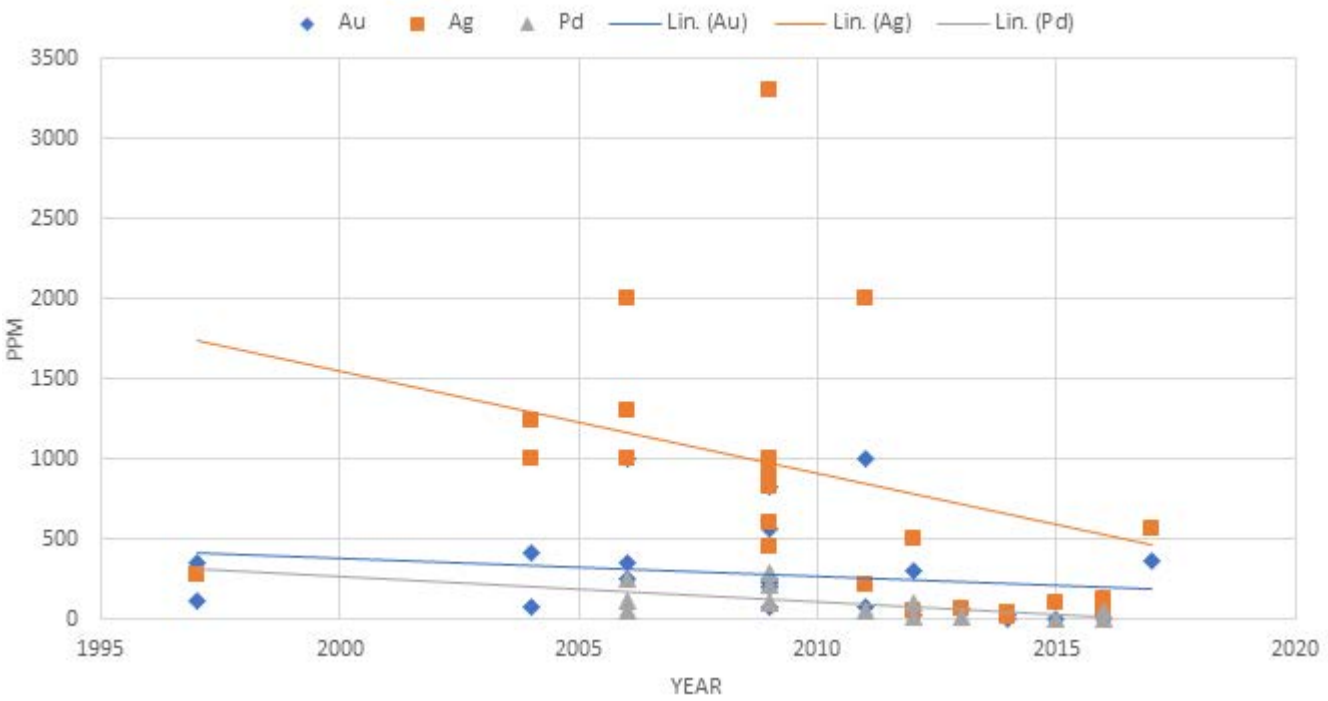

Figure 11. Precious metals composition data and change in composition over time

According to (a summary) Goodship & Stevels[41], PCB's contain roughly 40 % metals, 30 % polymers and 30 % ceramics. [41] This is shown in Figure 12, which shows the average composition of PCB's as shown in tables 1 and 2.

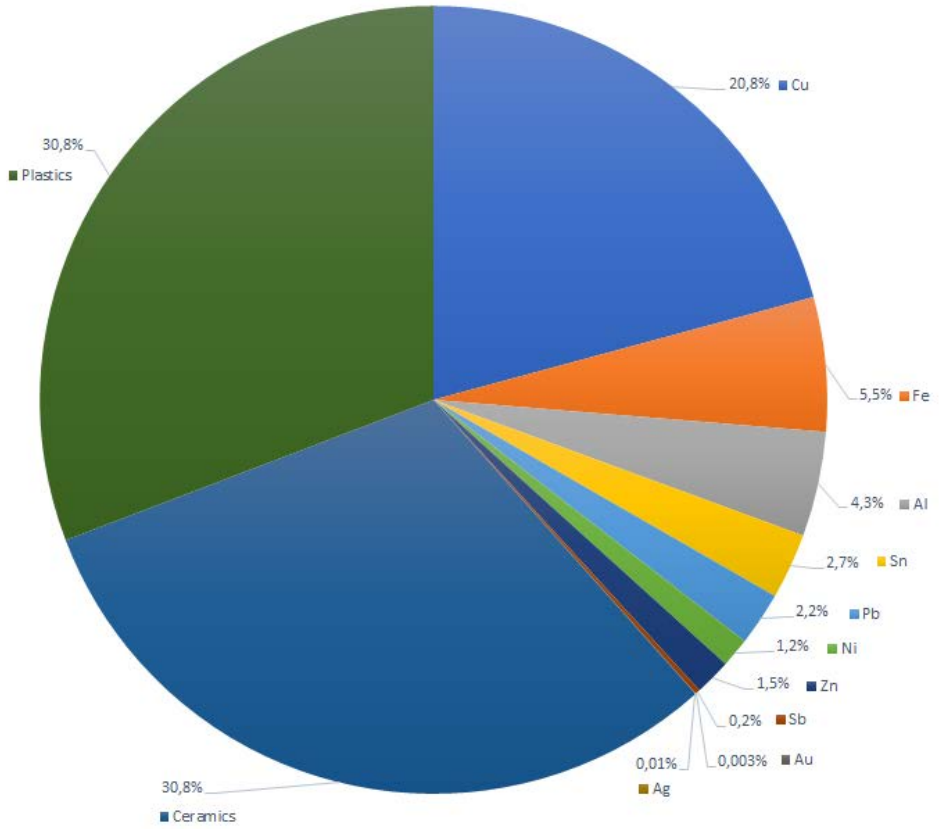

Figure 12. Visualization of average PCB composition from tables 1 and 2

3.3 Current and future trends

Due to remarkable development and growth of electronic industry in last two decades, both the number of consumers and businesses producing electronic products have increased phenomenally, while the prices of new electronic products have decreased. When paired with the fact that the average lifetime of an electronic product has diminished as well, the result is a massive generation of end-of-life products. This means that the amount of electronic scrap and thus wasted printed circuit boards have grown and will likely continue to grow in the near future. [1]

According to Ghosh et al., in 2015 nearly 45 million tons of electronic waste was annually produced, and this number was projected to grow significantly [1]. Another source, the global e-waste monitor forecasts the annual amount in 2018 to be 50 million tonnes [42]. Figure 13 shows the amounts of e-waste generated worldwide from 2010 to 2014 and a projection from 2015 to 2018. Figure is from a statistic portal using 22500 different sources. [43]

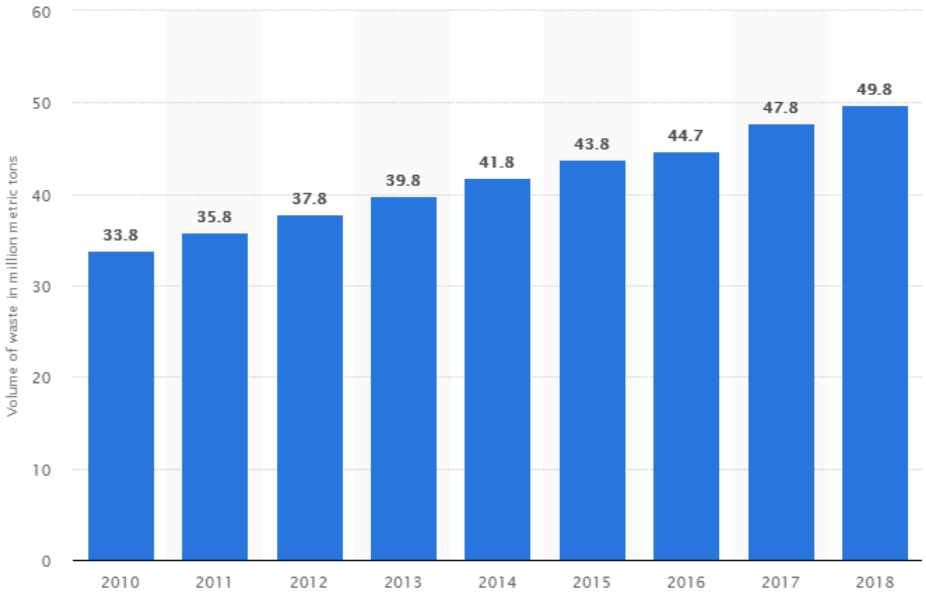

Figure 13. Generation of WEEE between 2010 – 2014, forecast of WEEE generated worldwide between 2015-2018(in million metric tons) [43]

In addition to growing amount of WEEE in global scale, the content of precious metals like gold, silver and palladium has been declining. In the past WEEE contained relatively high content of precious metals, but due to rapid technological advancements that amount has decreased. However, this amount is still higher than in primary sources of precious metals (ores). [44]

Gold is the most economically interesting side-stream in WEEE processing. Due to high price of gold, the manufacturers of EEE (electronic and electrical equipment) have been reducing the required amount using electrodeposition and other advanced processing methods. [44]

In printed circuit boards gold and gold alloys are used for their chemical resistance and thermal properties as well as electrical properties. These properties are primarily needed in temporary connections between circuit boards, components and hardware. A connector surface requires optimal chemical and thermal resistance and electric conductivity for binary signals to travel through. In addition to metallic gold, alloys containing nickel, silver and palladium are used. [44]

Gold containing connectors are diverse in number. First type of connector are sockets. Sockets connect CPU's to motherboard and can be divided in three categories: ball grid array (BGA), land grid array (LGA) and pin grid array (PGA). These connector types are shown in figure 14. As an example, gold content in PGA socket depends on the length of connector pins, which has decreased from 2.57 mm to 1.27 mm. [44]

Figure 14. Gold containing contact types [44]

Another gold containing connector type is the Peripheral Component Interconnect (PCI). PCI's connect functional extension modules to motherboard, such as graphic-, audio- and network cards. In addition to PCI, dual inline memory modules (DIMM), that connect RAM (Random Access Memory) to motherboards contain high gold concentration as well. In addition, there are numerous other minor gold containing contacts, including USB ports, Ethernet, audio, video and battery contacts. [44]

In general, precious metals (gold, silver, palladium) are used as contact materials or protective plating layers due to electrical conductivity and chemical resistance [45]. An article from 2005 estimated that the concentration of silver in PCB's would increase, as it would replace the use of lead as solder material due to European Union regulation [46]. However, the data shown in chapter 3.2. proves that this was not the case. Thin films of silver and tin are used to protect vulnerable sites (conductive copper lines, contacts) from oxidation[47]. Palladium is chemically resistant and physically durable metal and thus is an optimal material to form protective plating in PCB's [48]. In addition, the behavior of gold, silver and palladium in pyrometallurgical copper production has been an object of interest in recent studies [49-51].

Table 3 below shows the difference between amounts of metals found in natural minerals versus PCB material. The compositions show a range of results reported in source, between years 1993 – 2010. As seen from the table, regardless of the decrease in precious metal content in recent years, the copper, gold and silver content of PCB's is much higher than in natural minerals. [52]

Table 3. Average mineral composition and PCB composition

Metal	Ores (%)	PCB's (%) [1]	PCB's (%) [2]
Copper	0.5 - 3.0	12.0 - 29.0	20.8
Zinc	1.7 - 6.4	0.1 - 2.7	1.5
Tin	0.2 - 0.85	1.1 - 4.8	2.7
Lead	0.3 - 7.5	1.3 - 3.9	2.2
Iron	30 - 60	0.1 - 11.4	5.5
Nickel	0.7 - 2.0	0.3 - 1.6	1.2
Gold	0.0005	0.0029 - 0.112	0.003
Silver	0.0005	0.01 - 0.52	0.0098

PCB[1] = values from source [52], PCB[2] = values from tables 1 and 2

The economically interesting metals with significant concentration were gold, silver and copper. According to data shown in chapter 3.2, the concentration of gold and silver has been declining (silver more abruptly than gold) while the copper concentration has apparently risen. These trends are specified in figures 15 and 16. However, these trends are not necessarily the truth, as the results varied significantly depending on sources used (experimental method used, origin product of PCB's etc.). This uncertainty describes the PCB concentrations well, as they seem to vary depending on multiple factors.

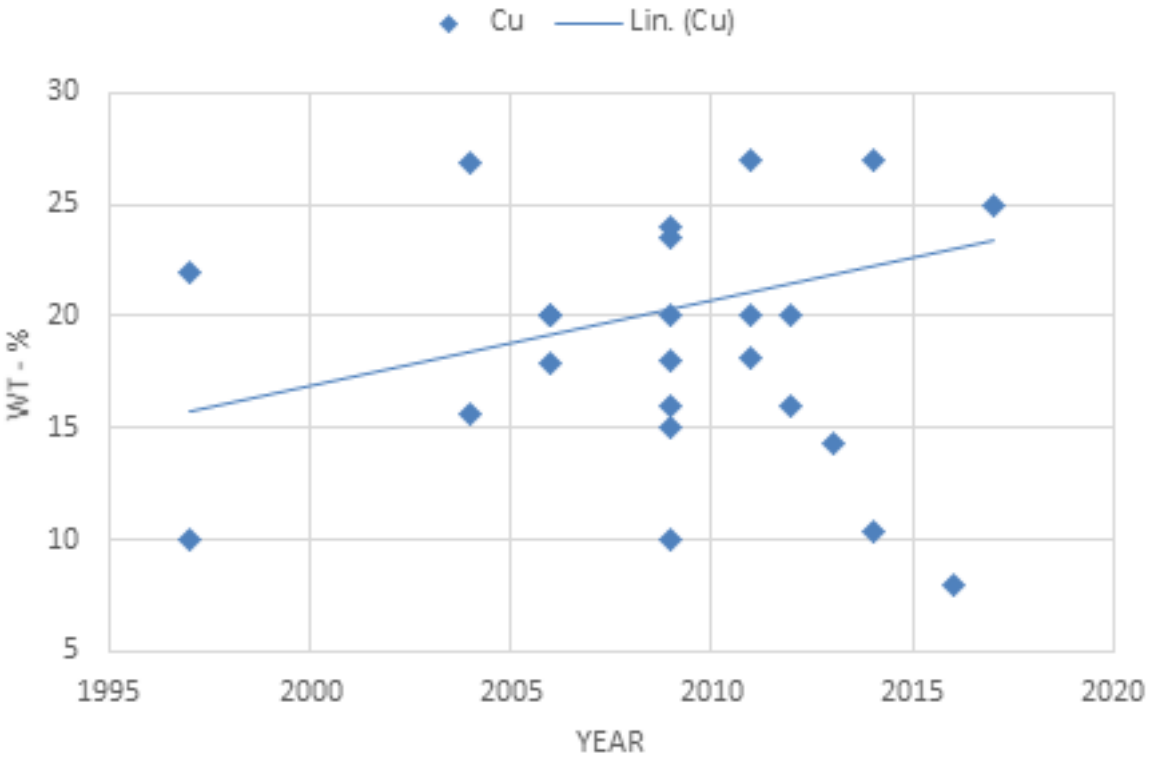

Figure 15. Trend of copper concentration in PCB's (in wt-%)

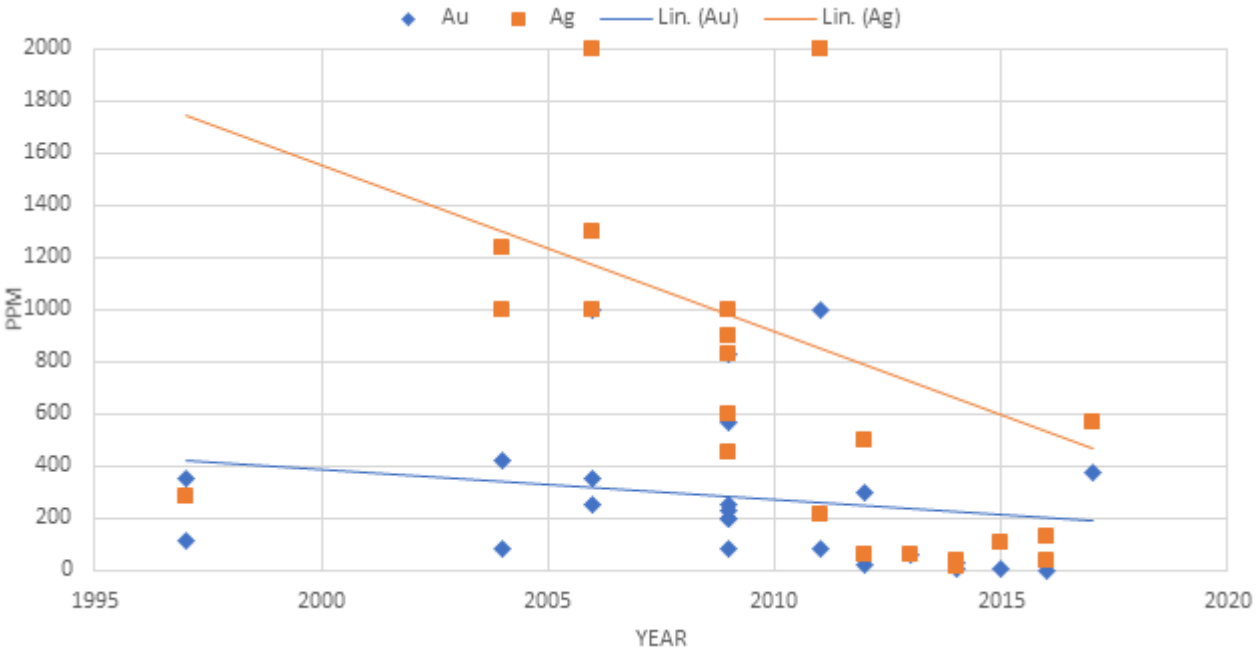

Figure 16. Trend of gold and silver concentrations (in ppm)

4 Melting behavior of PCB's

This chapter describes the theoretical melting behavior of a PCB piece. First, in part 4.1, a technique called lumped capacitance method is introduced to model the melting time and progress over time. Part 4.2. lists the thermal properties of PCB component materials that are needed for the analysis. Part 4.3. combines the technique and parameters from parts 4.1. and 4.2. to form an analysis of the melting behavior. Finally, part 4.4 specifies the melting of plastic components in PCB structure.

4.1 Lumped capacitance method

The melting of a PCB sample is considered a transient process. When a PCB piece lands on top of molten slag layer, outer layer of the object experiences a drastically higher temperature than the core of the sample. As a result, thermal energy starts to transfer into the piece through conduction, convection and/or radiation. Heat transfer also happens inside the structure of the PCB sample. [53]

Several methods exist for modeling the heat transfer inside a sample, most of which are based on approximations or graphical and numerical methods. The key question is if any steep temperature gradients form within the examined specimen. This is more than likely to happen as PCB contains several different materials with different thermal properties (metals, plastic and ceramics). [53]

The simplest way to model transient heat transfer is called the *lumped capacitance method (LCM)*, which is introduced here to understand the basic principles of heat transfer. This method is based on net energy of the studied object. Equations below show the relation between transferred heat from object surface and the changing rate of the objects internal energy in equation (4), which can be further described with equation (5).

$$-\dot{E}_{out} = \dot{E}_{var} \tag{4}$$

$$-hA(T - T_{\infty}) = \rho V c \frac{dT}{dt} \tag{5}$$

where h is the heat transfer coefficient of the material, A is area of an object, T temperature, ρ is density, V is volume, c is heat capacity of the material and $\frac{dT}{dt}$ change of temperature over time t.

By defining the temperature differences according to equations (6) and (7):

$$\theta \equiv T - T_\infty \tag{6}$$

$$\theta_i \equiv T_i - T_\infty \tag{7}$$

We can now write equation (5) in following form (8)

$$\frac{\rho V c}{hA} ln \frac{\theta}{\theta_i} = t \tag{8}$$

which can further be written as (9)

$$\frac{\theta}{\theta_i} = \frac{T - T_\infty}{T_i - T_\infty} = \exp[-t(\frac{hA}{\rho V c})] \tag{9}$$

Equation (9) shows that the temperature difference between solid object and fluid reaches zero when time grows to infinity. Equations (5) and (6) can be used to solve either the time t needed for an object to reach a specific temperature T or vice versa.

From equation (9) we can derive thermal time constant τ, which is defined in equation (10):

$$\tau = \frac{1}{hA}(\rho V c) = RC \tag{10}$$

In equation (7), R is called convective thermal resistance and C is lumped thermal capacitance of the object material. The name of this method is derived from these values, both of which describe the ability of an object to transfer heat to or from the surrounding environment. If either R or C grows, more time is required for an object to achieve thermal equilibrium. The above equations show that the *lumped capacitance method* is a

tempting method to use due to its simplicity, but in the case of PCB's this method could be inefficient due to multiple materials present. Below is a method for testing if lumped capacitance method is accurate enough.

The presence of temperature gradients within an object is described with a dimensionless variable called the *Biot's number, Bi*. Biot's number describes the relation of conduction and convection, more accurately the ratio of thermal resistance caused by these transfer mechanisms. For lumped capacitance method to be accurate enough, Biot's number should be $Bi \ll 1$. This means a value of $Bi < 0{,}1$ [53].

Figure 17 shows the effect of Biot's number on the stationary thermal profile of an object experiencing thermal convection. The temperatures are in relation of $T_\infty < T_2 < T_1$.

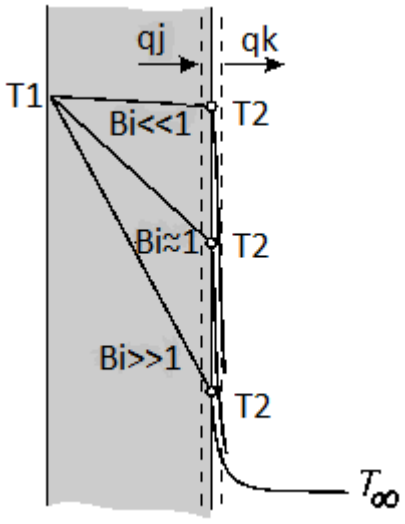

Figure 17. Different thermal profiles [53]

Biot's number can be calculated using equation (11):

$$\frac{T_1 - T_2}{T_2 - T_\infty} = \frac{(\frac{l}{kA})}{(\frac{1}{\alpha A})} = \frac{R_j}{R_k} = \frac{\alpha l_k}{k} \equiv Bi \tag{11}$$

where l_k is a characteristic length (volume divided by area) for objects with varying geometry and α is the thermal diffusivity of a material, defined in equations (12) and (13).

$$l_k \equiv \frac{V}{A} \tag{12}$$

$$\alpha = \frac{k}{\rho c} \tag{13}$$

Using the characteristic length and equation (9) following relations can be formed

$$\frac{\alpha A t}{\rho V c} = \frac{\alpha t}{\rho c l_k} = \frac{\alpha l_k}{k}\frac{k}{\rho c}\frac{t}{l_k} = \frac{\alpha l_k}{k}\frac{\alpha t}{l_k^2} \tag{14}$$

From equation (14), we can get another dimensionless value for characterizing transient thermal transfer phenomena, *Fourier's number, Fo*.

Thus, equations (15) and (16) can be formed as:

$$\frac{\alpha A t}{\rho V c} = Bi * Fo \tag{15}$$

or

$$Fo \equiv \frac{\alpha t}{l_k^2} \tag{16}$$

From three major heat transfer phenomena (radiation, convection, conduction), the dominant heat transfer phenomena in a slag – sample system is most likely radiation and conduction. Radiation is likely to be dominant when the sample is on top of the slag. Conduction becomes dominant when the sample is submerged. In this thesis the examined sample is assumed to submerge and be covered by slag almost instantly. Thus, the primary heat transfer into the sample is considered to be by conduction.

Due to layered nature of the PCB sample, heat conduction and melting are not constant through the sample. The copper layers, other metallic components and solders transfer heat better than polymer or ceramic components.

4.2 Thermal properties of PCB's

The most common materials in PCB's and their thermal properties are shown in tables 4-6 below. Properties shown are heat capacity, density, heat transfer coefficient, volumetric heat capacity and thermal diffusivity. The materials are divided into three groups: metals, ceramics and polymers. The arithmetic mean is mathematical average of each element value. Arithmetic mean is deemed to be enough in this work, since only the general behavior is of interest.

Table 4. Thermal properties of metals in PCB

	Heat capacity cp [J/kg*K]	Density ρ [kg/m^3]	Thermal conductivity k [W/m*K]	Volumetric heat capacity *[J/m^3*K]*	Thermal diffusivity α [m^2/s]	Reference/ Arithmetic mean
Metals (max 40%)	**417.4**	**7742.1**	**146.7**	**$3.03*10^{6}$**	**$4.8*10^{-5}$**	Arithmetic mean
Cu	386	8933	401	$3.45*10^{6}$	$1.2*10^{-4}$	[53]
Fe	448	7870	80.2	$3.53*10^{6}$	$2.3*10^{-5}$	[54]
Al	900	2702	237	$2.43*10^{6}$	$9.7*10^{-5}$	[54]
Pb	129	11340	35.3	$1.46*10^{6}$	$2.4*10^{-5}$	[55]
Zn	388	7140	116	$2.77*10^{6}$	$4.2*10^{-5}$	[55]
Ni	443	8900	90.7	$3.94*10^{6}$	$2.3*10^{-5}$	[54]
Sn	228	7310	66.6	$1.67*10^{6}$	$4.0*10^{-5}$	[55]

Table 5. Thermal properties of ceramics in PCB

	Heat capacity cp [J/kg*K]	Density ρ [kg/m^3]	Thermal conductivity k [W/m*K]	Volumetric heat capacity *[J/m^3*K]*	Thermal diffusivity α [m^2/s]	Reference/ Arithmetic mean
Ceramic (max 30%)	**800.2**	**3380.0**	**27.0**	**2.70*10^{6}**	**$1.1*10^{-5}$**	Arithmetic mean
SiO2 (Silica)	740	2650	1.4	$1.96*10^{6}$	$4.2*10^{-6}$	[54]
Al2O3 (Alumina)	770	3970	39	$3.06*10^{6}$	$1.2*10^{-5}$	[54]
MgO (Magnesia)	940	3560	37.7	$3.35*10^{6}$	$1.3*10^{-5}$	[56]
CaO (Burnt lime)	751	3350	30	$2.51*10^{6}$	$1.2*10^{-5}$	[57,58]

Table 6. Thermal properties of plastics in PCB

	Heat capacity cp [J/kg*K]	Density ρ [kg/m^3]	Thermal conductivity k [W/m*K]	Volumetric heat capacity *[J/m^3*K]*	Thermal diffusivity α [m^2/s]	Reference/ Arithmetic mean
Plastics (max 30%)	**1408.3**	**1412.2**	**0.24**	**$1.99*10^6$**	**$1.2*10^{-7}$**	Arithmetic mean
Polyethylene (HD)	1850	950	0.33	$1.76*10^6$	$1.9*10^{-7}$	[54]
Polypropylene	1925	903	0.24	$1.74*10^6$	$1.4*10^{-7}$	[54]
Epoxides	1000	1900	0.23	$1.90*10^6$	$1.2*10^{-7}$	[55]
Poly(vinylchloride)	1005	1400	0.15	$1.41*10^6$	$1.1*10^{-7}$	[59]
Poly(tetrafluroethane)	1000	2170	0.25	$2.17*10^6$	$1.2*10^{-7}$	[59]
Nylon	1670	1150	0.25	$1.92*10^6$	$1.3*10^{-7}$	[54]

The above tables 4-6 show heat capacity, density and heat transfer coefficient values from cited sources. Volumetric heat capacity and thermal diffusivity are calculated using previous values with equations (17) and (18). Finally, reference column shows mathematical average calculated from shown values and the sources cited.

$$Volumetric\ heat\ capacity\ (Vhc) = \rho * c \tag{17}$$

$$Thermal\ diffusivity\ (\alpha) = \frac{k}{Vhc} = \frac{k}{\rho * c} \tag{18}$$

Metals and ceramics are surprisingly close in thermal properties according to arithmetic averages, but each sum of each phase needs to be considered. It is essential to consider the difference of metals and ceramics compared to plastic fraction. Figure 18 is a graphical presentation of these differences in the form of thermal diffusivity. Thermal diffusivity measures the rate of transfer of heat through material. The scaling is logarithmic and averages and all values are taken from tables 4-6. Tables 7-9 show the melting points of PCB fractions. Figure 19 shows the melting points of elements listed in tables 7-9.

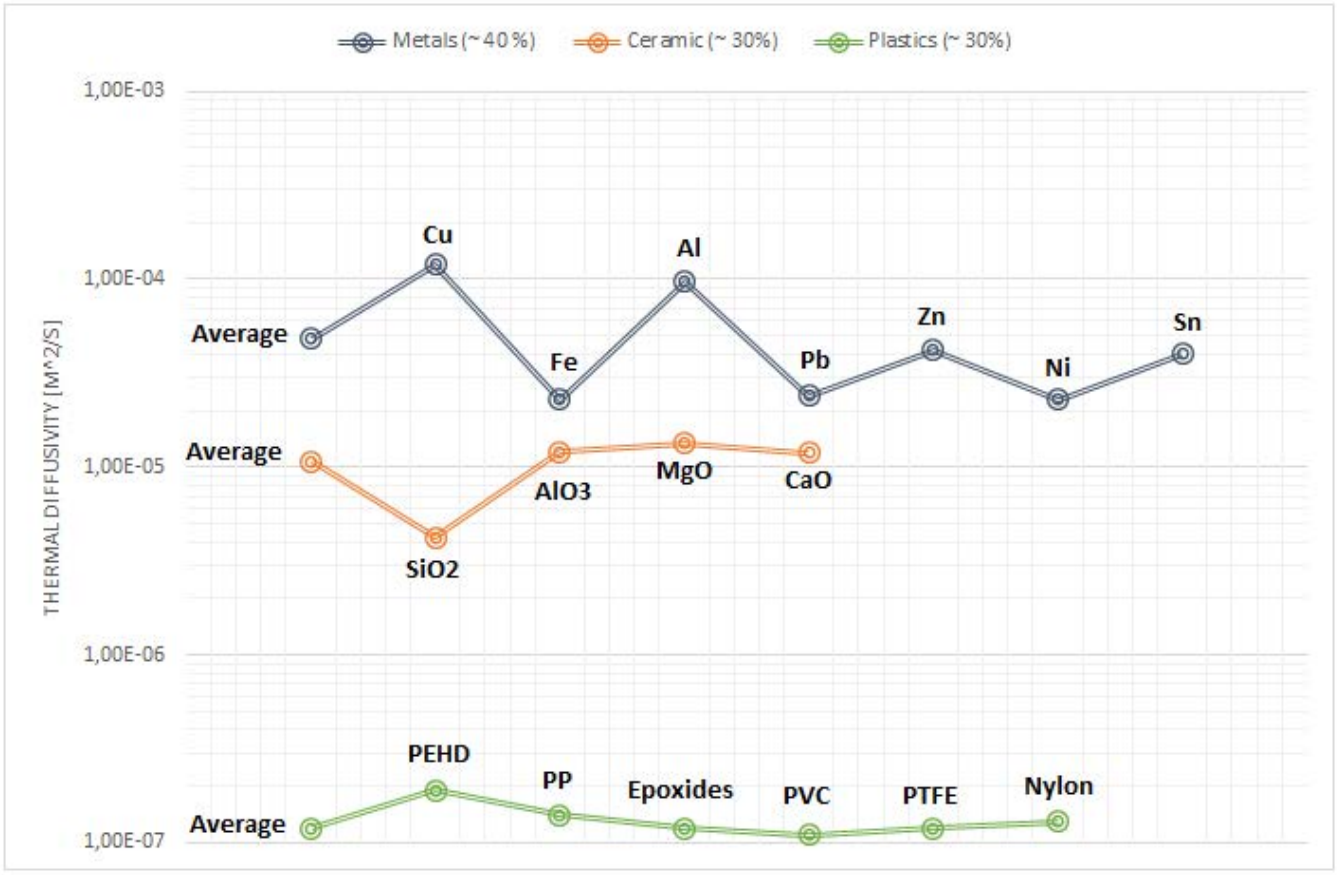

Figure 18. Thermal diffusivity of PCB materials

Table 7. Melting points of metallic fraction [60]

Element	Cu	Fe	Al	Pb	Zn	Ni	Sn	Ag	Au
Melting point (°C)	1084	1538	660	328	420	1453	232	960	1063

Table 8. Melting points of ceramic fraction [57,61]

Element	SiO2	Al2O3	MgO	CaO
Melting point (°C)	1726	2054	2826	2613

Table 9. Melting points of plastic fraction [62]

Element	Polyethylene (PEHD)	Polypropylene (PP)	Polyvinylchloride (PVC)	Polytetrafluroethylene (Teflon)	Nylon
Melting point (°C)	141	179	260	327	220

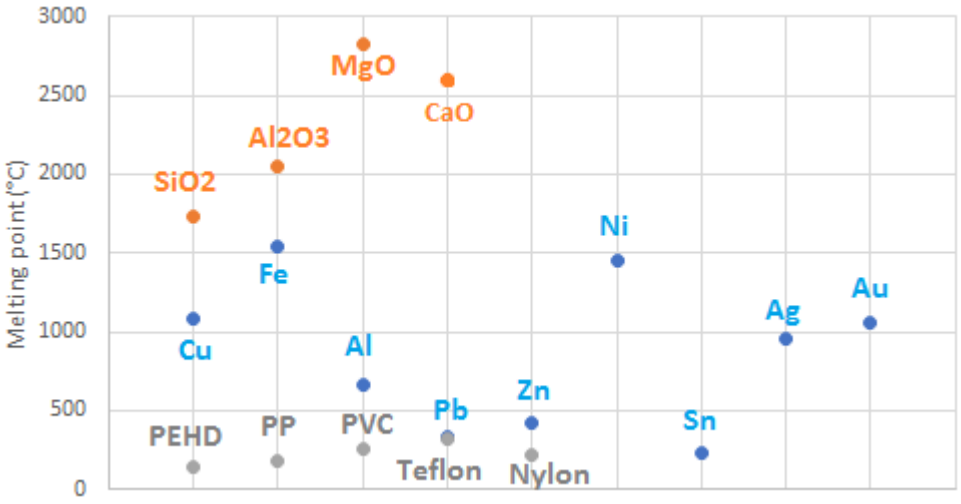

Figure 19. Melting points of elements in PCB's [60-62]

In contrast to thermal diffusivity, ceramic fraction requires very high temperatures to melt. However, even if the melting temperatures are high for ceramics, they will heat up to these temperatures relatively fast compared to plastics. As an observation, MgO has the highest melting temperature of nearly 3000 °C, but its content is low compared to other ceramics. Metallic fraction has the greatest deviation in melting temperatures, between 250 and 1500 °C. Plastics melt around 200 °C, which is low compared to the other fractions.

4.3 Thermal conduction through PCB structure

To begin modelling the thermal heat flow through a PCB structure, first the structure needs to be defined. Figures 20 and 21 show a cross-section of the structure. Figure 18 is a SEM image of a cross-section of a typical PCB piece. Figure 19 is a description of different phases or parts shown in figure 18.

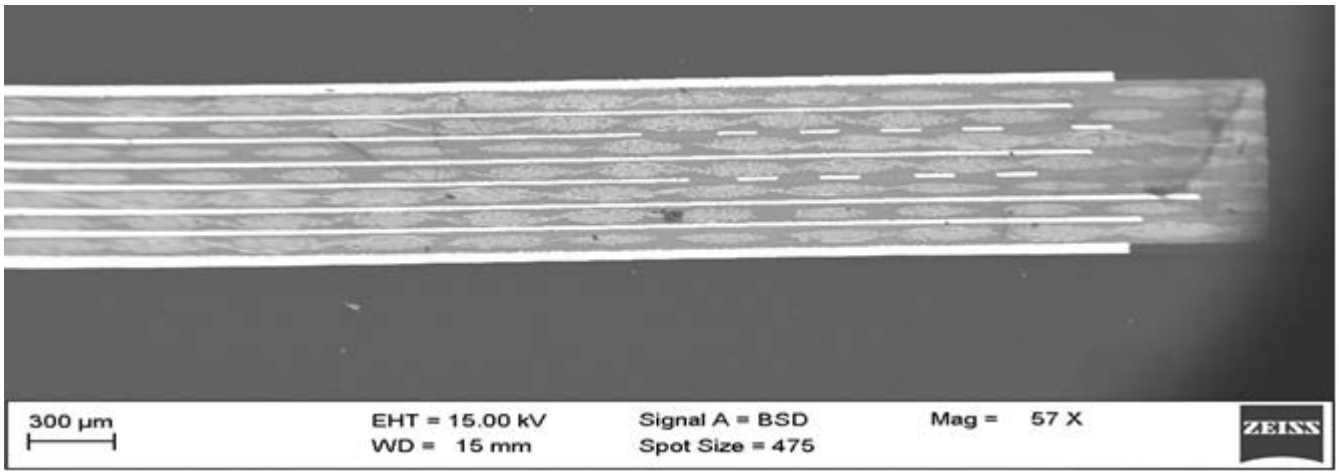

Figure 20. SEM image of PCB cross-section

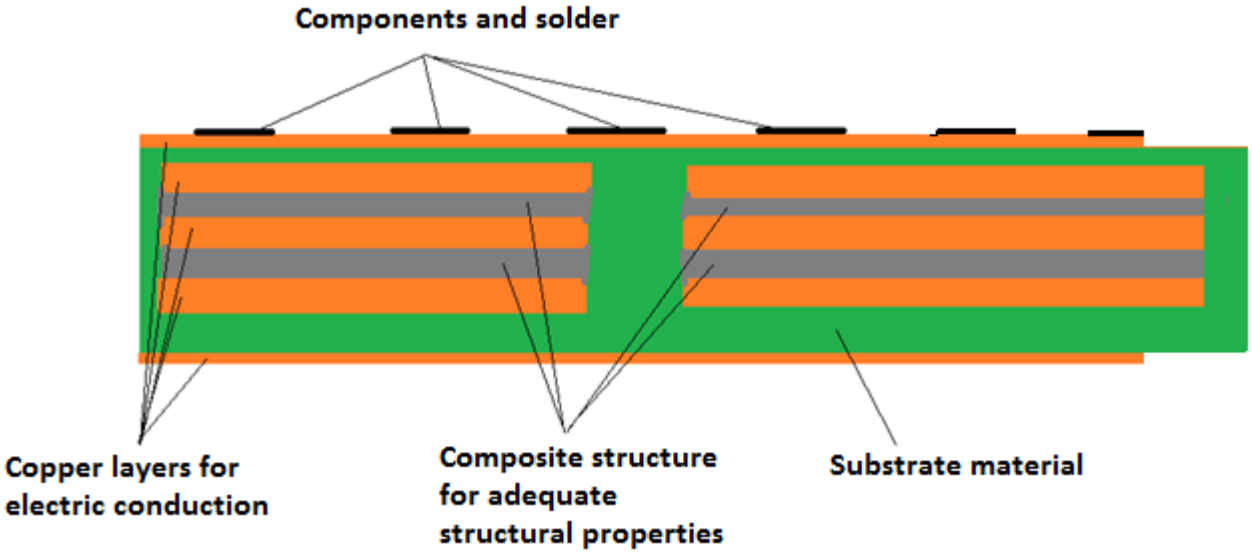

Figure 21. An illustration of PCB materials

The illustration above shows a simplified structure of a PCB piece. The copper layers, components and solder contain metals, whereas the composite structure is comprised of ceramics and substrate materials contain plastics.

As stated earlier, all three major layers have different thermal properties. To solve the thermal flow through such an object is complicated. The purpose of this thesis is to examine the thermal flow as a function of time for a sample that is roughly 5 mm x 5 mm x 1 mm in size. First, the Biot's number is calculated for metals, ceramics and plastics using equation (11). The numbers are calculated for each fraction of the used sample size and a weighted average. If the results are less than 0.1, then the lumped capacitance

method is viable for this thesis. The weighted average in table 10 is calculated using equation (19), with weight factors (w_i) of 0.4 for metals and 0.3 for ceramics and plastics.

Table 10. Biot's numbers

	Biot's number
Metals	$3.3*10^{-7}$
Ceramics	$4.1*10^{-7}$
Plastics	$5.0*10^{-7}$
Weighted Average	$3.2*10^{-7}$

$$\bar{x} = \frac{\sum_{i=1}^{n} w_i x_i}{\sum_{i=1}^{n} w_i} \tag{19}$$

In equation (19) w_i is the weighing factor and x_i is a datapoint.

Table 10 shows that the Biot's numbers are low enough to justify the use of lumped capacitance method. Figure 22 shows temperature as a function of time calculated using the lumped capacitance method (equation (8)). The values used are shown in table 11.

Table 11. Values used in figure 17.

	Thermal conductivity ***k*** ***[W/m*s]***	*Heat transfer coefficient* ***h*** ***[W/m^2*s]***	*Density* ***ρ*** ***[g/cm^3]***	*Heat capacity* ***c [J/m^3*°C)***
Metals	146.70	146.70	7.74	391.40
Ceramics	27.00	27.00	3.38	800.20
Plastics	0.24	0.24	1.41	1408.33
Weighted Average	66.85	66.85	4.53	819.12

Heat transfer coefficient h is calculated using characteristic length l_k and equation (20).

$$h = \frac{k}{l_k} \tag{20}$$

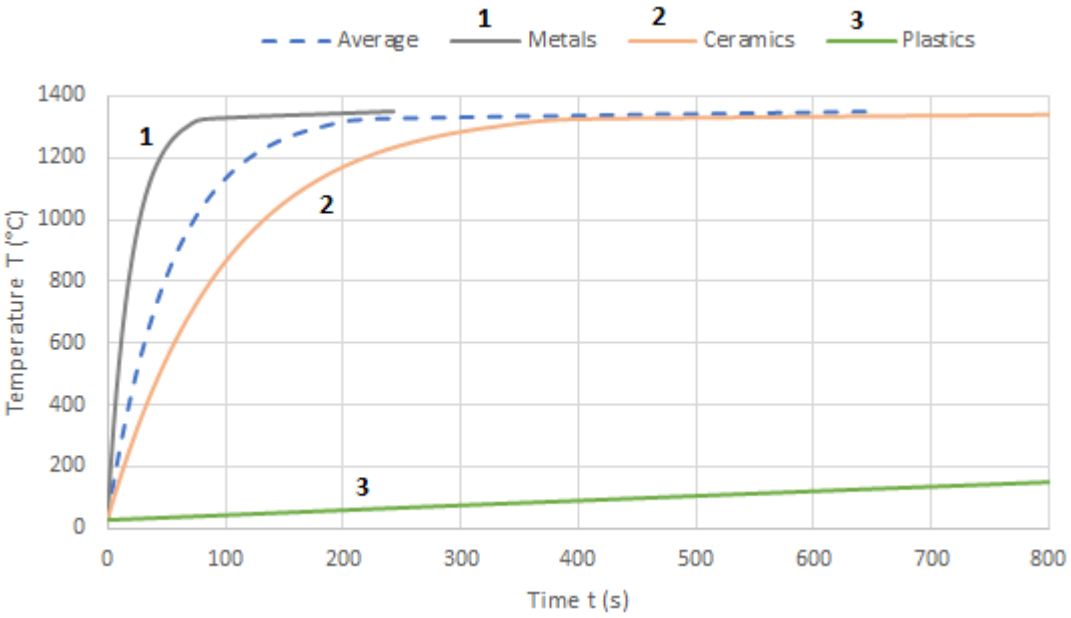

Figure 22. Temperature VS Time using weighted averages for PCB sample

Starting from room temperature of 25 °C, figures 22 that it would take approximately 3 minutes for the PCB sample to reach a temperature of 1350 °C. This was the temperature used in the experiments in this thesis. The properties of metal and ceramic fraction are again somewhat similar, while plastic fraction differs drastically.

When considering the melting behavior of a PCB piece, figures 20 and 21 clearly show that the structure is the deciding factor. Heating times differ significantly for each fraction and when this data is compared with the melting temperatures in figure 19, the metallic fraction starts to melt quickly when dropped to molten slag. The ceramic fraction has higher melting temperatures than the temperature used in experiments. Thus, the ceramic components may mix with the slag in solid state. However, the effect of silica as a flux in the slag may lead to considerably lower melting temperatures of the ceramic fraction, resulting in melting already in the experimental temperature. Finally, the melting of the plastic fraction is the most difficult to describe, since it's thermal diffusivity is poor and melting temperature low.

4.4 Pyrolysis of plastics

Pyrolysis refers to a process, which involves chemical and thermal decomposition under the absence of oxygen. The breakdown of plastics happens via depolymerization, in which the macromolecular structure of polymeric material breaks down into smaller molecules. Organic material typically degrades to coke and gases. The gaseous components can be further divided into condensable and non-condensable gases. The process of decomposition of plastic material in relation to temperature is shown in figure 23. [63]

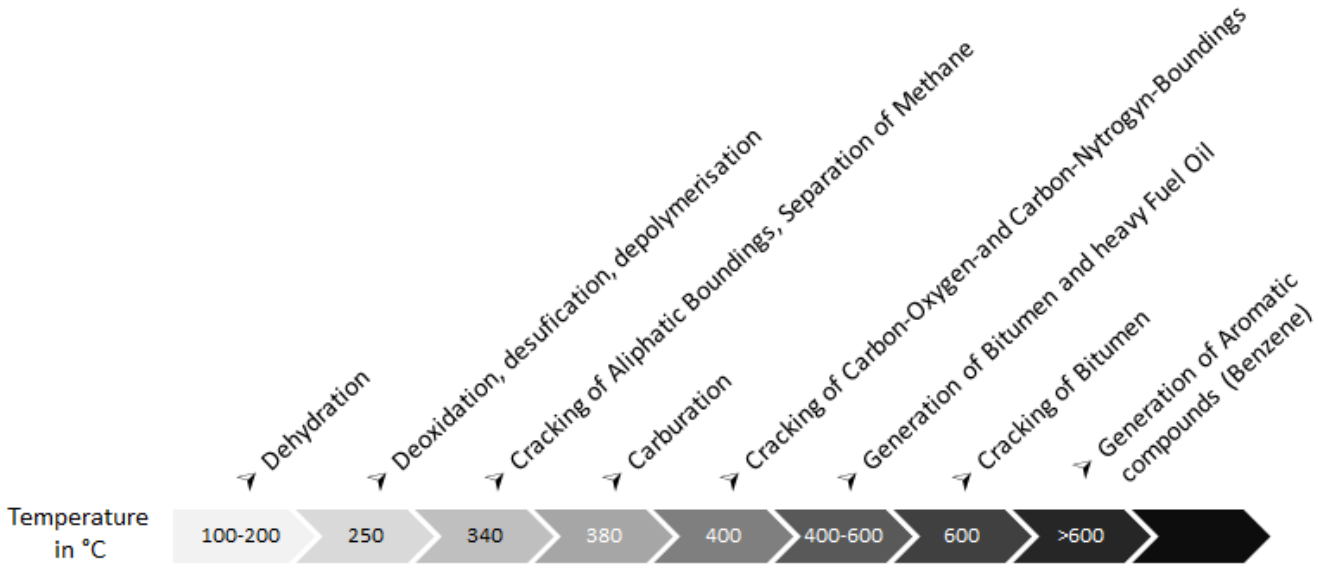

Figure 23. Thermal decomposition of organic material VS temperature [63]

Pyrolysis of plastics is potentially hazardous and environmentally toxic due to halogenated flame retardants. These can cause the formation of carcinogenic substances, more specifically polybrominated dibenzo dioxins/furans (PBDD/F) [64].

The additive flame retardants include polybrominated diphenyl ethers (DBPE and TBPC). In addition, halogens (Br and Cl) and Sb in some cases, are collected in gases, oil and solid residue. When in contact with hydrogen, which is formed in the dehydration of the polymer structure, Cl and Br form gaseous HBr and HCl. These are corrosive gases and may cause problems in gas purification equipment. [63] Sb is a toxic substance and a suspected carcinogen. [65]

Figure 24 shows an example of a polymer chain of one flame retardant substance and figure 25 shows the structure of PCDD/F (PolyChlorinated Dibenzo Dioxin/Furan) and PBDD/F.

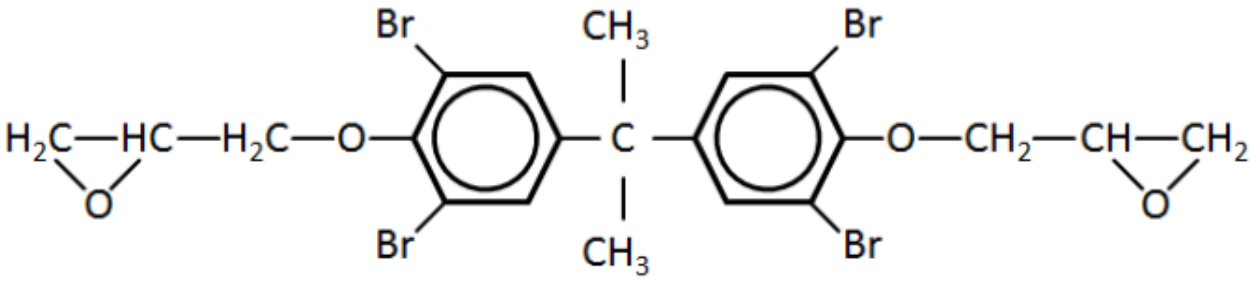

Figure 24. A flame retardant polymer chain, DGETBBA [63]

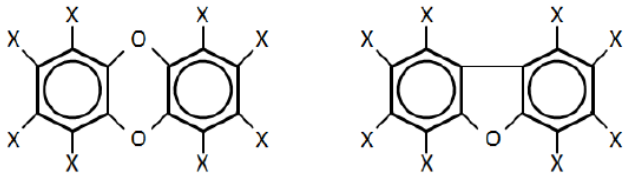

Polychlorinated dibenzodioxins (PCDD) X= H, Cl

Polybrominated dibenzodioxins (PBDD) X= H, Br

Polychlorinated dibenzofurans (PCDF) X= H, Cl

Polybrominated dibenzofurans (PBDF) X= H, Br

Figure 25. PCDD/F and PBDD/F [63]

Part II: Experimental

As stated in the introduction, the goal for the experimental part is to find out the time interval in which the PCB sample will melt and where the resulting phases end up. Part II first introduces the experimental setup in chapter 5. Results of the experiments are shown and discussed in chapter 6. Finally, conclusions and suggestions for future work are presented in chapter 7.

5 Experimental setup

Chapter 5 introduces the experiments conducted in this thesis. First, the experimental setup is introduced. Then, chapter 5.1 describes the samples characteristics. Then, chapter 5.2. presents the formation of fayalite slag and its meaning to the experiments. Chapter 5.3. goes through the sample preparation for analysis. Finally, chapter 5.4. presents the analysis methods.

The experimental setup is based on the same setting as used in previous thesis [3]. The experiments were conducted in a vertical tube-shaped furnace, into which a cone-shaped crucible (outer diameter of 22 mm, Finnish special glass, FIN) holding slag and sample was suspended. The temperature around the crucible was 1350 °C. The crucible contained fayalite slag, which was given enough time to melt. This time was 5 minutes. The gas atmosphere was inert argon gas, otherwise the slag would react with oxygen in an air atmosphere and this was not desirable. The major difference compared to the previous thesis was that the WEEE sample was dropped from a hole on top of the furnace into the molten slag. [3]

Figure 26 is a photograph of the furnace used in experiments. Below the furnace is the quenching vessel, on the left is the gas system and bottom right corner shows the control equipment (temperature measurement and gas flow control).

Figure 26. Furnace used in experiments

The furnace in figure 26 is a Lenton 16/450 single phase vertical tube furnace, that is heated electrically using four silicon carbide (SiC) heating elements. Furnace had two alumina tubes (Friedrichs feld AL23, Ger) with inner diameters of 35 mm and 22 mm. The larger tube was called a working tube and had the heating elements positioned on the inner circumference in spiral shape. The smaller alumina tube was enveloped inside the larger working tube and spanned from the top lid of the furnace to 20 mm above the geometrical center line of the furnace. The bottom part of the inner tube was defined as the experimental hot-zone, which was at the experiment temperature of 1350 °C. The temperature was monitored using a S-type /Pt/Pt-10Rh thermocouple (Johnson Matthey Noble metals, UK).

Figure 27 shows an illustration of the experimental setup in the furnace. The silica crucibles were suspended in a chassis made of platinum wire. Mixed slag powder in a crucible was first inserted to the bottom part of the furnace and the furnace was sealed.

The argon gas flow was then turned on and given 5 minutes to fill the tube. After 5 minutes the crucible was raised to the hot zone, where it remained for 5 minutes for the slag to melt. After this, the sample was dropped into the crucible from the top of the furnace through a small re-sealable hole. Time was taken from the moment the sample was dropped through the hole to the moment the sample was quenched. The quenching was done by pulling the platinum wire from the top of the furnace, which caused the hook-like wire contact with the crucible chassis to straighten. This caused the crucible to fall out of the bottom part into a quenching vessel filled with ice water. Thus, the structure of the slag remained as it was within the furnace hot-zone.

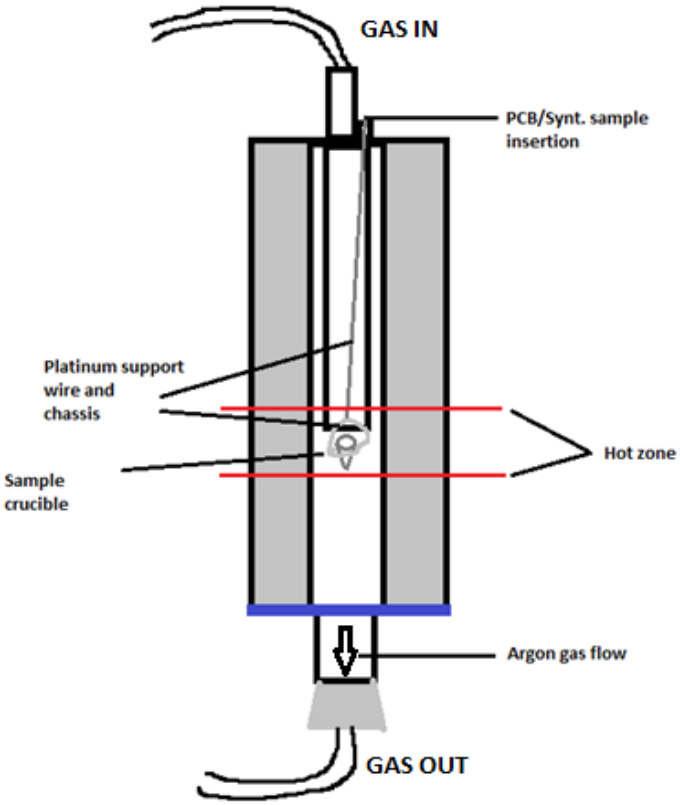

Figure 27. An illustration of the furnace structure

5.1 Sample characteristics

The samples examined were pieces of printed circuit board, that were cut from a disassembled mobile phone motherboard. The size of the pieces was approximately 5

mm x 5 mm x 1 mm. As a comparison sample, copper-nickel alloy (33 wt-% copper and 67 wt-% nickel) pieces wrapped in aluminum foil were used. The size of these comparison pieces was 5 mm x 5 mm x 1 mm as well. Figure 28 shows an example piece of used PCB sample, roughly 5 x 5 x 1 mm. Figure 29 shows components used for "synthetic PCB" sample – pieces of Ni-Cu alloy (66 wt-% Ni /34 wt-% Cu) wrapped in aluminum foil.

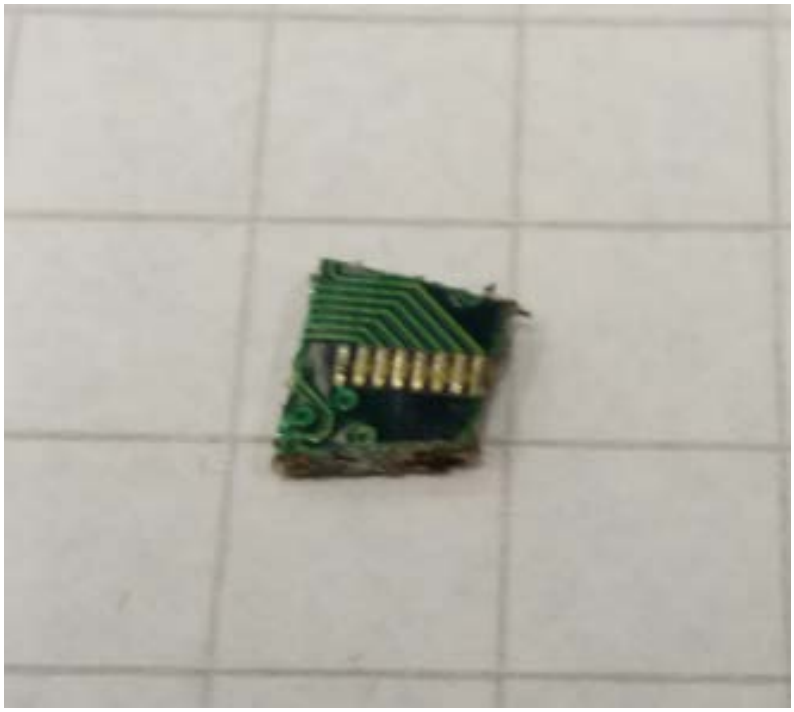

Figure 28. PCB Sample

Figure 29. Components for synthetic samples

The reaction times for the samples were 25, 60, 120 and 300 seconds. Each time interval was repeated multiple times. Initially 40-second samples were melted as well, but these could not be properly prepared for SEM analysis. This was due to bubble-like formation out of cross-section plane in vacuum during carbon coating. The vacuum used in carbon coating step was much weaker than in SEM, so the 40-second samples were discarded because of risk of contaminating SEM chamber. One plausible reason for the bubbles could be a formation of oil from the polymer fraction of PCB's, but this could not be confirmed.

5.2 Slag

The synthetic slag composition used in the melting tests was initially the same that was used in P.I. Guntoro's thesis [3]. This slag consists of hematite (Iron(III) oxide, 99.998%, Alfa Aesar, no mention of particle size) and silica (Silicon dioxide, 99.995%, Alfa Aesar, -40 mesh powder) powders. Fayalite consists of FeO - Fe_2O_3 – SiO_2 structure. The amount of slag used for each experiment was such that a molten bath would form at the bottom of a cone-shaped crucible. This amount was determined by an educated guess and then trial and error. The amount used was at first about 0.5 - 0.7 grams of slag powder and later 1 gram. This amount was observed to form samples with adequate structure.

Important factors in fayalite-slag melting behavior were oxygen partial pressure in the furnace and Fe/SiO ratio. The ratio commonly used in flash smelting furnace is about 1.5-2 (60-67 % SiO, 40-33 % FeO_x). The thermodynamic behavior of the melting point can be seen in figure 30 [66]. In this figure the boundary curves are shown as solid lines and oxygen partial pressure (in bars) as dotted lines.

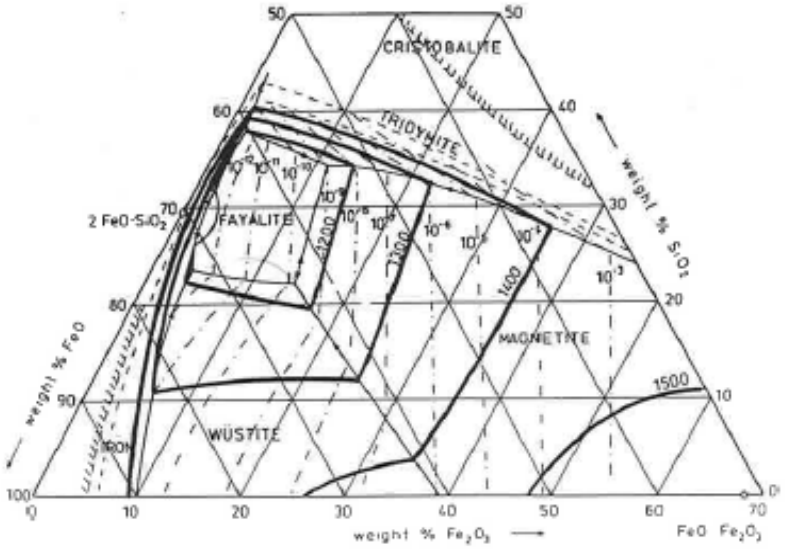

Figure 30. Projection of the liquidus surface of the system FeO-Fe_2O_3-SiO_2 [66]

While defining the experiment conditions, the melting of synthetic slag proved difficult. Many factors, including temperature, gas atmosphere and slag composition, were tested before a working test set-up was found. These conditions were following:

Table 12. Experiment conditions

Temperature (°C)	Gas atmosphere	Slag composition
1350	Inert (Argon)	Fe_2O_3 - Fe (s) - SiO_2

The hematite – iron – silica ratio used was 50 – 20 – 30 (wt-%). It is acknowledged by the author that the selected experimental conditions differ from the conditions used in a Flash Smelting furnace. The differences include fluxing agents like Ca and Mg and temperature. Nevertheless, for the purpose of this thesis, the slag needs to be in molten state and have a fayalitic structure. Thus, the conditions in table 12 were deemed justifiable.

Figures 31 and 32 show the difference in composition of quenched slag structure without and with metallic iron mixed in composition, respectively. The slag was in the furnace hot-zone at 1350 °C for 25 minutes in Argon atmosphere. In figure 31 the slag is only

partially molten. This slag consisted of silica and hematite powder. Figure 30 shows that the addition of metallic iron to the starting mixture enabled complete melting of the slag.

Figure 31. Hematite - Silica structure

Figure 32. Hematite - Iron - Silica structure in silica crucible

5.3 Sample preparation

The samples produced in experimental setup were cone shaped crucibles with solidified slag. To produce a cross-section of the sample, the crucible was first cast into an epoxy mold. The produced epoxy piece was then sawed through at a site, which looked the most interesting by visual examination. The cross-section side of resulting piece was then ground step by step from 120, 240, 400, 800, 1200 and 4000 particles per ft^2 and polished using 3 µm and 1µm synthetic diamond particle polishing spray. Finally, the samples were cleaned using ultra-sound and submerged in ethanol. For SEM analysis the samples were carbon-coated using carbon evaporation. Figures 33 and 34 show crucibles before any preparation steps, figure 35 shows a crucible cross section cast in epoxy and figure 36 shows a finished sample ready for SEM analysis.

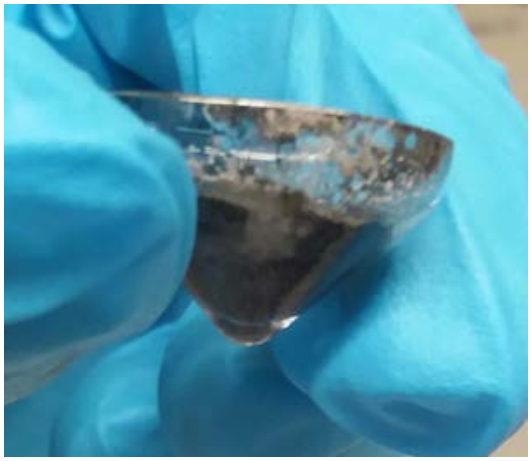

Figure 33. Sample crucible photographed from side

Figure 35. Sawed crucible cross-section

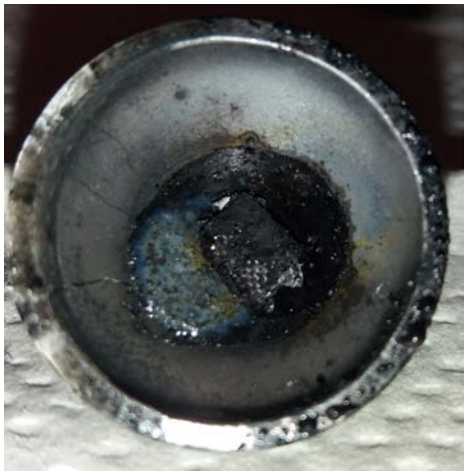

Figure 34. 25 s PCB sample photographed from above

Figure 36. Finished, carbon-coated sample

5.4 SEM and EDS Analysis

The samples were analyzed using Scanning Electron Microscopy (SEM) and X-ray Energy Dispersive Spectrometry (EDS).

Scanning electron microscopy is a widely used, non-destructive analysis technique. It uses an electron beam probe to produce images of sample surface down to nanoscale magnifications. The equipment used in this thesis analysis was TESCAN MIRA3, which used Schottky-type emitter to produce the electron beam. [67,68] Images were produced using Backscattered Electron (BSE) detector. BSE detects electrons, that originate from the scanning electron beam and are reflected or back-scattered from sample interaction volume. Back-scattering phenomena is caused by interactions of electrons with samples atoms. This causes heavier elements (high atomic number) to deflect electrons more strongly than lighter elements (low atomic number). Therefore, heavier elements appear brighter in BSE images, which is practical in determining the chemical composition of a sample. [69] Figure 37 shows the analysis setup. TESCAN MIRA SEM is on the left, with EDS analysis sensor attached on the side and the SEM operating interface and Thermo-Scientific NSS Spectral Imagining software are shown on the right side.

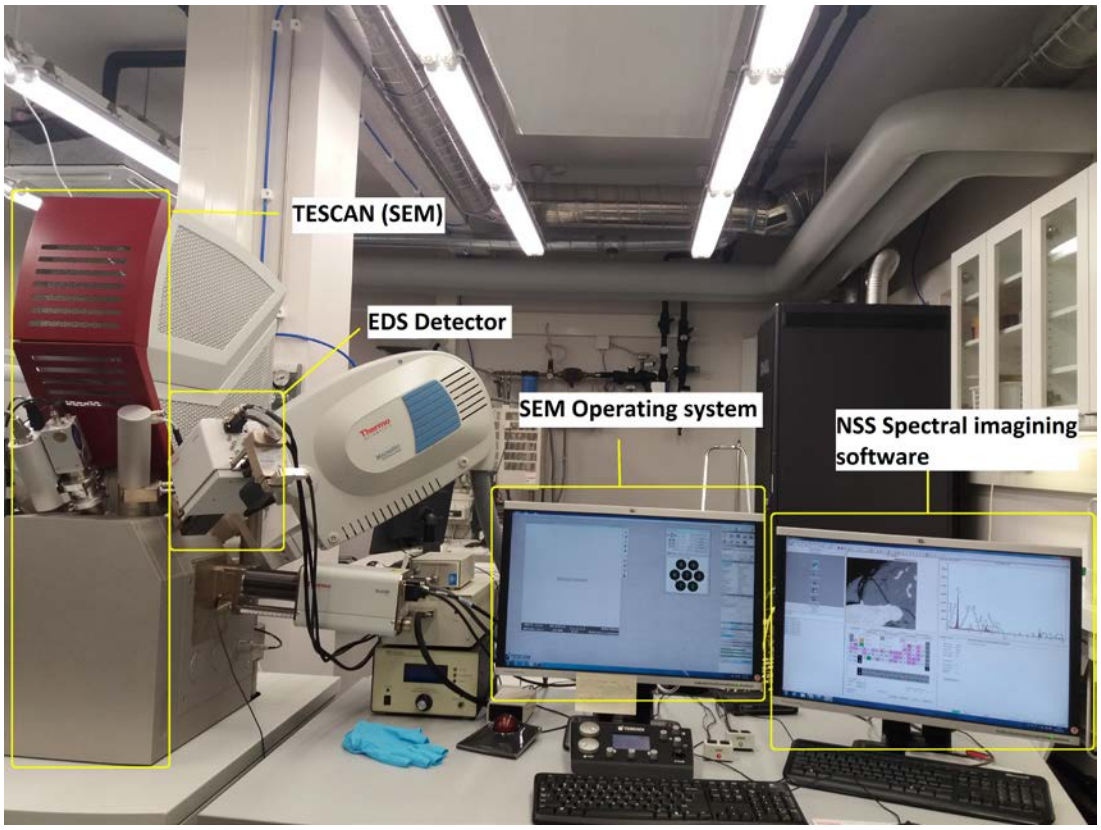

Figure 37. SEM-EDS analysis setup

Composition of samples was analyzed using Energy Dispersive X-ray Spectroscopy (EDXS or EDS). It is based on electron bombardment of the inspected sample surface, which causes unique interaction or electromagnetic emission sets from individual atomic structure. The resulting X-ray emission from atoms in a sample are measured and a spectrum of elements can be formed. The elemental composition is based on this spectrum. The EDS analysis may not be the most reliable in identifying some elements (such as Re etc.), due to the X-ray energy values being similar. Although, in purpose of this thesis (approximately identifying elements and their location in samples), EDS was accurate enough. [69]

6 Results and discussion

Results from the WPCB and synthetic sample analyses are presented in this chapter. The analysis consists of SEM pictures of different magnifications, and EDS analysis is conducted for interesting sites based on these pictures. As a common observation, the PCB samples themselves contain very little, if any iron. For the sake of clarity, all iron found in the analyses is considered to originate from the synthetic slag. This chapter shows an overview BSE images and EDS sites, additional data is found in appendixes A-D. In all the figures, the black background is epoxy (casting material), dark-grey cup is crucible wall and light-grey phase is slag. Chapter 6.3. briefly describes the possible evidence of pyrolysis filmed during PCB containing experiments.

6.1 PCB containing samples

When observing the PCB sample results, the melting of PCB structure starts at the outer copper layers and moves towards the center of the sample. Because there are different material layers the melting is not constant. Copper layers and lead-tin solders are likely to melt almost instantaneously, while ceramic structures and plastic parts take more time to melt. Furthermore, pyrolysis of plastic is a factor in the melting behavior.

Figure 38 shows an overview of the 25 seconds PCB sample. It shows a still noticeable PCB structure on top of molten slag, indicating that 25 seconds is much too short to melt the whole PCB sample. Although the slag phase has melted (5-minutes pre-melting before PCB-sample introduction), some light-grey sites of metallic iron are visible throughout the slag, which is an indication that the slag has not reached an equilibrium state. For the purpose of this work this is not an issue, as the aim is just to investigate the thermal behavior of PCB piece in contact with a molten slag matrix. In addition, with longer pre-melting times, considerable amounts of the slag dripped through the silica crucible, resulting in a diminished slag volume left in the crucible.

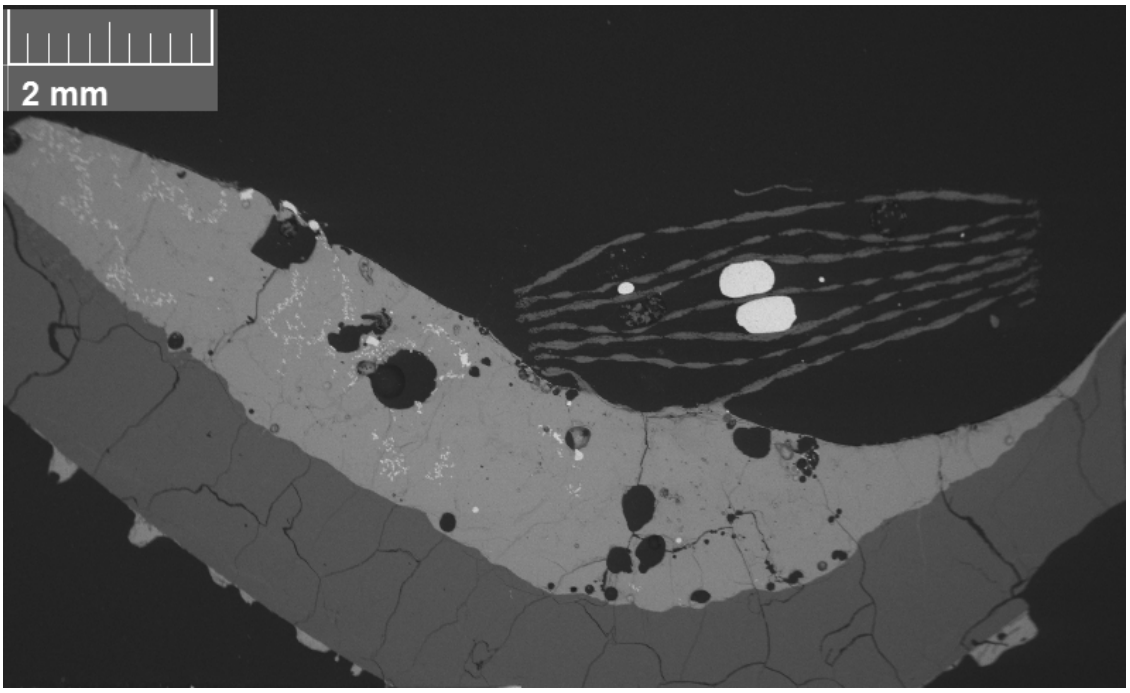

Figure 38. 25 s PCB sample overview

Figure 39 shows the analyzed EDS sites from 25 seconds PCB sample. Sites A and B consist of copper, still within the solid-state PCB structure. Sites C to F show a slag-PCB layer, where copper from upper layers of the PCB sample has formed droplets mixed with iron, nickel, lead and tin. Site G shows sites of metallic iron.

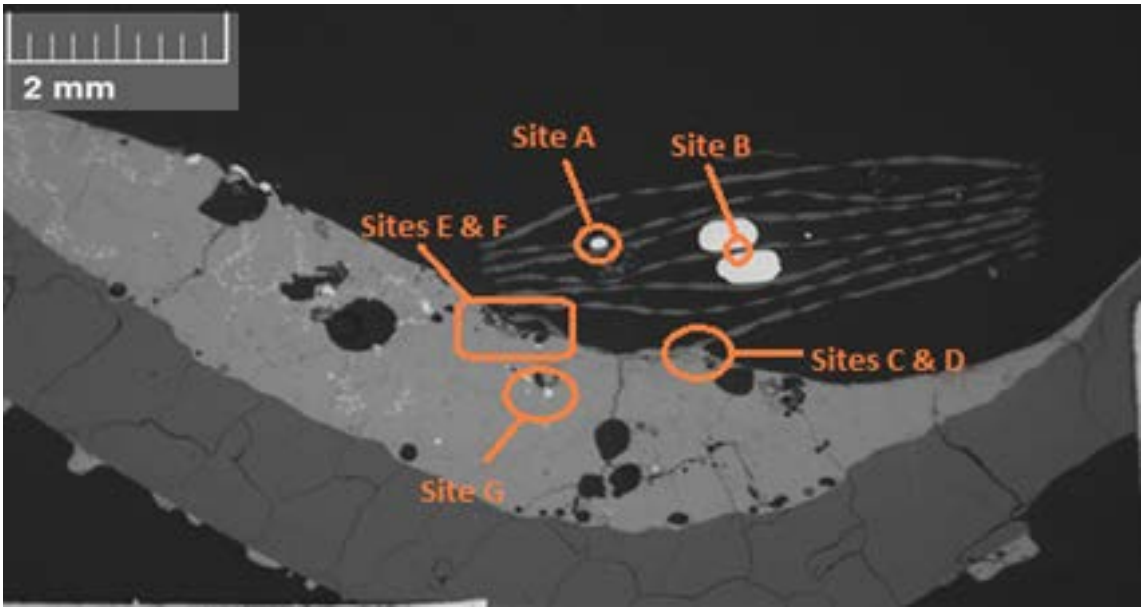

Figure 39. EDS analysis sites

Figure 40 shows an overview of the 60 seconds PCB sample and figure 41 shows the analyzed EDS sites. In this sample, the PCB piece seems to have dropped near the right-side crucible wall. The 60-second sample does not clearly show a PCB piece, but traces of it are visible, specifically at site A. To the right side of the slag there are white areas, which are primarily copper mixed with minor trace metals such as nickel, lead and tin. Sites B, C and E focus on these areas. 60-seconds has not been long enough to allow the copper alloy droplets to start settling through the slag layer towards the bottom of the crucible. Finally, site D verifies more metallic iron present in the sample.

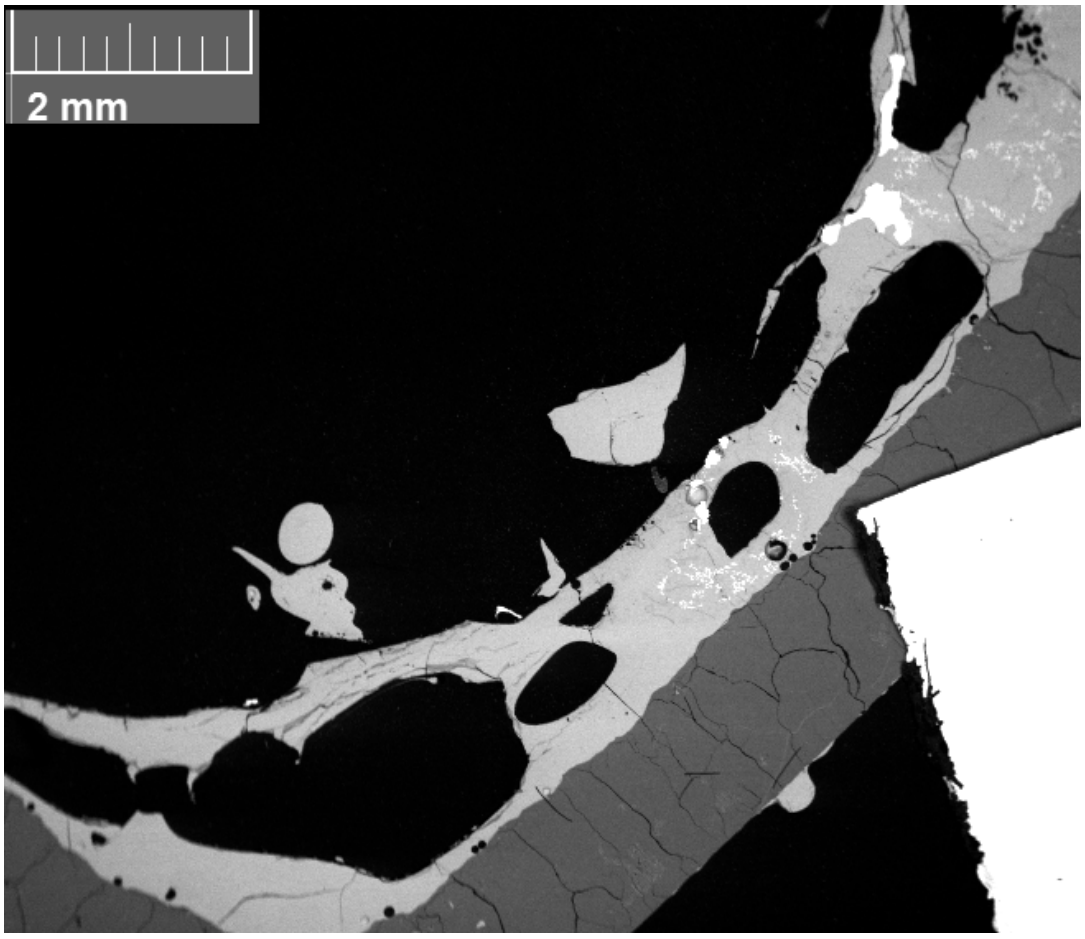

Figure 40. 60 s PCB sample overview

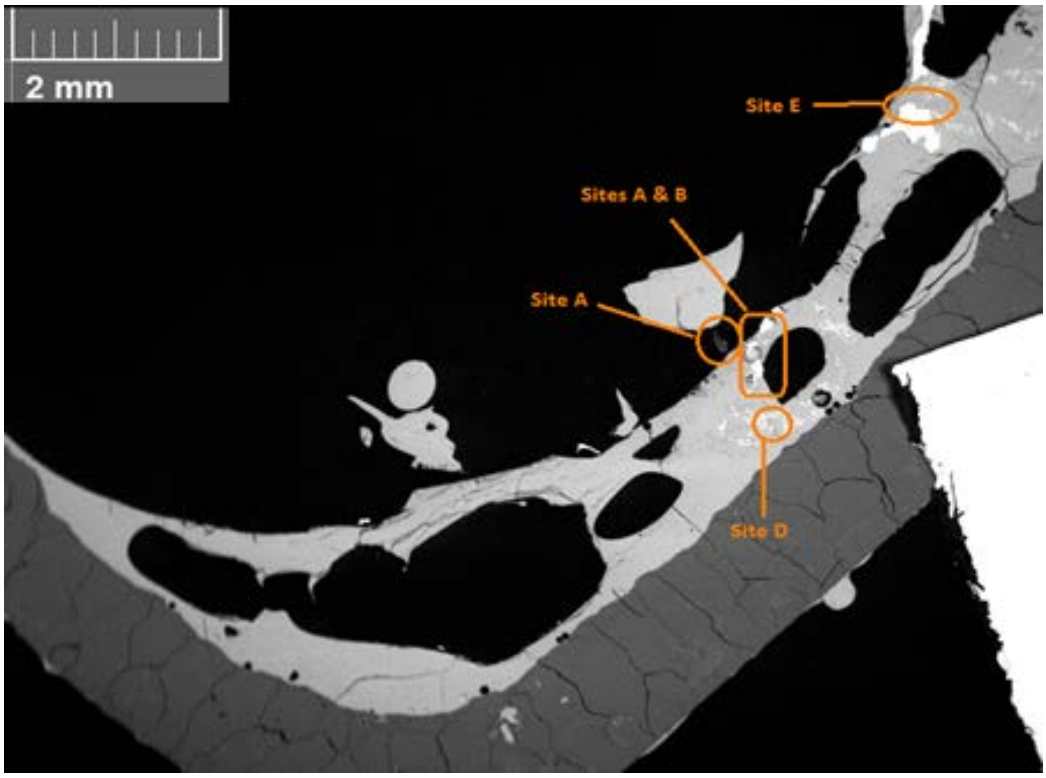

Figure 41. EDS Analysis sites

Initially, the 120-second sample shown in figure 42 did not show copper anywhere else than in the small dots on the right-hand side of partly molten remains of the PCB piece. This sample shows the biggest problem of the experimental setup and sample preparation technique used. As the epoxy samples are cut, it is almost a matter of chance how much of the molten metal droplets ends up in the analyzed cross-section. However, this sample was re-ground to see if any metal traces could be found when moving inward to the sample and the results are shown below.

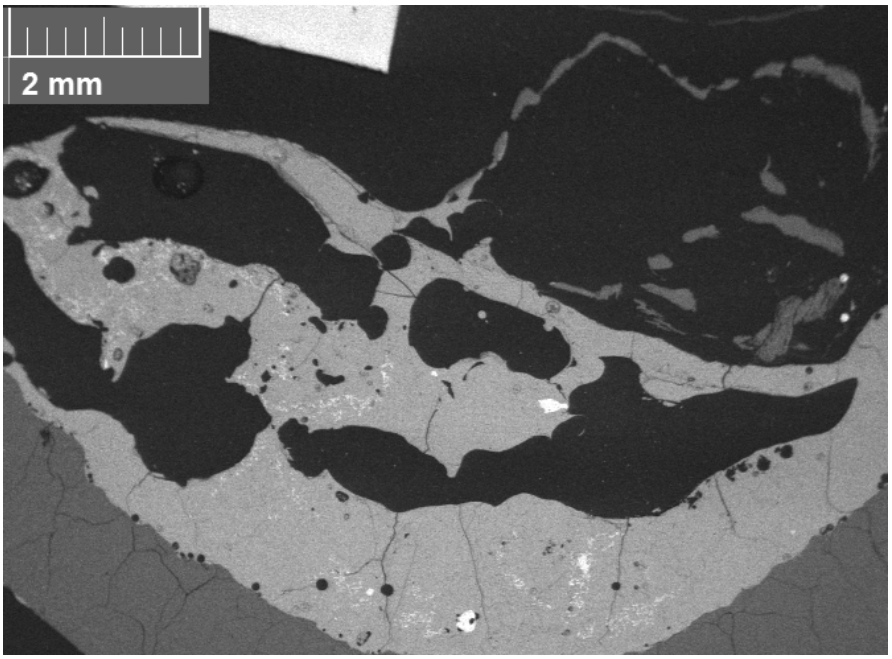

Figure 42. 120 s PCB sample overview

The re-ground sample shown in figure 43 revealed significantly more information. The structure of the PCB piece is clearly visible on upper center part with copper droplets in between. Smaller molten metal droplets can be seen near the PCB structure, on the bottom part of the crucible and on the right-hand side, mixed with the slag matrix.

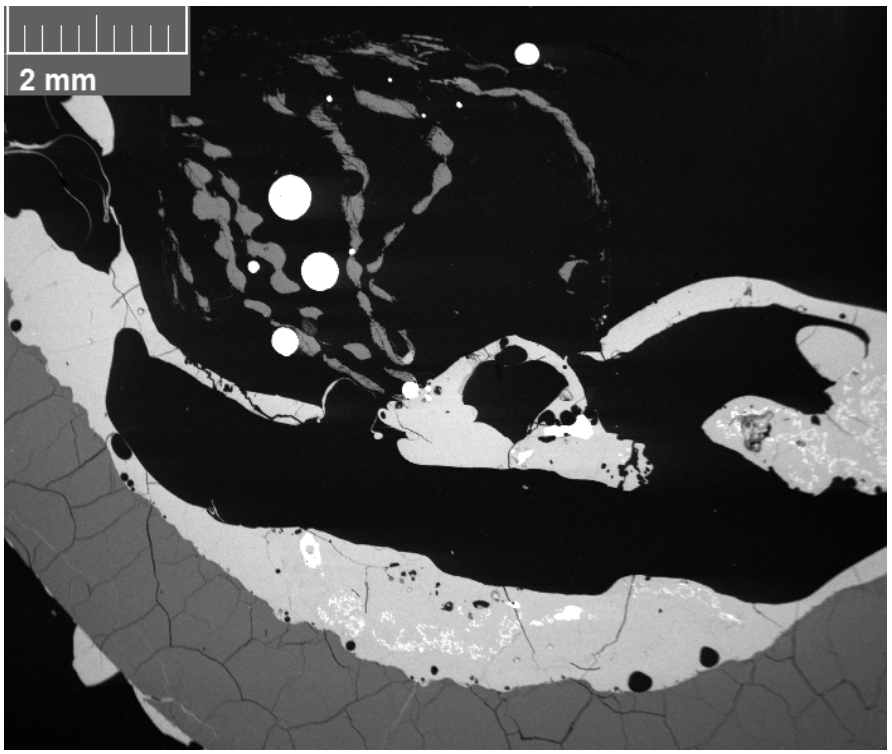

Figure 43. 120 s PCB re-grind overview

Figure 44 shows the EDS analysis sites of the 120 s re-ground sample. A partial PCB structure with copper droplets is found above molten slag layer. Inside the slag there are multiple metal containing sites, that are most likely copper. Site A shows such a droplet in contact with the fayalite slag structure. Peculiarly, all other sites of interest (B-F) show copper and minor traces of other base metals (Ni, Sn, Pb). Site B has a droplet of almost pure iron, mixed with noticeable copper area. Sites C, E and F have an iron-copper-nickel-lead-tin mix, which is also found to be a typical droplet composition in the 300 s sample.

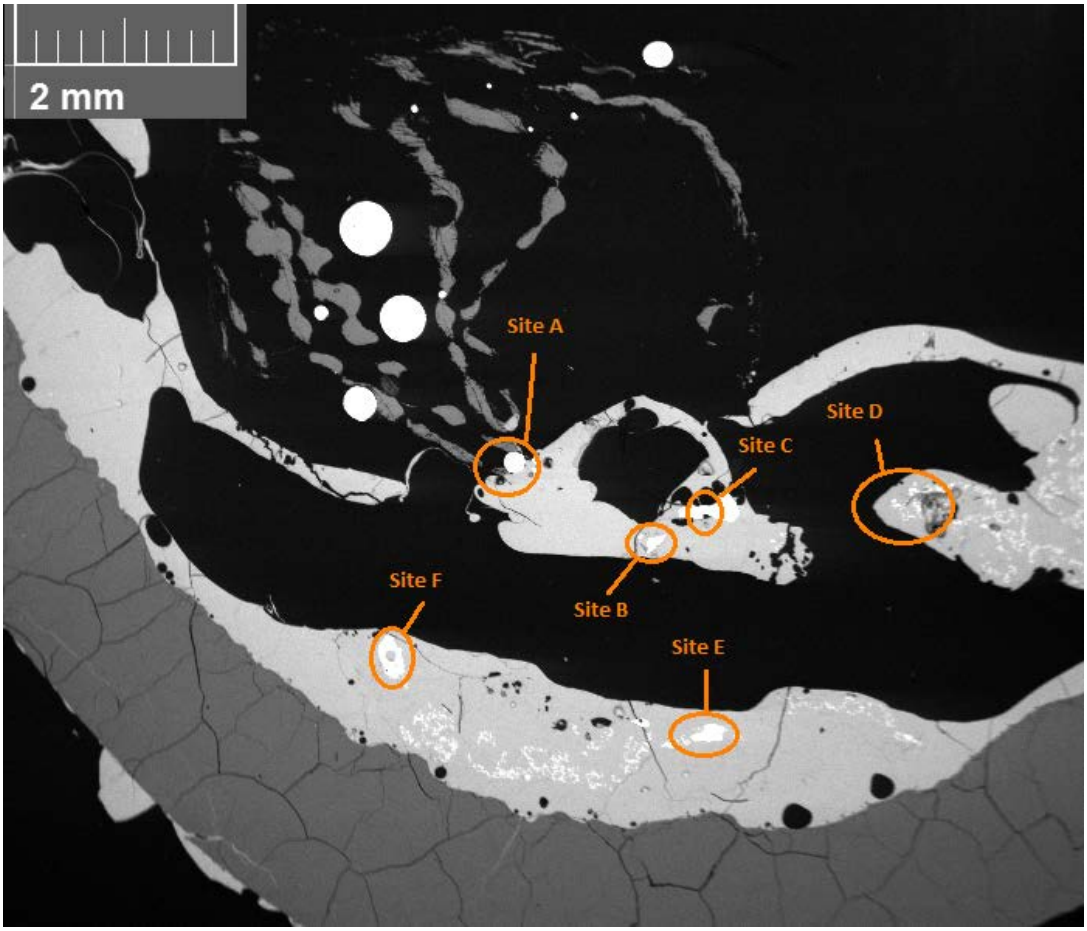

Figure 44. EDS Analysis sites

Figure 45 shows an overview of the 300 seconds PCB sample. After this time, the PCB structure seems to have melted almost entirely and molten metallic material has formed droplets, which have gathered in the middle-bottom area of the crucible. It seems evident

that with a slightly longer reaction time, the rest of the copper alloy droplets would also have begun to settle towards the bottom of the crucible.

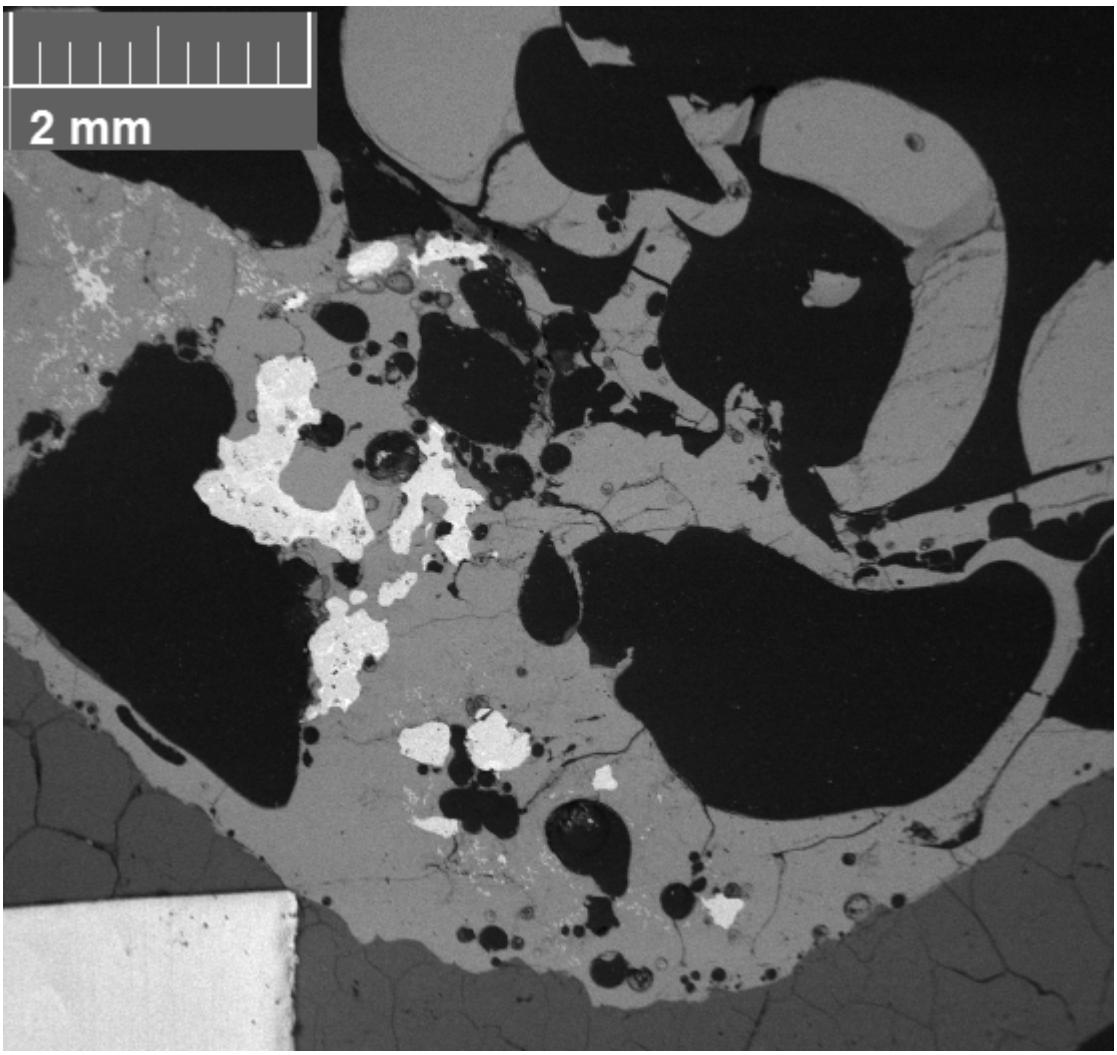

Figure 45. 300 s PCB Sample overview

Figure 46 shows the EDS analysis sites of the 300 seconds PCB sample. The sites A, B and C each had a similar metal mix structure as encountered in previous samples (Cu-Fe mix with minor traces of Ni, Pb and Sn). Sites D, E and F had similar structure to A – C. This sample shows how the copper has mixed with metallic iron, lead, tin and other minor metal traces and spread along the slag layer, with insufficient time to reach the bottom of the crucible.

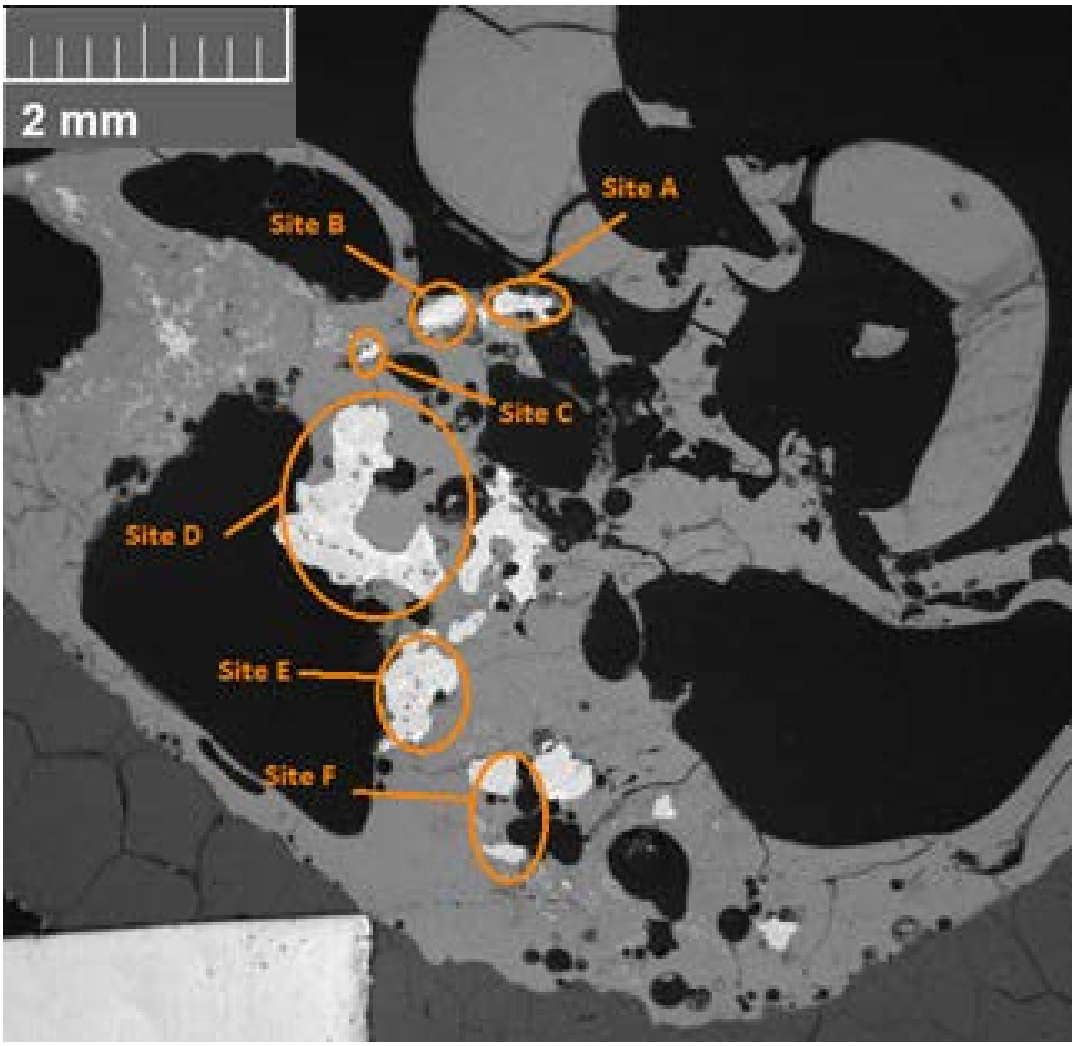

Figure 46. EDS Analysis sites

The results of PCB samples show that the structure of the sample does melt gradually between 1 to 5 minutes. After 5 minutes the structure seems to be nearly completely broken down, but it is possible that there is some error in the results due to inspecting only single cross-sections. The melting behavior described using lumped capacitance method in chapter 4.2. supports this timeframe, although the difference in thermal properties of plastic fraction compared to metal and ceramic fraction needs more specific consideration.

When considering the melting time and differences in fraction melting behavior inside an operational copper furnace, the 5 minutes melting time seems beneficial. The important factor to the process is how the molten metal alloy droplets moves through the slag layer to the bottom of the furnace.

Copper mixes with other metals to form alloy droplets. The composition of these droplets varies according to position and proximity to the PCB piece. These droplets contain copper, nickel, lead, tin and minor traces of gold and silver. Copper has the largest volume and thus forms the base matrix. Unreacted metallic iron from the slag mixture is mixed with these droplets from. Minor metals form small droplets inside the copper matrix. This can clearly be seen from figure 47 (120 s PCB sample, site C). This behavior can be attributed to the fact, that platinum group metals (like platinum and palladium) have high melting points, and thus they may exist in solid state inside the liquid copper alloy droplet. Another reason may be the quenching, which, although rapid, is not instantaneous and thus allows some time for possible minor element segregation. This platinum group metal segregation has been reported by Avarmaa et al. in copper matte – iron silicate slag system [49].

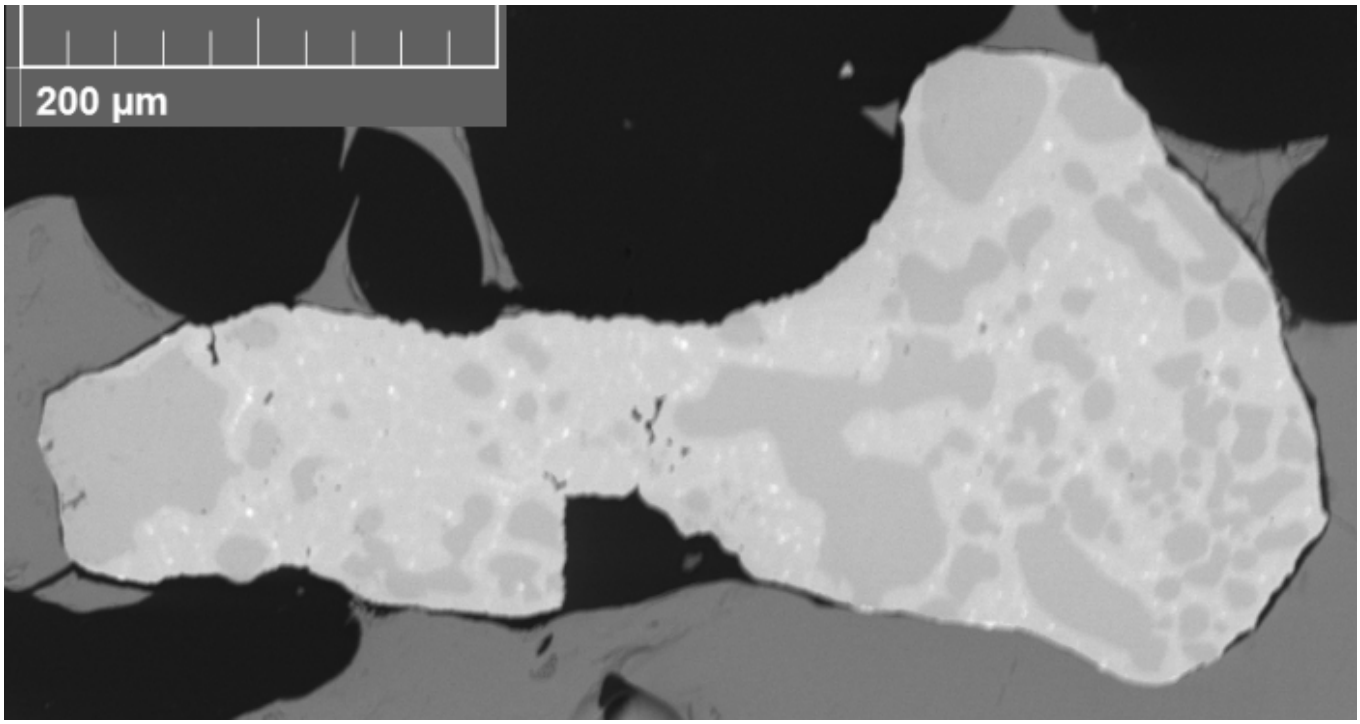

Figure 47. 120 second PCB sample, site C

The metal droplets do not dissolve in the slag but traverse through it. Given enough time, the droplets appear to settle at the bottom of the silica crucible, due to differences in densities between the metals alloys and slag. This is the same principle that happens in a flash smelting furnace settler.

6.2. Synthetic sample results

Figures 48 and 49 show the 25 seconds synthetic samples. The synthetic sample has stayed on top of the molten slag and has melted more thoroughly than the PCB sample at same time interval. Molten metal droplets have started to mix into the slag close to the main alloy area. The alloy droplet is located near upper-left corner of the crucible.

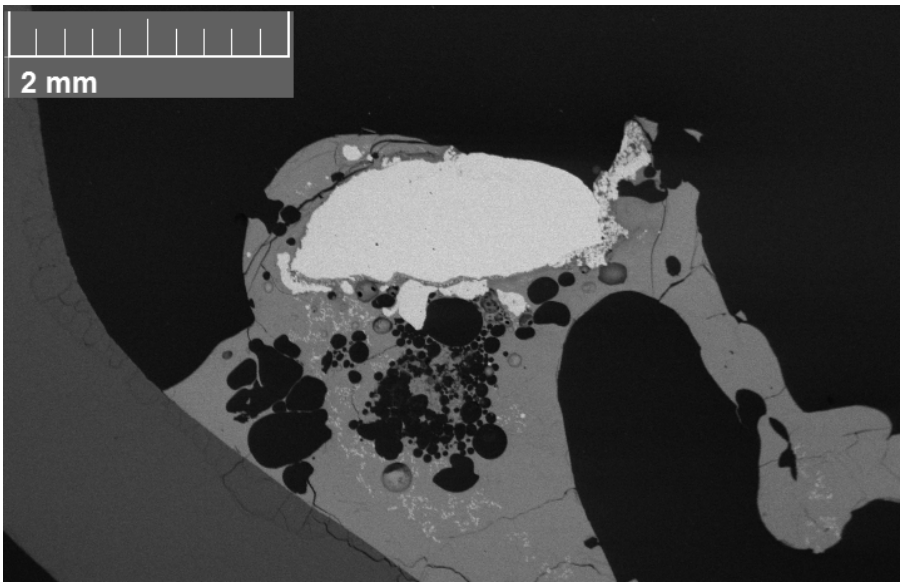

Figure 48. 25 seconds synthetic sample overview

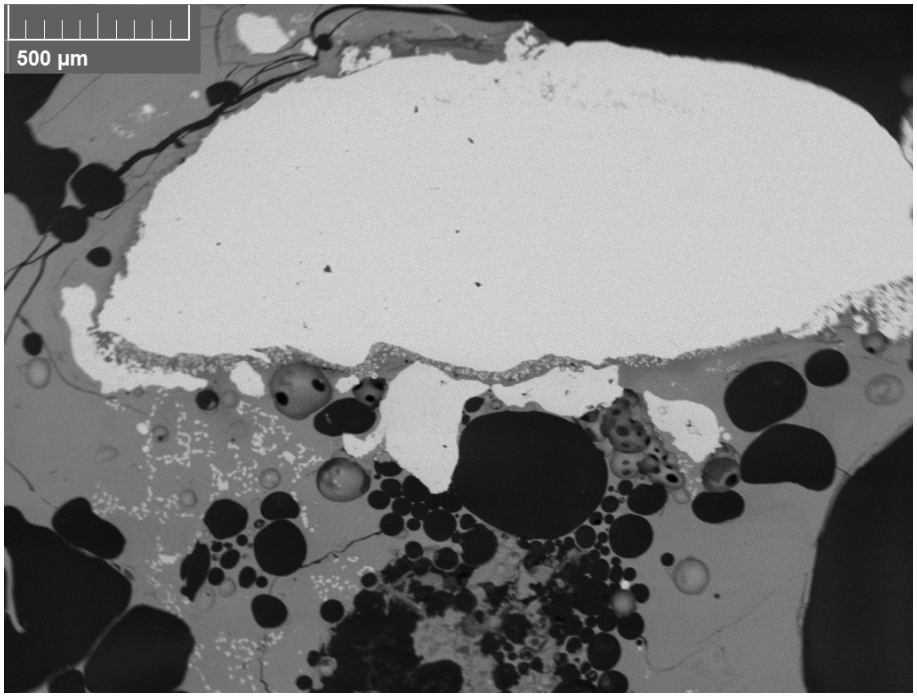

Figure 49. Sample site

The 60 seconds synthetic sample looks similar to the 25 seconds sample. The figure 50 shows, that the sample droplet seems thoroughly molten and has mixed to slag from outer layers.

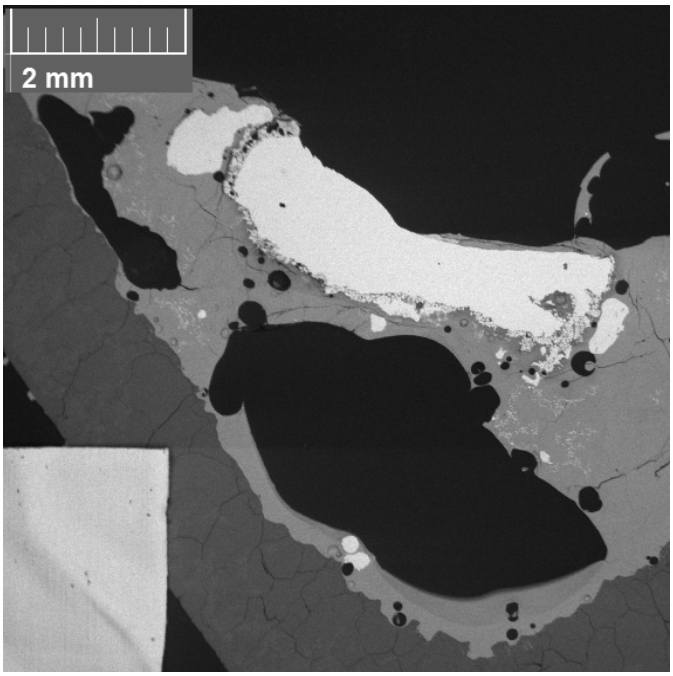

Figure 50. 60 s synthetic sample overview

Figure 51 shows an overview of the 120 second synthetic sample. The sample has formed a sizeable droplet in the middle of the sample and to the right-hand wall of the crucible.

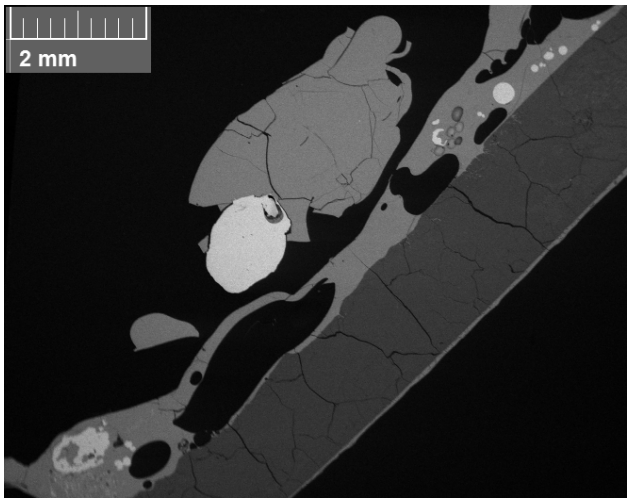

Figure 51. 120 seconds synthetic sample overview

Figure 52 is an overview of the 300-second synthetic sample. The sample droplet has traversed through slag and is almost entirely settled at the bottom of the crucible. Severe slag penetration through the crucible is also visible.

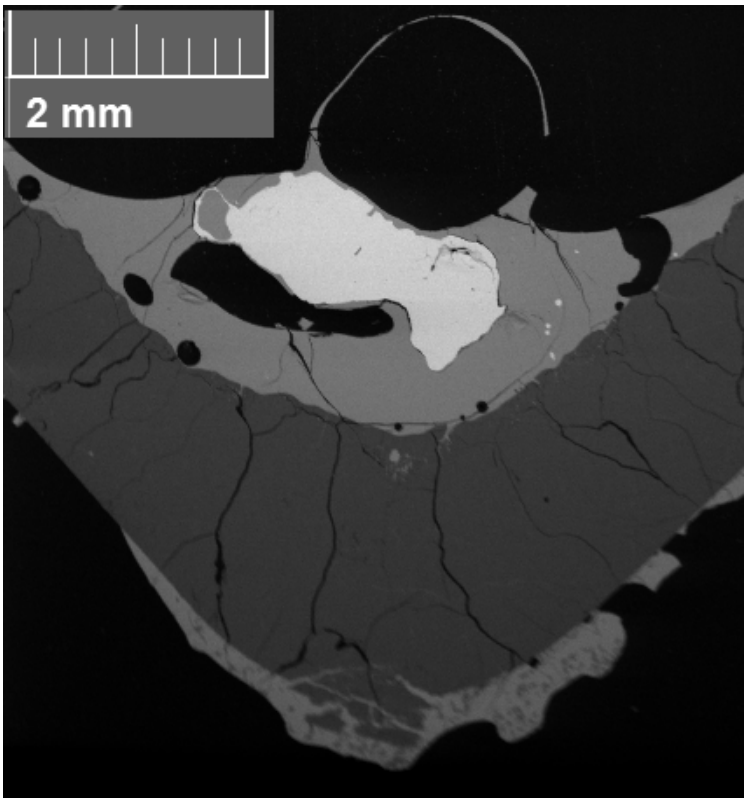

Figure 52. Overview of 300 second synthetic sample

6.3. Pyrolysis of plastic fraction

The plastic fraction was not found in the EDS analyses. However, some black, charred like residue was observed to exit the furnace when the gas seal was opened for quenching of PCB samples. This black residue did not occur during the quenching of synthetic samples. Figure 53 is a still shot from a video clip showing the black residue exiting the furnace due to the gas flow.

Figure 53. Black residue floating in quenching vessel

7. Conclusions

The recent change in metal concentrations, especially regarding copper, gold and silver, raises the question how the overall PCB composition changes and how it affects the process used for recycling. Due to this, the research studying secondary materials processing is important as the amount of scrap materials is certain to increase and the amount of primary materials to decrease in near future. In addition, the composition, structure and change in composition over recent decades was reviewed.

The behavior of PCB pieces was examined using silica crucibles, which were suspended in a vertical tube furnace. The pieces were dropped on top of molten slag inside crucible, and then given time to melt or react between time intervals of 25 seconds, 60 seconds, 120 seconds and 300 seconds. After each time interval, the crucible was quenched in ice water bath. The samples were then analyzed using SEM and EDS.

The key research questions were: How the PCB piece behaved in molten slag as a function of time, how long did it take for the piece to melt, where the resulting metal, polymer and ceramic fractions ended up and in what form.

When WPCB pieces are dropped on top of fayalite slag under inert atmosphere and at 1350 ° C, they will submerge into the slag and start to melt gradually. The melting time was between 2-5 minutes. This corresponded with the results calculated in the theoretical part, chapter 4. The most abundant metal in WPCB scrap was copper, followed by base metals of lead, tin and nickel plus gold and silver as precious metals. All these metals were identified in metal droplets found in WPCB containing samples (in EDS analyses). The metallic fraction of WPCB's formed droplets that tended to settle towards the bottom of the silica crucible. This was due to differences between densities of slag and metals. This was the optimal result for practical purposes. The ceramic fraction was difficult to distinguish, but it is most likely mixed with the slag phase. Plastic fraction experienced pyrolysis and formed solid, carbon-based compound, liquid oils or gases. The additives in plastic fraction, mainly halogenic fire retardants and possible carcinogenic compounds, are most likely to cause problems in industrial scale.

For future work, first the insertion of PCB material directly into the molten slag could be studied as opposed to dropping the material from above. This would enable a systematic experimental series investigating if the thermal conditions inside slag affects the melting and possible reactions of WPCB when compared to the results of this thesis. Another point of interest would be the distance traveled in the slag layer and how the direct insertion affects the molten PCB materials descent through. Second, the source and final location of precious metals (gold and silver) should be revised further. As this thesis only inspected the base structure of PCB's and especially gold is more often found in connectors and components on top of the base structure. Third interest could be to study variation in sample size. As this thesis only focused on one size of samples, assessing the effect of particle size could give beneficial information on melting and other operational data, such as feeding of material into an industrial process like FS furnace. Finally, the method of analysis used in this thesis could be developed further into a three-dimensional analysis, such as X-ray computed microtomography, instead of cross-sectional analysis. This would give a better understanding of the size distribution and location of the metal droplets in the slag.

References

1. Ghosh B, Ghosh M, Parhi P, Mukherjee P, Mishra B. Waste printed circuit boards recycling: An extensive assessment of current status. *J Clean Prod*. 2015;94:5-19.

2. Khaliq A, Rhamdhani MA, Brooks G, Masood S. Metal extraction processes for electronic waste and existing industrial routes: A review and australian perspective. *Resources*. 2014;3(1):152-179.

3. Guntororo PI. *Experimental investigation of matte-slag interactions in copper flash smelting.* Aalto University, School of Chemical Technology; 2017.

4. Kojo IV, Jokilaakso A, Hanniala P. Flash smelting and converting furnaces: A 50 year retrospect. *JOM*. 2000;52(2):57-61.

5. LI X, XIAO T. Production enhancement and operation parameter's optimization of the flash smelting furnace based on numerical simulation. Third international conference on CFD in the minerals and process industries CSIRO, Melbourne, Australia . 2003:155.

6. Taskinen P, Kolhinen T, Anjala Y. The influence of reaction shaft conditions on the behaviour of impurities in flash smelting and direct blister smelting. Outotec Research Oy. Pori, Finland.

7. Vaarno J, Jarvi J, Ahokainen T, Laurila T, Taskinen P. Development of a mathematical model of flash smelting and converting processes. Third Internatianal Conference on CFD in the Minerals and Process Industries, Melbourne. 2003:147-154.

8. Davenport WG, King MJ, Schlesinger ME, Biswas AK. *Extractive metallurgy of copper.* 4 th ed. Elsevier; 2002.

9. Beychok M. Schematic diagram of an outukumpu flash smelter and its waste heat boiler. http://en.citizendium.org/wiki/File:Flash_Smelter_Waste_Heat_Boiler.png. Updated 2009. Accessed 7/5, 2018.

10. Seetharaman S, McLean A, Guthrie R, Sridhar S. *Treatise on process metallurgy.* Vol 2. Elsevier; 2013.

11. Li J, Shrivastava P, Gao Z, Zhang H. Printed circuit board recycling: A state-of-the-art survey. *IEEE transactions on electronics packaging manufacturing*. 2004;27(1):33-42.

12. Scarlett JA. *An introduction to printed circuit board technology.* Ayr, Scotland: Electrochemical Publications Limited; 1984.

13. Sparkfun. PCB basics. https://learn.sparkfun.com/tutorials/pcb-basics. Accessed 01/22, 2018.

14. Rocchetti L, Amato A, Beolchini F. Printed circuit board recycling: A patent review. *J Clean Prod*. 2018.

15. Li J, Zeng X. Ch 13, recycling printed circuit boards. In: *WEEE handbook.* Tsinghua: Woodhead Publishing limited; 2012:287-311.

16. Flandinet L, Tedjar F, Ghetta V, Fouletier J. Metals recovering from waste printed circuit boards (WPCBs) using molten salts. *J Hazard Mater*. 2012;213:485-490.

17. Guo J, Guo J, Xu Z. Recycling of non-metallic fractions from waste printed circuit boards: A review. *J Hazard Mater*. 2009;168(2-3):567-590.

18. Zhang S, Forssberg E. Mechanical separation-oriented characterization of electronic scrap. *Resour Conserv Recycling*. 1997;21(4):247-269.

19. Iji M, Yokoyama S. Recycling of printed wiring boards with mounted electronic components. *Circuit World*. 1997;23(3):10-15.

20. Zhao Y, Wen X, Li B, Tao D. Recovery of copper from waste printed circuit boards. *Miner Metall Process*. 2004;21(2):99-102.

21. Kim B, Lee J, Seo S, Park Y, Sohn HY. A process for extracting precious metals from spent printed circuit boards and automobile catalysts. *JOM*. 2004;56(12):55-58.

22. Shuey S, Vildal E, Taylor P. Pyrometallurgical processing of electronic waste. SME Annual Meeting. 2006:06-037.

23. Kogan V. Process for the recovery of precious metals scrap by means of hydrometallurgical technique. *Patent Application, WO*. 2006;6006(013568):A3.

24. Ogunniyi I, Vermaak MKG, Groot D. Chemical composition and liberation characterization of printed circuit board comminution fines for beneficiation investigations. *Waste Manage*. 2009;29(7):2140-2146.

25. Hageluken C. Improving metal returns and eco-efficiency in electronics recycling-a holistic approach for interface optimisation between pre-processing and integrated metals smelting and refining. Electronics and the Environment, 2006. Proceedings of the 2006 IEEE International Symposium on. IEEE. 2006:218-223.

26. Park YJ, Fray DJ. Recovery of high purity precious metals from printed circuit boards. *J Hazard Mater*. 2009;164(2-3):1152-1158.

27. Yu J, Williams E, Ju M. Review and prospects of recycling methods for waste printed circuit boards. Sustainable Systems and Technology, 2009. ISSST'09. IEEE International Symposium on. IEEE, 2009:1-5.

28. Hino T, Agawa R, Moriya Y, Nishida M, Tsugita Y, Araki T. Techniques to separate metal from waste printed circuit boards from discarded personal computers. *Journal of material cycles and waste management*. 2009;11(1):42-54.

29. Wang W, Sun J, Ma C, et al. Study on the gasification and melting characteristics of electronic waste. . 2009;3:574-577.

30. Reuter M, Hudson C, van Schaik A, Heiskanen K, Meskers C, Hagelüken C. UNEP (2013) metal recycling: Opportunities, limits, infrastructure, a report of the working group on the global metal flows to the international resource panel. *United Nations Environmental Programme UNEP (....Paris.Retrieved from http://scholar.google.com/scholar*. 2013.

31. Luda MP. Recycling of printed circuit boards. In: *Integrated waste management-volume II.* InTech; 2011.

32. Kavander K. Kullan syanidivapaa liuotus piirikorttiromusta. Masters thesis. Aalto University, Espoo, Finland. 2016. https://aaltodoc.aalto.fi/handle/123456789/20940

33. Elomaa H, Seisko S, Junnila T, et al. The effect of the redox potential of aqua regia and temperature on the au, cu, and fe dissolution from WPCBs. *Recycling*. 2017;2(3):14.

34. Theo L. Integrated recycling of non-ferrous metals at boliden ltd. ronnskar smelter. Electronics and the Environment, 1998. ISEE-1998. Proceedings of the 1998 IEEE International Symposium on. Ieee. pp:42-47.

35. Yamane LH, de Moraes VT, Espinosa DCR, Tenório JAS. Recycling of WEEE: Characterization of spent printed circuit boards from mobile phones and computers. *Waste Manage*. 2011;31(12):2553-2558.

36. Oguchi M, Sakanakura H, Terazono A, Takigami H. Fate of metals contained in waste electrical and electronic equipment in a municipal waste treatment process. *Waste Manage*. 2012;32(1):96-103.

37. Jascisak J, Havlik T, Turek P, Klimko J. Quo vadis recycling. Conference proceedings. 2017(first):142.

38. Havlik T, Orac D, Berwanger M, Maul A. The effect of mechanical–physical pretreatment on hydrometallurgical extraction of copper and tin in residue from printed circuit boards from used consumer equipment. *Minerals Eng*. 2014;65:163-171.

39. Hadi P, Ning C, Ouyang W, Lin CSK, Hui C, McKay G. Conversion of an aluminosilicate-based waste material to high-value efficient adsorbent. *Chem Eng J*. 2014;256:415-420.

40. Maurell-Lopez S, Gül S, Friedrich B, et al. Metallurgical fundamentals for an autother-mal melting of WEEE in a top blown rotary converter. Proceedings of EMC. 2011:1.

41. Goodship V, Stevels A. *Waste electrical and electronic equipment (WEEE) handbook.* Elsevier; 2012.

42. Balde CP, Wang F, Kuehr R, Huisman J. The global e-waste monitor 2014: Quantities, flows and resources. United Nations University, International Telecommunication Union, and International Solid Waste Association. 2015.

43. Statista 2018. Forecast of electronic waste generated worldwide from 2010 to 2018 (in million metric tons). https://www.statista.com/statistics/499891/projection-ewaste-generation-worldwide/. Updated 2018. Accessed 5/23, 2018.

44. Klimko J, Orac D, Havlik T, Jascisak J. Gold in personal computers. Quo Vadis Recycling. Conference proceedings. 2017(first):176-177-181.

45. Lu Y, Xu Z. Precious metals recovery from waste printed circuit boards: A review for current status and perspective. *Resour Conserv Recycling*. 2016;113:28-39.

46. Petter P, Veit HM, Bernardes AM. Evaluation of gold and silver leaching from printed circuit board of cellphones. *Waste Manage*. 2014;34(2):475-482.

47. Yamane LH, de Moraes VT, Espinosa DCR, Tenório JAS. Recycling of WEEE: Characterization of spent printed circuit boards from mobile phones and computers. *Waste Manage*. 2011;31(12):2553-2558.

48. Philpott J. Palladium plating of printed circuits. *Platinum Metals Review*. 1960;4(1):12-14.

49. Avarmaa K, Johto H, Taskinen P. Distribution of precious metals (ag, au, pd, pt, and rh) between copper matte and iron silicate slag. *Metallurgical and Materials Transactions B*. 2016;47(1):244-255.

50. Avarmaa K, O'Brien H, Taskinen P. Equilibria of gold and silver between molten copper and FeO x-SiO 2-al 2 O 3 slag in WEEE smelting at 1300° C. Advances in Molten Slags, Fluxes, and Salts: Proceedings of the 10th International Conference on Molten Slags, Fluxes and Salts 2016. Springer, Cham. 2016:193-202.

51. Avarmaa K, O'Brien H, Klemettinen L, Taskien P. Precious metals recoveries through secondary copper smelting. *Journal of Cleaner Production*.

52. Bizzo W, Figueiredo R, de Andrade V. Characterization of printed circuit boards for metal and energy recovery after milling and mechanical separation. *Materials*. 2014;7(4555-4566).

53. Incropera FP, Dewitt DP, Bergman TL, Lavine AS. *Principles of heat and mass transfer.* 7 th edition ed. Singapore: John Wiley & Sons Singapore Pte. Ltd; 2013.

54. Callister WD, Rethwisch DG. *Fundamentals of materials science and engineering.* 5 th edition ed. Singapore: John Wiley & sons; 2016.

55. The Engineering Toolbox. Specific heat of common substances. https://www.engineeringtoolbox.com/specific-heat-capacity-d_391.html. Accessed 30.1.2018, 2018.

56. AZO Materials. Magnesia - magnesium oxide (MgO) properties & applications. https://www.azom.com/properties.aspx?ArticleID=54. Accessed 6/21, 2018.

57. Landolt H, Börnstein R. Calcium oxide (CaO) debye temperature, heat capacity, density, melting and boiling points, hardness. In: Madelung O, Rössler U, Schulz M, eds. *Group III condensed matter book series (volume 41B).* Berlin, Heidelberg: Springer; 1999. https://doi-org.libproxy.aalto.fi/10.1007/b71137.

58. Landolt H, Börnstein R. Calcium oxide (CaO) electrical and thermal transport properties. In: Madelung O, Rössler U, Schulz M, eds. *Group III condensed matter book series (volume 41B).* Berlin, Heidelberg: Springer; 1999. https://doi.org/10.1007/10681719_232.

59. Osswald TA, Menges G. *Material science of polymers for engineers.* 3 rd edition ed. Munich, Germany: Hanser Publishers; 2012.

60. The Engineering Toolbox. Metals - melting temperatures. https://www.engineeringtoolbox.com/melting-temperature-metals-d_860.html. Accessed 7/19, 2018.

61. Hlavac J. Melting temperatures of refractory oxides: Part I. *Pure and Applied Chemistry*. 1982;54(3):681-688.

62. Polymer properties database. Melting points of polymers. http://polymerdatabase.com/polymer%20physics/Polymer%20Tm%20C.html. Accessed 7/19, 2018.

63. Diaz F, Florez S, Friedrich B. High recovery recycling route of WEEE: The potential of pyrolysis. . 2015:1.

64. Yang X, Sun L, Xiang J, Hu S, Su S. Pyrolysis and dehalogenation of plastics from waste electrical and electronic equipment (WEEE): A review. *Waste Manage*. 2013;33(2):462-473.

65. Li J, Zheng B, He Y, et al. Antimony contamination, consequences and removal techniques: A review. *Ecotoxicol Environ Saf*. 2018;156:125-134.

66. M. K, Vartiainen A. Kuonat kuparin ja nikkelin liekkisulatuksessa. In: *Kuonametallurgia.* Helsinki: INSKO; 1993.

67. TESCAN. Mira3. https://www.tescan.com/en-us/technology/sem/mira3. Accessed 7/14, 2018.

68. TESCAN. Sem. https://www.tescan.com/en-us/technology/sem. Accessed 7/14, 2018.

69. Goldstein J, Newbury. *Scanning electron microscopy and X-ray microanalysis.* Springer US; 2003.

Appendix A

25 s PCB Sample, EDS sites (A-G) and results

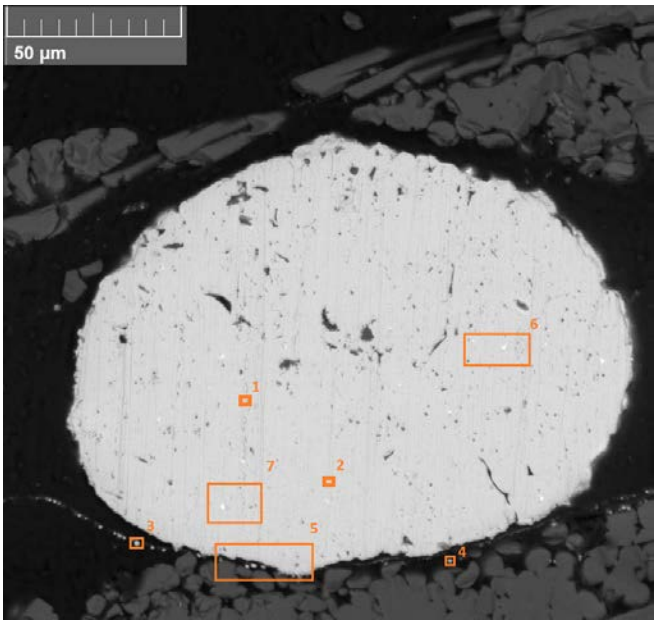

Figure 54. Site A and EDS data points

Point of analysis	***O-K***	***Mg-K***	***Al-K***	***Si-K***	***S-K***	***Cl-K***	***Ca-K***	***Ti-K***	***Cr-K***	***Fe-K***
1	0.30	0.00	0.02	0.46	0.00		0.04	0.00	0.04	0.07
2	0.35	0.00	0.04	0.51	0.05		0.07	0.02	0.00	0.04
3	0.00	0.00	0.05	0.64	0.03	0.09	0.21	0.00	0.02	0.15
4	3.62	0.00	0.77	2.46	0.05	0.15	0.77	0.00	0.00	0.08
5	14.47	0.45	3.89	12.40	0.00		5.35	0.27	0.22	0.09
6	0.39	0.00	0.20	0.11	0.00		0.05	0.03	0.00	0.02
7	0.52	0.00	0.18	0.00	0.15		0.09	0.00	0.05	0.01
	Ni-K	**Cu-K**	**Zn-K**	**Ge-L**	**Se-L**	**Zr-L**	**Mo-L**	**Ag-L**	**Cd-L**	**Sn-L**
1	1.23	94.48	0.00	0.41	0.04	0.45		0.03	0.05	0.13
2	1.38	95.59	0.00	0.51	0.11	0.46		0.00	0.00	0.14
3	1.00	73.06	0.27	2.05	0.13	0.25		0.01	0.00	0.00
4	1.00	65.73	0.28	2.03	0.20	0.06		0.04	0.04	0.00
5	0.56	36.92	0.00	0.70	0.44	0.00	0.39	0.00	0.00	0.00
6	1.08	95.93	0.00	0.46	0.34	0.00		0.01	0.00	0.12
7	1.23	95.71	0.00	0.00	0.00	0.00	0.00	0.00	0.00	0.22
	Sb-L	**Te-L**	**Re-M**	**Au-M**	**Pb-M**					
1	0.03	0.05	3.80	0.00	0.10					
2	0.00	0.05	4.62	0.11	0.01					
3	0.00	0.06	2.76	0.05	0.10					
4	0.00	0.46	2.14	0.00	0.12					
5	0.00	5.30	0.93	0.00	0.00					
6	0.00	0.00		0.00	0.77					
7	0.08	0.00		0.00	0.96					

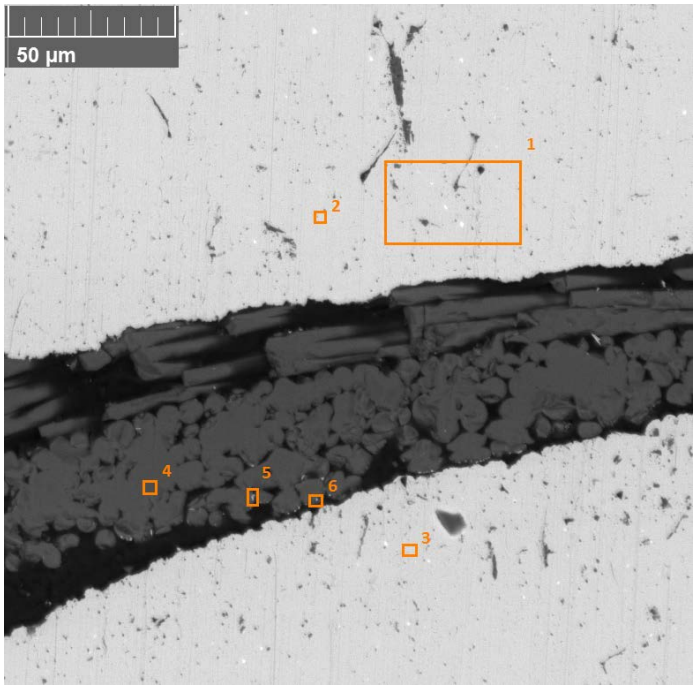

Figure 55. Site B and EDS data points

Point of analysis	***O-K***	***Mg-K***	***Al-K***	***Si-K***	***K-K***	***Ca-K***	***Ti-K***	***Cr-K***	***Fe-K***	***Ni-K***
1	0.69	0.75	0.45	0.07	0.01	0.00	0.00	0.02	0.00	0.15
2	0.37	0.48	0.21	0.00	0.00	0.00	0.00	0.02	0.01	0.18
3	0.52	0.57	0.19	0.00	0.00	0.07	0.00	0.02	0.00	0.05
4	40.73	0.72	7.16	25.22	0.27	13.20	0.57	0.50	0.14	0.07
5	9.72	0.44	3.43	11.03	0.00	4.20	0.37	0.04	0.06	0.05
6	19.43	0.15	5.48	18.99	0.00	8.21	0.62	0.21	0.10	0.06
	Cu-K	**Zn-K**	**Ge-L**	**Se-L**	**Ag-L**	**Cd-L**	**Sn-L**	**Sb-L**	**Te-L**	**Tl-M**
1	94.20	0.34	0.07	0.53	0.04	0.03	0.12	0.13	0.01	
2	97.66	0.34	0.00	0.31	0.00	0.00	0.00	0.02	0.03	
3	97.96	0.25	0.00	0.34	0.00	0.06	0.09	0.00	0.00	
4	0.83	0.07	0.00	0.00	0.09	0.71	2.84	0.00	15.54	
5	56.13	0.38	0.97	0.62	0.13	0.07	0.00	0.00	5.02	0.41
6	32.45	0.32	0.94	0.47	0.18	0.00	0.00	0.00	9.63	0.81

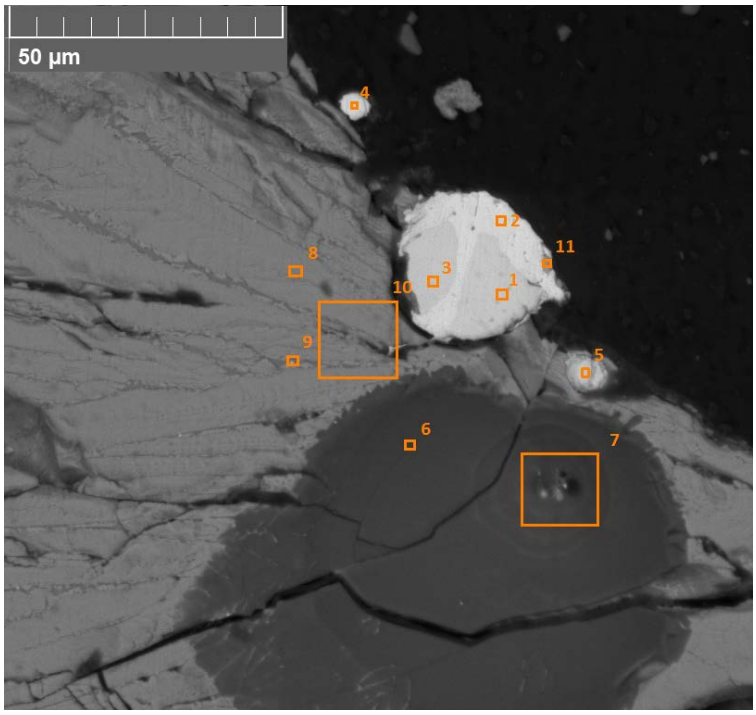

Figure 56. Site C and EDS data points

Point of analysis	***O-K***	***Mg-K***	***Al-K***	***Si-K***	***P-K***	***S-K***	***Ca-K***	***Ti-K***	***Fe-K***	***Ni-K***
1	0.00	0.54	0.02	0.07	0.06	0.02	0.07	0.00	85.44	1.79
2	0.45	0.00	0.05	0.54		0.00	0.07	0.01	3.99	0.07
3	0.00	0.46	0.03	0.14		0.00	0.07	0.00	87.46	0.29
4	0.57	0.00	0.08	0.88		0.00	0.14	0.02	2.31	0.00
5	0.35	0.46	0.04	0.25		0.05	0.11	0.00	82.78	0.71
6	57.26	0.00	0.00	46.88		0.00	0.00	0.02	1.27	0.03
7	52.82	0.00	0.00	42.11		0.00	0.00	0.02	3.11	0.05
8	27.16	0.29	0.10	16.86		0.00	0.38	0.00	45.14	0.00
9	28.09	0.00	0.81	15.91		2.19	2.08	0.29	30.08	0.00
10	26.66	0.00	0.19	15.84		0.00	0.33	0.02	42.47	0.00
11	13.25	0.53	0.10	6.12	0.15	0.90	0.28	0.00	46.58	0.00
	Cu-K	**Zn-K**	**Ge-L**	**Se-L**	**Zr-L**	**Mo-L**	**Sn-L**	**Sb-L**	**Te-L**	**Ta-L**
1	8.48	0.13	0.23	0.38	0.02		0.00	0.00	0.00	
2	91.44	0.27	0.28	0.00	0.00		0.18	0.00	0.00	
3	8.28	0.02	0.00	0.35	0.00	0.29	0.04	0.03	0.04	
4	91.97	0.11	0.38	0.00	0.00		0.37	0.00	0.00	
5	10.29	0.03	0.00	0.27	0.03		0.07	0.07	0.00	
6	0.10	0.03	0.00	0.00	0.00	2.26	6.29	2.43	0.27	
7	1.30	0.00	0.00	0.00	0.00	1.80	5.02	1.81	0.24	0.21
8	0.00	0.00	0.00	0.01	0.35		0.37	0.00	0.00	4.38
9	16.13	0.81	0.30	0.24	0.00		0.00	0.00	3.19	
10	2.08	0.00	0.20	0.00	0.00	0.46	0.00	0.00	0.30	2.66
11	11.25	0.06	0.17	0.27	0.00	0.42	0.00	0.00	0.00	

	Os-M	Au-M	Hg-M	Tl-M	Pb-M
1		0.00			0.02
2	1.95	0.00			0.00
3		0.00			0.12
4	3.25	0.00			0.07
5		0.00			0.00
6		0.00			0.00
7		0.00			0.00
8		0.00	0.92	0.85	0.00
9		0.25			1.24
10		0.00			0.00
11		0.13			0.00

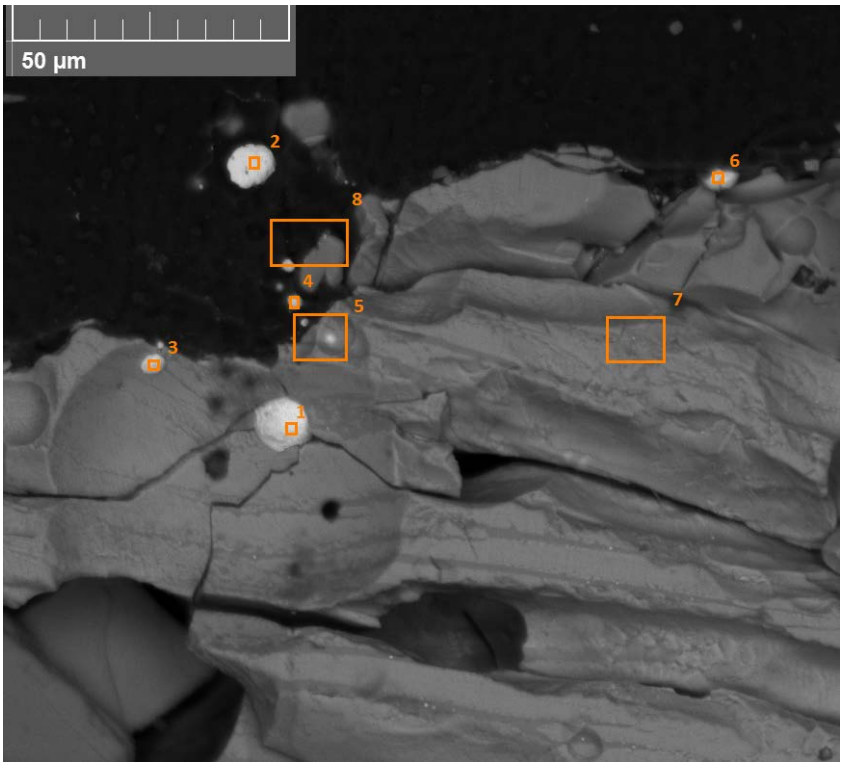

Figure 57. Site D and EDS data points

Point of analysis	*O-K*	*Mg-K*	*Al-K*	*Si-K*	*S-K*	*Ca-K*	*Ti-K*	*Cr-K*	*Fe-K*	*Ni-K*
1	1.89	0.00	0.10	1.31	0.15	0.20	0.00	0.00	13.37	0.14
2	0.40	0.00	0.07	0.79	0.00	0.14	0.00	0.01	1.32	0.00
3	2.87	0.50	0.22	1.15	0.00	0.26	0.01	0.00	3.63	0.89
4	1.83	0.00	0.11	2.00	0.00	0.23	0.03	0.00	2.49	1.31
5	20.74	0.00	0.69	12.01	0.00	1.41	0.25	0.02	24.77	0.04
6	1.68	0.32	0.30	0.98	0.29	0.62	0.00	0.01	2.52	0.07
7	22.32	0.00	1.06	16.29	0.00	2.72	0.36	0.12	31.59	0.03
8	13.32	0.57	1.71	7.48	0.00	2.62	0.32	0.11	3.35	0.03

	Cu-K	Zn-K	Ge-L	Se-L	Sr-L	Mo-L	Ag-L	Sn-L	Te-L	Ba-L
1	86.33	0.19	0.55	0.00			0.00	0.12	0.00	
2	93.35	0.27	0.24	0.00			0.00	0.21	0.00	
3	89.95	0.25	0.90	0.60	2.93		0.09	0.19	0.00	
4	83.96	0.31	0.93	0.00			0.05	0.33	0.00	
5	7.26	0.00	0.18	0.00			0.00	0.00	1.75	0.14
6	91.44	0.29	0.73	0.39	2.08		0.00	0.21	0.00	
7	0.05	0.00	0.00	0.00		0.34	0.00	0.00	2.97	0.38
8	4.65	0.00	0.10	0.16			0.00	0.00	3.58	0.96

	Ta-L	Os-M	Tl-M	Pb-M
1		2.62		0.17
2		2.12		0.00
3		1.34		0.00
4		2.12		0.05
5	0.48		0.74	0.00
6		0.87		0.00
7	2.85			0.00
8			0.56	0.00

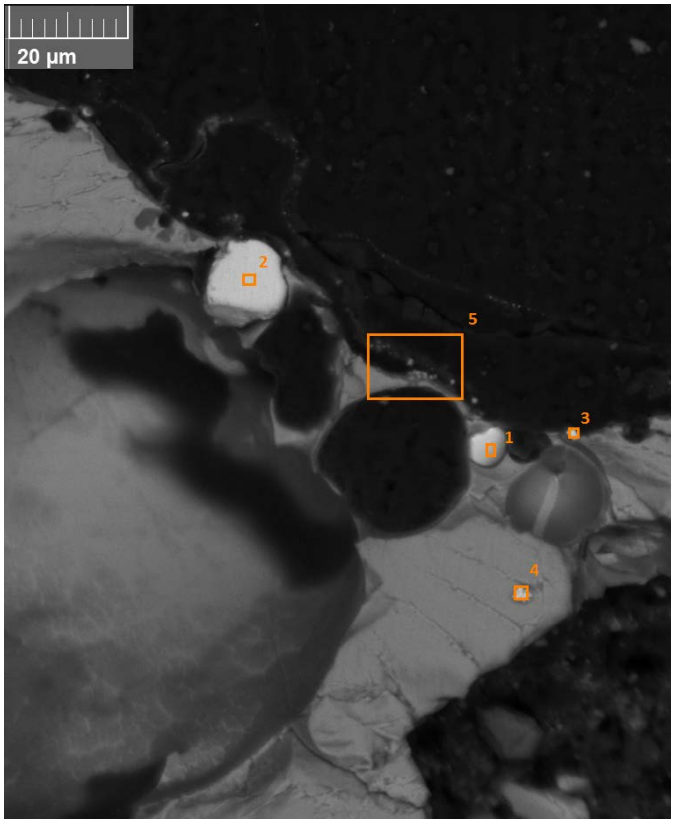

Figure 58. Site E and EDS data points

Point of analysis		***O-K***	***Mg-K***	***Al-K***	***Si-K***	***S-K***	***Cl-K***	***K-K***	***Ca-K***	***Fe-K***	***Ni-K***
	1	1.17	0.69	0.03	0.72	0.02		0.00	0.14	86.69	0.22
	2	0.00	0.64	0.03	0.09	0.00		0.01	0.16	92.40	0.19
	3	8.09	1.33	0.00	3.56	0.00		0.03	0.36	6.66	0.00
	4	4.86	3.06	0.00	2.20	0.00		0.04	0.31	6.12	0.00
	5	30.54	0.12	0.25	17.36	0.00	0.80	0.00	0.68	39.69	0.00
		Cu-K	**Zn-K**	**As-L**	**Se-L**	**Zr-L**	**Ag-L**	**Cd-L**	**Sn-L**	**Sb-L**	**Te-L**
	1	3.90	0.00		0.47	0.09	0.00	0.00	0.00	0.00	0.00
	2	2.91	0.00		0.41	0.00	0.02	0.06	0.13	0.04	0.00
	3	54.68	0.18	24.53	2.16	0.00	0.22	0.18	0.14	0.59	0.08
	4	55.23	0.01	18.37	1.60	0.00	0.15	0.13	0.04	0.36	0.00
	5	1.06	0.18		0.42	1.25	0.00	0.00	0.38	0.00	0.15
		Ta-L	**Hg-M**	**Tl-M**	**Pb-M**						
	1				0.07						
	2				0.00						
	3		1.05		0.00						
	4				0.00						
	5	3.26		2.92	0.00						

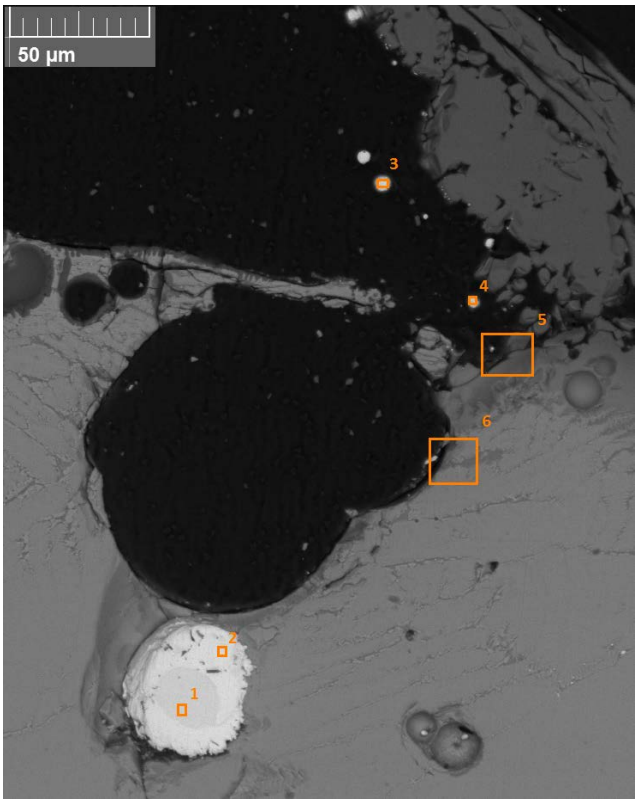

Figure 59. Site F and EDS data points

Point of analysis	***O-K***	***Mg-K***	***Al-K***	***Si-K***	***P-K***	***S-K***	***Cl-K***	***Ca-K***	***Ti-K***	***Cr-K***
1	0.31	0.25	0.01	0.07	0.12	0.01		0.00	0.00	0.00
2	0.55	0.00	0.05	0.00		0.00		0.00	0.01	0.01
3	0.27	0.00	0.04	0.73		0.00		0.32	0.00	0.00
4	0.00	0.45	0.14	0.00		0.10		0.35	0.00	0.01
5	23.16	0.00	3.21	12.33		0.00	0.13	4.72	0.37	0.22
6	28.46	0.87	0.28	14.79		0.00		1.17	0.00	0.04
	Fe-K	**Ni-K**	**Cu-K**	**Zn-K**	**Ge-L**	**Se-L**	**Ag-L**	**Cd-L**	**Sn-L**	**Sb-L**
1	66.31	11.82	19.79	0.06	0.00	0.19	0.04	0.03	0.00	0.09
2	14.90	4.73	78.14	0.04	0.22	0.00	0.00	0.10	0.19	0.01
3	2.92	6.08	87.37	0.00	0.19	0.00	0.00	0.06	0.21	0.00
4	2.90	5.16	82.16	0.20	0.72	0.25	0.01	0.00	0.28	0.00
5	8.55	0.12	1.39	0.00	0.00	0.00	0.00	0.00	0.00	0.00
6	34.43	0.01	0.38	0.00	0.00	0.30	0.00	0.00	0.00	0.00
	Te-L	**Ta-L**	**Os-M**	**Pt-M**	**Au-M**	**Hg-M**	**Tl-M**			
1	0.04			0.00	0.00					
2	0.03		0.00	0.00	0.00					
3	0.00		1.62	0.00	0.00					
4	0.15	0.54		0.00	0.84					
5	4.67	0.97		0.00	0.23		1.38			
6	0.80	3.93		0.83	0.00	1.36	1.12			

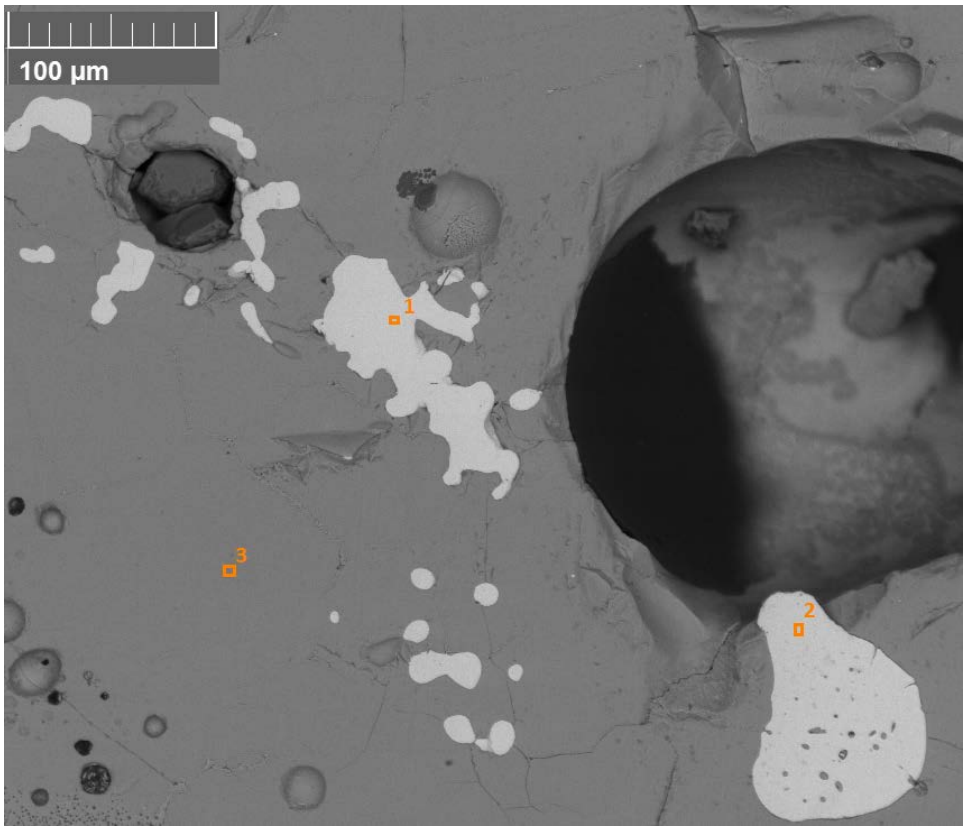

Figure 60. Site G and EDS data points

Point of analysis	***O-K***	***Mg-K***	***Al-K***	***Si-K***	***S-K***	***Fe-K***	***Ni-K***	***Cu-K***	***Se-L***	***Mo-L***
1	0.00	0.38	0.01	0.10	0.01	97.62	0.11	0.14	0.39	
2	0.00	0.41	0.03	0.09	0.01	97.93	2.00	0.00	0.38	
3	33.90	0.17	0.00	18.44	0.00	45.33	0.00	0.00	0.00	0.45
	Sn-L	**Sb-L**	**Ta-L**							
1	0.05	0.06								
2	0.10	0.10								
3	0.30	0.00	4.73							

Appendix B

60 s PCB sample, EDS sites (A-F) and results.

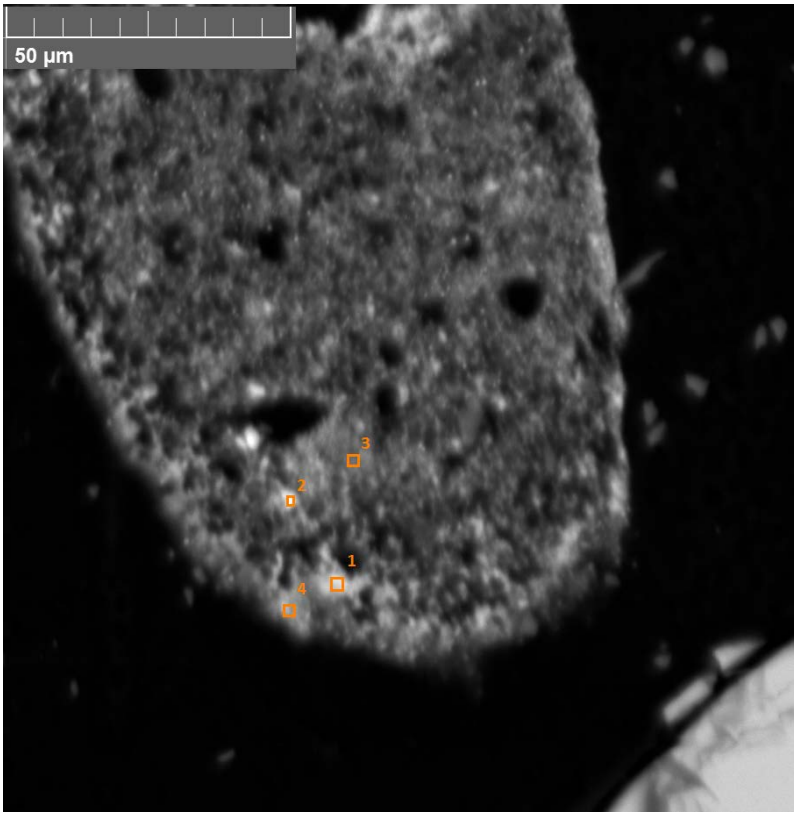

Figure 61. Site A and EDS data points

Site A looks similar to solid PCB structure. EDS analysis also suggests this.

Point of analysis	***O-K***	***Mg-K***	***Al-K***	***Si-K***	***S-K***	***Cl-K***	***Ca-K***	***Ti-K***	***Fe-K***	***Co-K***
1	24.78	0.00	0.72	7.95	0.00	0.08	0.00	27.24	1.54	0.18
2	11.81	0.00	1.27	11.55	0.00	0.13	0.32	1.14	0.53	
3	10.19	0.65	1.22	7.28	0.07	0.25	0.04	0.73	0.44	
4	10.98	0.25	1.08	9.20	0.13	0.14	0.23	1.00	0.46	
	Ni-K	**Cu-K**	**Zn-K**	**Ge-L**	**Se-L**	**Ag-L**	**Cd-L**	**Sn-L**	**Ba-L**	**Au-M**
1	0.05	0.67	0.00	0.13	0.08	0.27	0.15	0.07		0.91
2	0.05	0.44	0.04	0.35	0.19	0.11	0.00	0.00	30.84	0.00
3	0.04	0.50	0.00	0.00	0.33	0.10	0.04	0.00	13.17	0.00
4	0.00	0.29	0.00	0.13	0.17	0.00	0.00	0.00	19.51	0.00

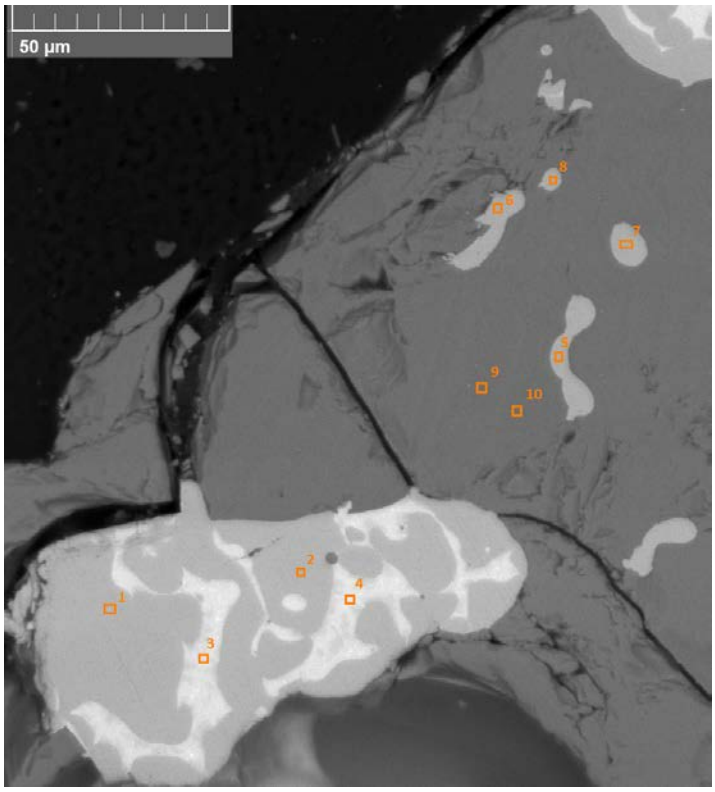

Figure 62. Site B and EDS data points

Point of analysis	***O-K***	***Mg-K***	***Si-K***	***Fe-K***	***Ni-K***	***Cu-K***	***Zn-K***	***Ge-L***	***Ag-L***	***Cd-L***
1	0.00	0.38	0.00	101.90	0.83	6.20	0.02	0.23	0.00	0.04
2	0.00	0.00	0.00	101.24	1.49	6.54	0.17	0.23	0.02	0.03
3	0.00	0.00	0.00	3.34	1.50	79.38	0.00	0.48	0.82	0.21
4	0.44	0.00	0.00	2.67	1.62	75.84	0.00	0.00	0.74	0.21
5	0.00	0.03	0.10	105.40	0.16	0.01	0.01	0.00	0.00	0.00
6	0.00	0.00	0.15	104.77	0.09	1.09	0.00	0.27	0.00	0.00
7	0.00	0.04	0.12	108.30	0.04	0.00	0.00	0.00	0.00	0.00
8	0.00	0.05	0.14	105.68	0.03	0.18	0.00	0.00	0.06	0.08
9	36.96	0.00	22.36	48.82	0.00	0.00	0.00	0.12	0.00	0.00
10	33.47	0.08	20.04	53.98	0.07	0.00	0.07	0.00	0.04	0.03
	Sn-L	**Pt-M**	**Au-M**	**Pb-M**						
1	0.28	0.02	0.00	0.00						
2	0.18	0.00	0.00	0.00						
3	28.97	0.00	0.11	0.52						
4	29.20	0.07	0.00	5.89						
5	0.32	0.00	0.01	0.00						
6	0.28	0.00	0.00	0.00						
7	0.32	0.00	0.00	0.00						
8	0.44	0.00	0.05	0.02						
9	0.00	0.00	0.00	0.00						
10	0.00	0.00	0.07	0.00						

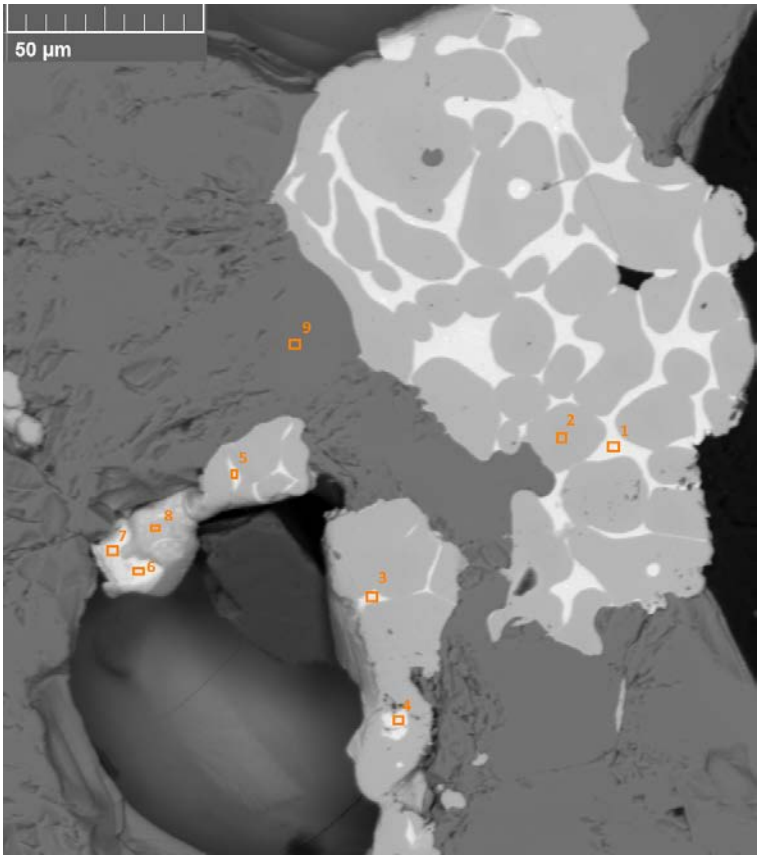

Figure 63. Site C and EDS data points

Point of analysis	***O-K***	***Si-K***	***Ca-K***	***Ti-K***	***Fe-K***	***Ni-K***	***Cu-K***	***Se-L***	***Br-L***	***Ag-L***
1	0.00	0.00	0.00	0.16	4.46	1.77	69.84	0.10		1.13
2	0.00	0.05	0.04	0.00	106.72	0.57	0.04	0.00		0.00
3	0.88	0.00	0.15	0.14	8.09	1.71	75.91	0.10		0.92
4	0.58	0.00	0.14	0.16	9.01	1.45	71.79	0.11		0.93
5	0.00	0.00	0.16	0.15	11.25	1.61	72.99	0.05		0.95
6	4.60	0.31	0.25	0.18	8.74	1.81	67.61	0.00		0.92
7	2.02	0.58	0.00	0.18	7.73	1.75	72.96	0.06		0.80
8	1.07	0.26	0.26	0.03	85.67	1.37	18.72	0.08	0.19	0.12
9	37.25	20.82	0.03	0.01	52.72	0.03	0.00	0.07		0.02

	Cd-L	**Sn-L**	**Sb-L**	**Te-L**	**Re-M**	**Au-M**	**Pb-M**
1	0.25	29.84	0.00	0.00	0.00	0.00	11.83
2	0.07	0.59	0.05	0.05	0.03	0.00	0.00
3	0.12	30.70	0.00	0.00	0.00	0.27	0.34
4	0.18	30.46	0.00	0.28	0.00	0.26	0.61
5	0.18	29.34	0.00	0.00	0.00	0.24	0.30
6	0.20	28.83	0.00	0.00	0.11	0.27	2.31
7	0.23	27.13	0.00	0.00	0.06	0.24	0.60
8	0.00	4.61	0.00	0.00	0.16	0.01	0.00
9	0.03	0.07	0.04	0.03	0.00	0.00	0.00

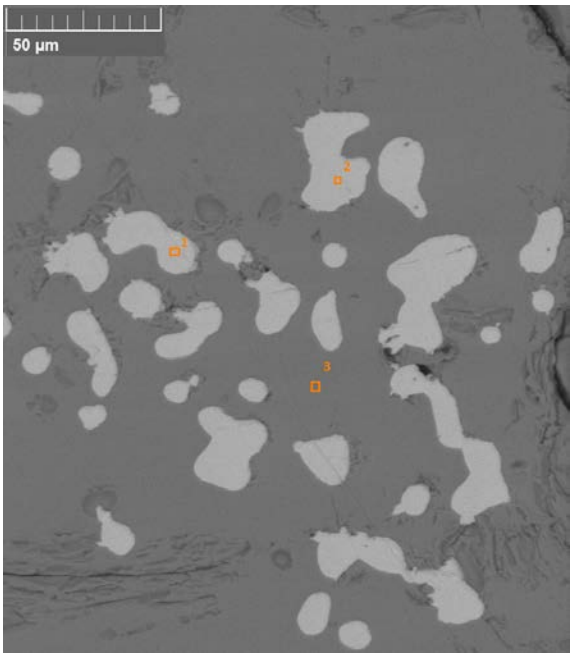

Figure 64. Site D and EDS datapoints

Point of analysis	***O-K***	***Mg-K***	***Si-K***	***Fe-K***	***Ni-K***	***Cu-K***	***Ag-L***	***Cd-L***	***Sn-L***	***Au-M***
1	0.00	0.11	0.11	108.49	0.01	0.08	0.00	0.00	0.07	0.06
2	1.17	0.00	0.09	109.79	0.14	0.09	0.00	0.00	0.00	0.07
3	36.99	0.00	20.88	53.27	0.00	0.00	0.04	0.10	0.02	0.19

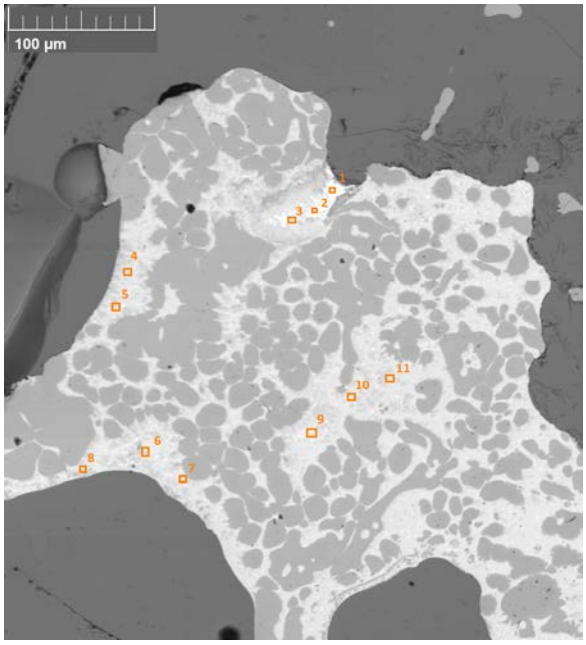

Figure 65. Site E and EDS data points

Point of analysis	*Elelement-standard*									
	O-K	**Si-K**	**Ca-K**	**Ti-K**	**Fe-K**	**Ni-K**	**Cu-K**	**Ge-L**	**Se-L**	**Ag-L**
1	5.37	0.44	0.12	0.10	2.12	2.00	65.25	0.00	0.00	1.48
2	4.83	0.00	0.08	0.10	1.23	2.16	66.74	0.29	0.09	1.42
3	7.83	0.10	0.08	0.00	0.80	1.47	42.13	0.00	0.04	0.81
4	0.55	0.00	0.08	0.21	1.56	2.51	75.35	0.00	0.08	0.94
5	0.45	0.00	0.00	0.09	2.69	2.44	88.54	0.00	0.00	0.00
6	1.01	0.00	0.00	0.06	1.60	2.72	83.60	0.00	0.14	0.64
7	0.00	0.00	0.42	0.21	2.04	3.37	75.00	0.00	0.13	0.92
8	1.49	0.78	0.03	0.09	2.14	2.49	79.25	0.00	0.00	0.78
9	0.41	0.01	0.10	0.14	1.76	2.42	83.88	0.00	0.16	0.77
10	0.43	0.00	0.10	0.10	2.55	2.99	86.94	0.00	0.11	0.49
11	0.47	0.00	0.41	0.12	1.12	3.09	84.47	0.00	0.16	0.48

Point of analysis	Elelement-standard					
	Cd-L	**Sn-L**	**Te-L**	**Re-M**	**Au-M**	**Pb-M**
1	0.38	23.77	0.00	0.18	0.12	15.03
2	0.37	22.59	0.00	0.00	0.00	12.92
3	0.28	16.01	0.00	0.23	0.00	37.28
4	0.19	30.22	0.24	0.00	0.00	0.48
5	0.00	16.95	0.00	0.00	0.13	0.20
6	0.15	21.19	0.15	0.00	0.28	0.31
7	0.21	31.17	0.09	0.00	0.12	1.13
8	0.17	26.00	0.14	0.14	0.06	1.94
9	0.18	24.35	0.00	0.00	0.18	0.37
10	0.12	20.45	0.27	0.00	0.11	0.19
11	0.03	22.54	0.00	0.00	0.15	0.28

Appendix C

120 s PCB sample, EDS Sites (A-E) and results

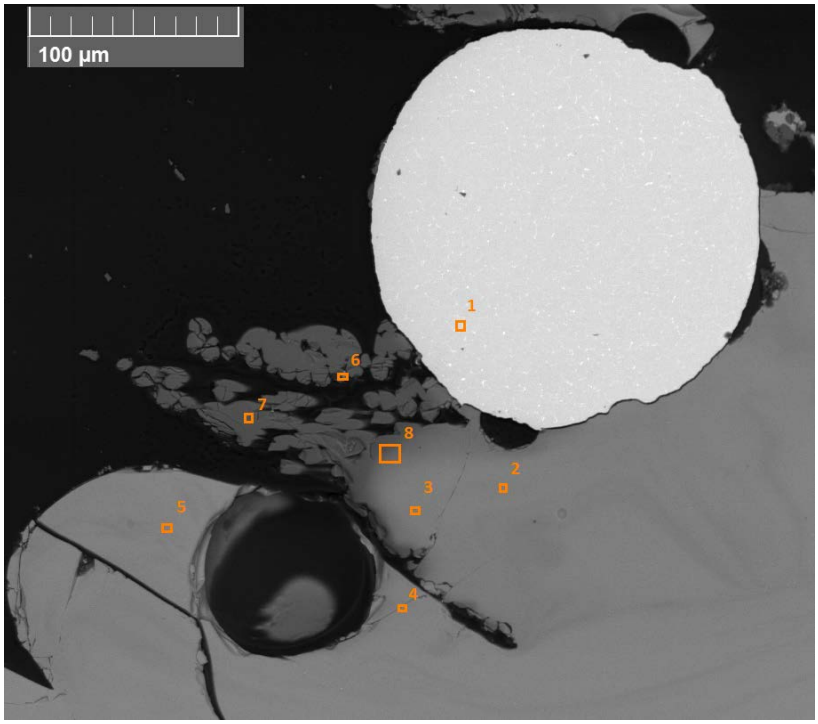

Figure 66. Site A and EDS data points

Point of analysis	O-K	Al-K	Si-K	Cl-K	Ca-K	Fe-K	Ni-K	Cu-K	Ag-L
1	1.08	0.00	0.00		0.00	3.26	0.05	76.93	0.04
2	38.64	0.45	20.40		0.38	35.20	0.00	0.08	0.00
3	40.20	0.70	19.84		1.10	34.00	0.00	0.08	0.00
4	37.82	0.08	18.74		0.26	37.41	0.00	0.00	0.00
5	38.02	0.71	18.91		0.69	33.43	0.10	0.07	0.00
6	0.00	0.07	0.33	0.32	0.13	0.21	0.00	0.05	0.00
7	0.00	2.87	9.86	0.15	3.21	0.45	0.02	0.08	0.04
8	43.05	2.30	21.75		4.45	24.76	0.00	0.04	0.00

Point of analysis	Sn-L	Sb-L	Te-L	Au-M	Pb-M
1	0.14	0.00	0.00	0.00	0.41
2	0.00	0.15	0.00	0.14	0.00
3	0.00	0.00	0.54	0.12	0.00
4	0.00	0.00	0.00	0.00	0.00
5	0.00	0.00	0.21	0.00	0.00
6	0.03	0.04	0.00	0.00	0.00
7	0.23	1.18	4.65	0.00	0.00
8	0.00	0.00		0.00	0.00

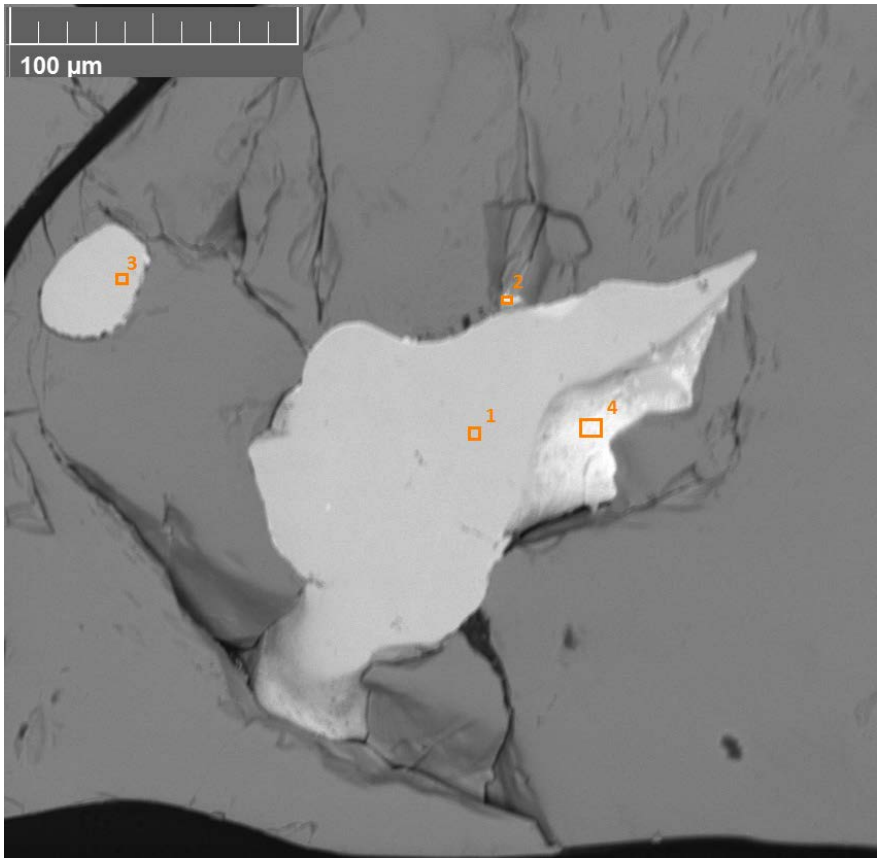

Figure 67. Site B and EDS data points

Point of analysis	O-K	Al-K	Si-K	Fe-K	Ni-K
1	0.00	0.01	0.07	85.78	0.00
2	1.44	0.03	0.66	9.32	0.02
3	0.00	0.00	0.11	77.92	0.00
4	1.28	0.10	0.06	29.06	0.06

Point of analysis	Cu-K	Ag-L	Sn-L	Au-M	Pb-M
1	0.00	0.00	0.08	0.00	0.00
2	1.94	0.00	0.12	0.00	0.04
3	4.77	0.00	0.08	0.00	0.00
4	47.94	0.34	14.48	0.00	0.19

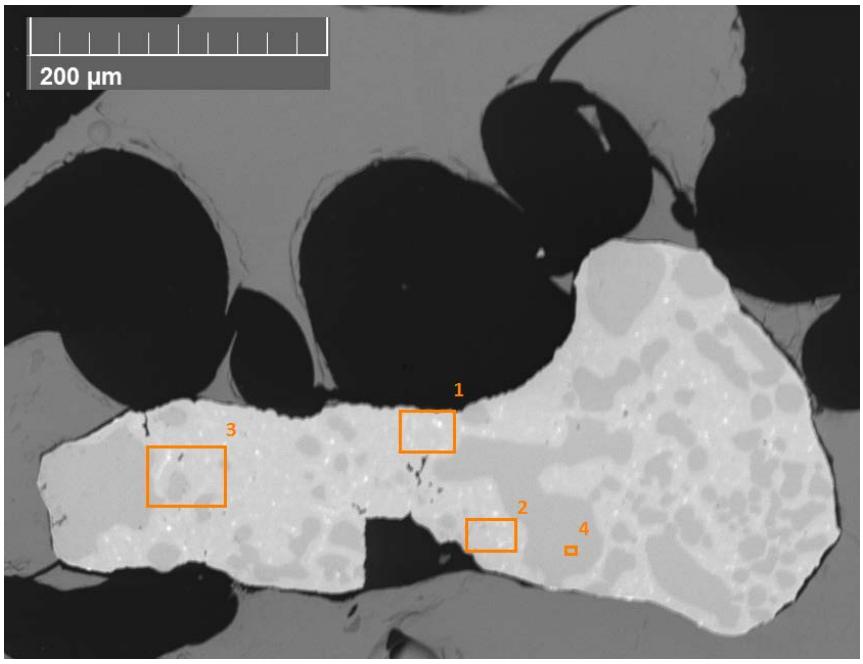

Figure 68. Site C and EDS data points

Point of analysis	O-K	Si-K	Fe-K	Ni-K	Cu-K
1	1.93	0.00	2.67	0.48	65.58
2	1.66	0.00	11.28	0.00	75.67
3	1.39	0.00	21.57	0.18	60.61
4	0.00	0.08	90.02	0.06	0.05

Point of analysis	As-L	Ag-L	Sn-L	Au-M	Pb-M
1	0.23	0.19	2.14	0.00	1.53
2		0.00	2.51	0.00	1.26
3		0.00	2.23	0.00	0.62
4		0.05	0.08	0.04	0.05

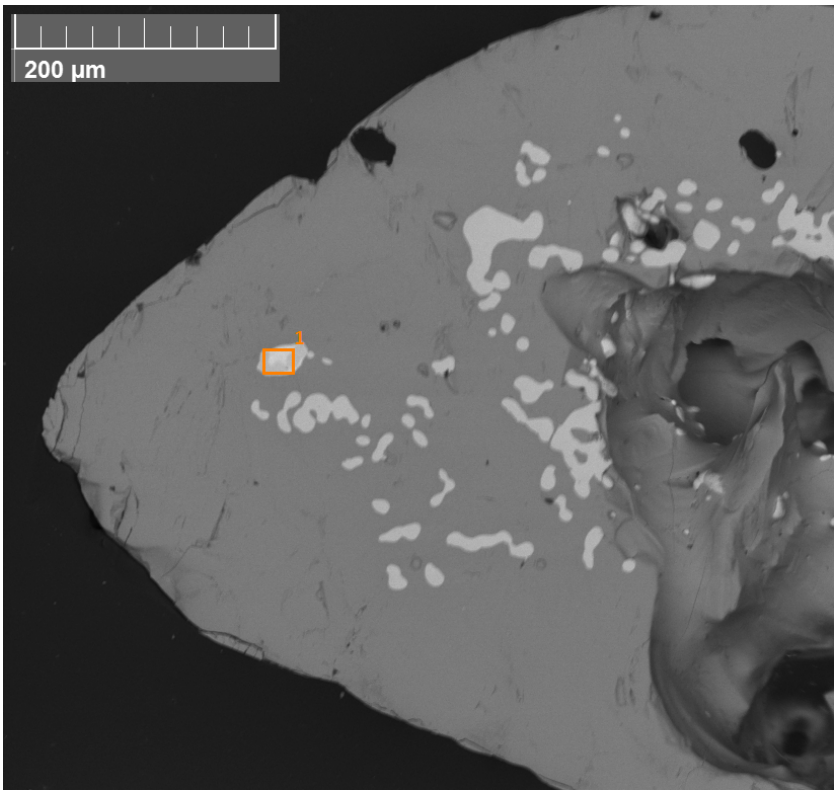

Figure 69. Site D and EDS data points

Point of analysis	O-K	Al-K	Si-K	Fe-K	Cu-K
1	3.77	0.11	1.69	49.78	29.70

Point of analysis	Sn-L	Sb-L	Bi-M
1	1.02	0.03	0.06

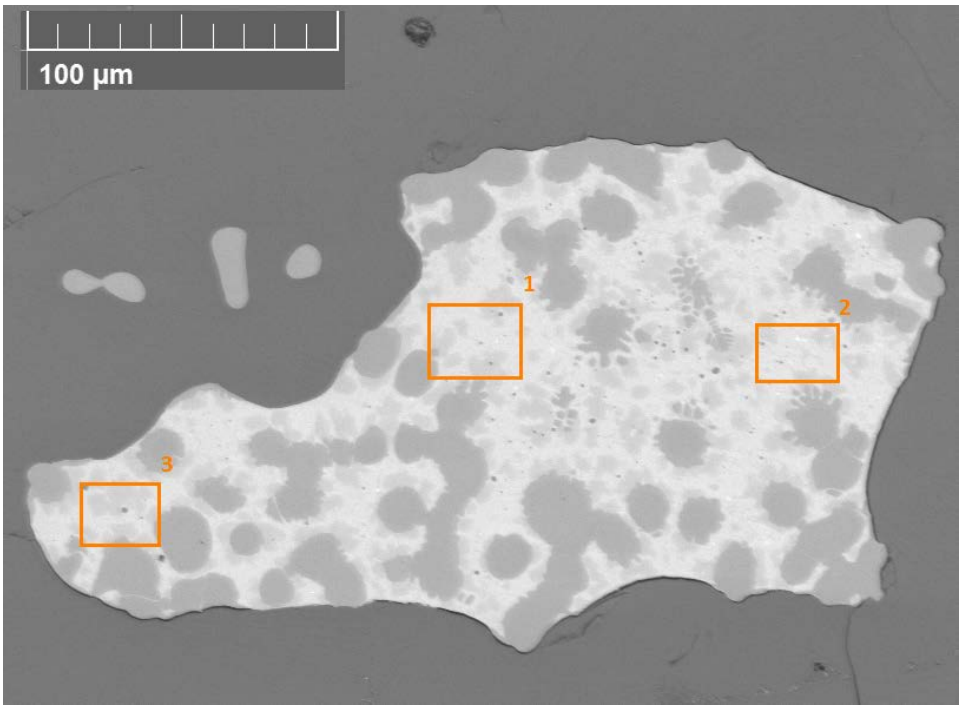

Figure 70. Site E and EDS data points

Point of analysis	*O-K*	*Fe-K*	*Ni-K*	*Cu-K*	*Ag-L*
1	0.00	2.92	2.17	63.21	0.67
2	1.15	3.34	2.45	62.33	0.74
3	1.43	7.55	2.11	62.23	0.45

Point of analysis	**Cd-L**	**Sn-L**	**Au-M**	**Pb-M**
1	0.09	21.43	0.08	0.43
2	0.17	23.26	0.02	0.82
3	0.13	17.71	0.10	0.26

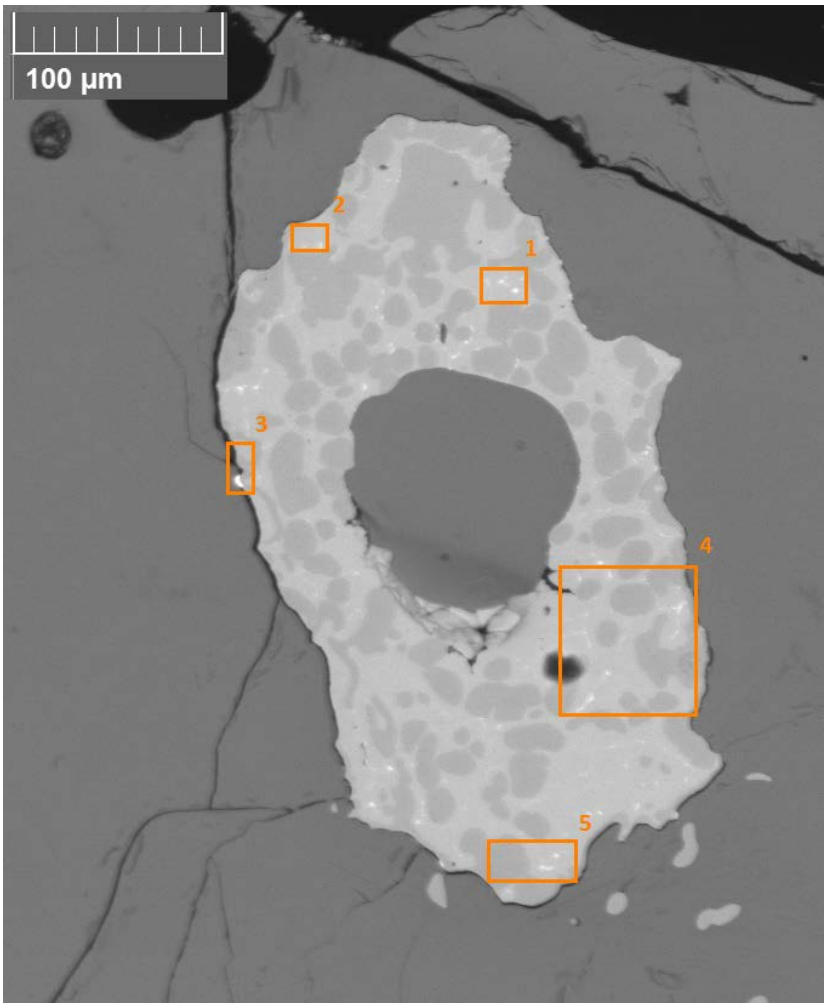

Figure 71. Site F and EDS data points

Point of analysis	*O-K*	*Al-K*	*Si-K*	*Fe-K*	*Co-K*
1	1.34	0.00	0.00	29.84	
2	1.81	0.00	0.00	16.73	
3	7.95	0.00	3.02	32.81	
4	3.67	0.22	1.83	39.64	
5	0.00	0.00	0.00	52.44	0.56

Point of analysis	**Cu-K**	**Ag-L**	**Sn-L**	**Pb-M**
1	52.85	0.07	0.60	2.44
2	63.78	0.07	0.63	2.79
3	33.15	0.00	0.00	4.34
4	42.35	0.00	0.27	1.10
5	32.15	0.00	0.30	1.14

Appendix D

300 s PCB sample, EDS sites (A-E) and results

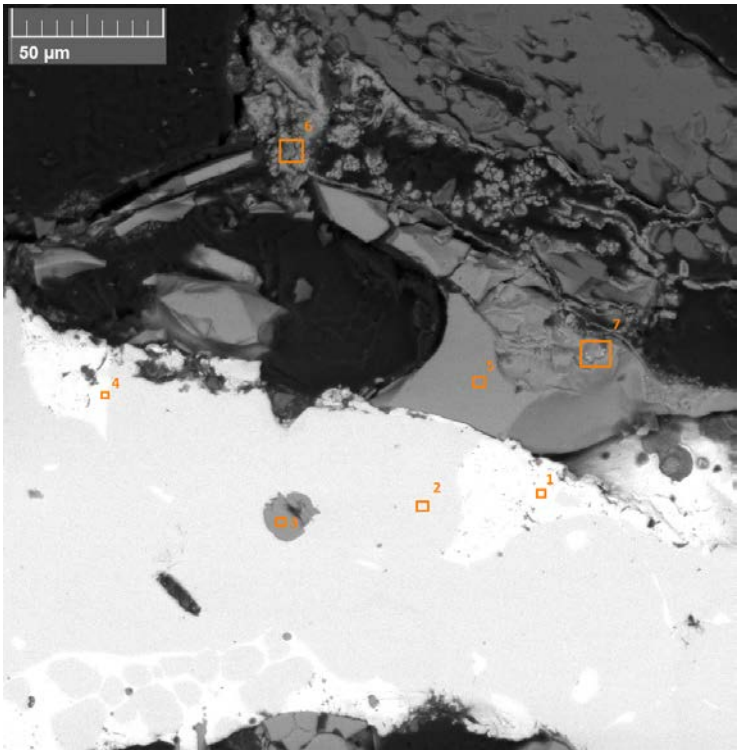

Figure 72. Site A and EDS data points

EDS analysis shows that the white section of the site A mainly comprises of iron and copper (copper white, iron light grey) and some lesser traces of lead, nickel and tin.

Point of analysis		***O-K***	***Mg-K***	***Al-K***	***Si-K***	***Cl-K***	***Ca-K***	***Fe-K***	***Ni-K***	***Cu-K***	***Zn-K***
	1	1.23	0.00	0.05	0.05		0.00	11.57	0.00	96.64	0.00
	2	0.00	0.21	0.02	0.01		0.03	98.96	0.00	10.15	0.14
	3	38.43	0.00	0.31	21.30		0.63	48.70	0.00	0.00	0.00
	4	1.25	0.00	0.00	0.01		0.00	4.17	0.07	97.39	0.00
	5	37.48	0.00	0.19	20.87		0.32	50.12	0.00	0.13	0.00
	6	28.43	0.01	0.00	2.41	0.10	0.32	67.92	0.18	0.12	0.20
	7	23.74	0.06	0.07	11.30		0.39	60.34	0.05	3.57	0.00
		Ge-L	**Ag-L**	**Cd-L**	**Sn-L**	**Te-L**	**Au-M**	**Pb-M**			
	1	0.00	0.86	0.17	5.40	0.00	0.00	0.13			
	2	0.00	0.00	0.00	0.16	0.00	0.00	0.00			
	3	0.00	0.00	0.00	0.00	0.32	0.00	0.00			
	4	0.43	1.41	0.28	9.28	0.00	0.00	0.22			
	5	0.00	0.00	0.00	0.00	0.17	0.05	0.00			
	6	0.12	0.00	0.00	0.00	0.00	0.00	0.04			
	7	0.26	0.00	0.00	0.00	0.05	0.04	0.00			

Data point 7 looked interesting and was subjected to a closer examination.

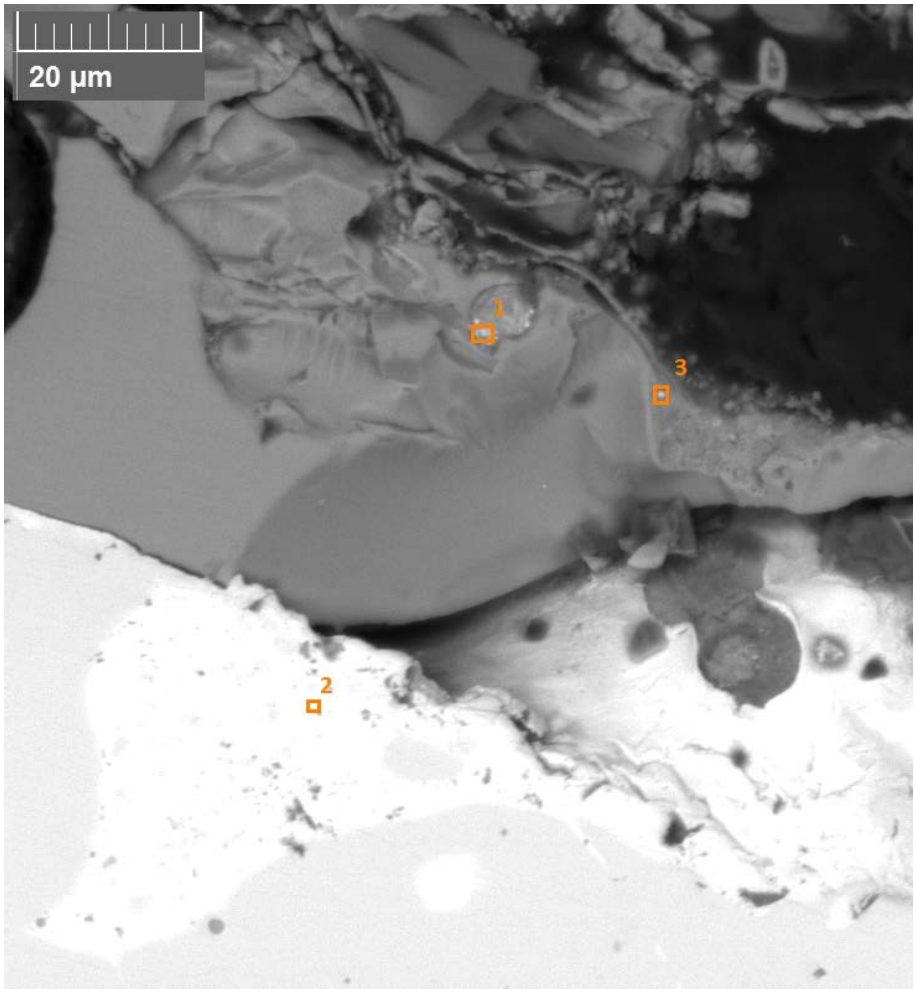

Figure 73. Site A2 and EDS data points

Point of analysis	***O-K***	***Mg-K***	***Si-K***	***Ca-K***	***Fe-K***	***Cu-K***	***Zn-K***	***Ge-L***	***Ag-L***	***Cd-L***	***Sn-L***
1	11.55	0.35	1.68	0.13	37.94	40.16	0.24	0.00	0.12	0.04	2.17
2	1.34	0.00	0.01	0.19	5.29	100.06	0.00	0.48	0.00	0.22	5.80
3	21.19	0.13	8.70	0.28	46.62	7.96	0.00	0.09	0.00	0.00	0.09
	Au-M	**Bi-M**									
1	0.00	0.02									
2	0.15	0.15									
3	0.04	0.00									

Data points 1 and 2 show minor traces of silver and gold.

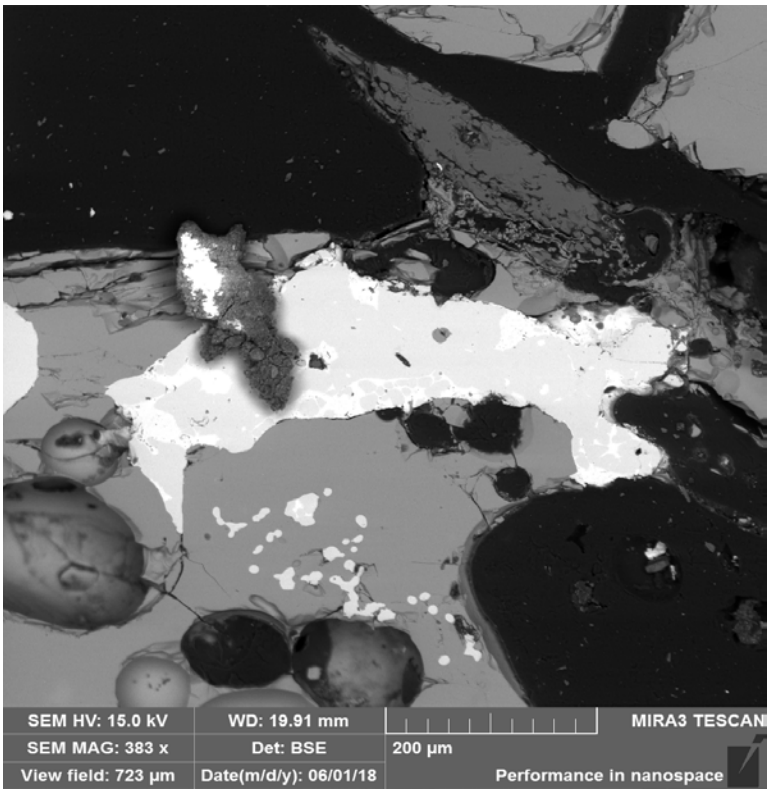

Figure 74. Site AB

Site AB shows a clear structural change of PCB sample piece to metallic iron-copper structure.

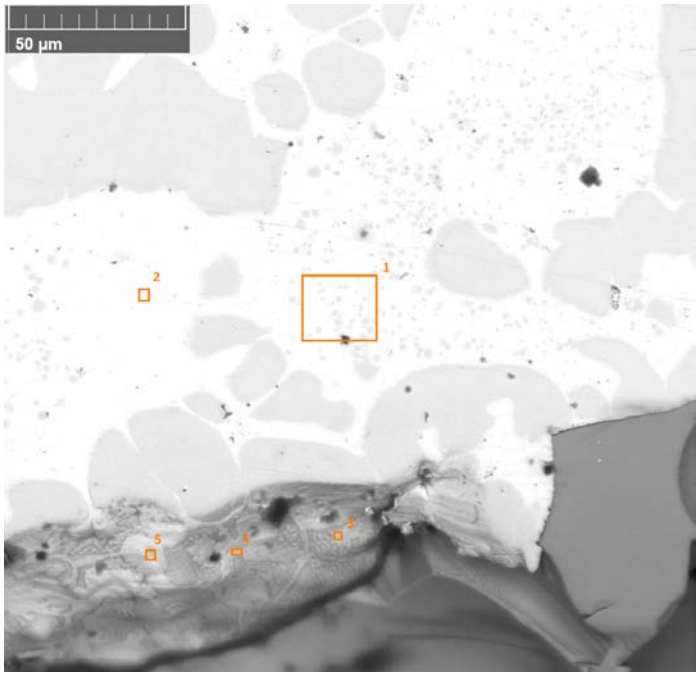

Figure 75. Site B and EDS data points

Point of analysis	***O-K***	***Mg-K***	***Al-K***	***Si-K***	***S-K***	***Cr-K***	***Fe-K***	***Ni-K***	***Cu-K***	***Zn-K***	***Ag-L***
1	0.00	0.00	0.09	1.85	0.04	0.00	23.84	0.00	76.85	0.32	0.50
2	0.18	0.00	0.06	0.01	0.03	0.00	3.46	0.05	97.12	0.15	0.96
3	2.85	0.01	0.08	0.85	0.02	0.00	57.59	0.00	44.35	0.22	0.44
4	2.81	0.11	0.00	1.54	0.00	0.02	18.09	0.00	83.90	0.18	1.16
5	1.68	0.00	0.06	0.00	0.00	0.00	11.88	0.00	89.95	1.66	1.45
	Cd-L	**Sn-L**	**Pb-M**	**Bi-M**							
1	0.12	2.30	0.00	0.15							
2	0.29	4.80	0.11	0.00							
3	0.09	2.39	0.00	0.00							
4	0.23	5.37	0.00	0.00							
5	0.23	6.06	0.02	0.00							

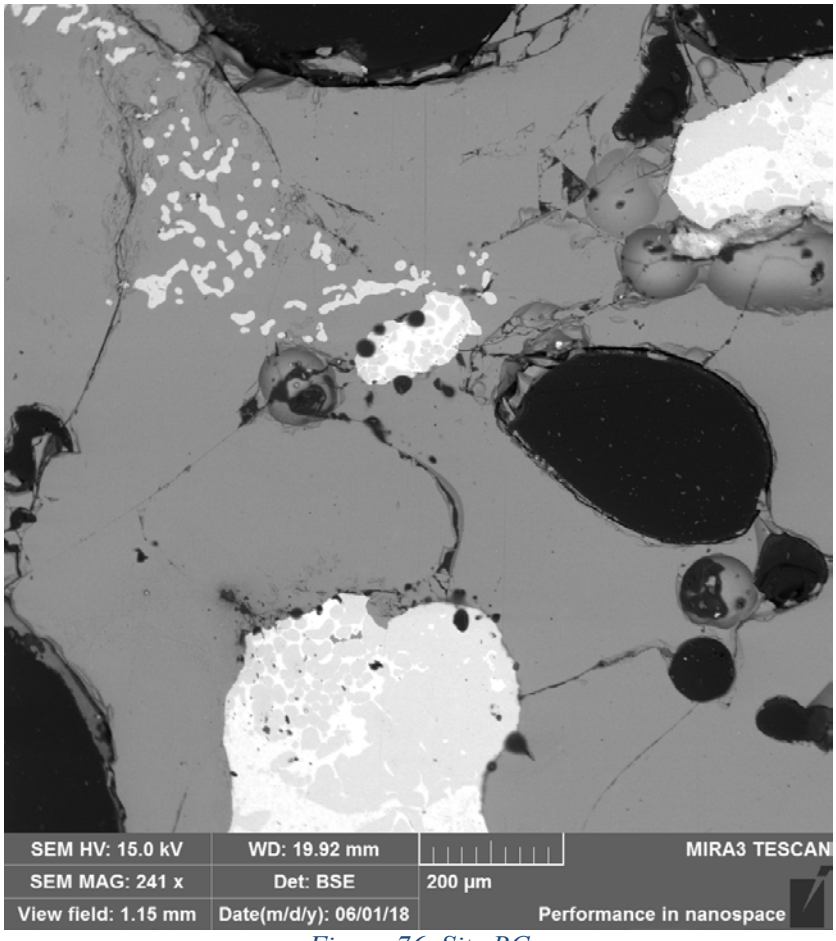

Figure 76. Site BC

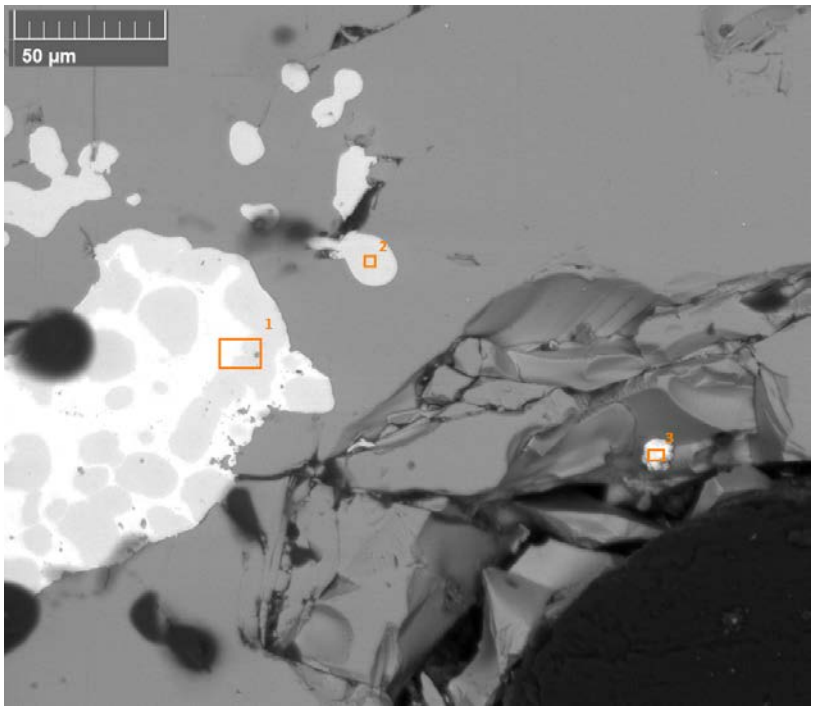

Figure 77. Site C and EDS data points

Point of analysis	***O-K***	***Al-K***	***Si-K***	***Fe-K***	***Co-K***	***Cu-K***	***Zn-K***	***Ge-L***	***Se-L***	***Ag-L***	***Sn-L***
1	1.70	0.14	0.58	56.05	1.93	46.20	0.16	0.00	0.14	0.38	3.24
2	0.00	0.00	0.08	105.35		0.07	0.09	0.23	0.00	0.00	0.15
3	4.15	0.00	0.00	8.39		102.15	2.51	0.08	0.00	0.00	0.00

Sites (D-F) all had similar structure to site AB.

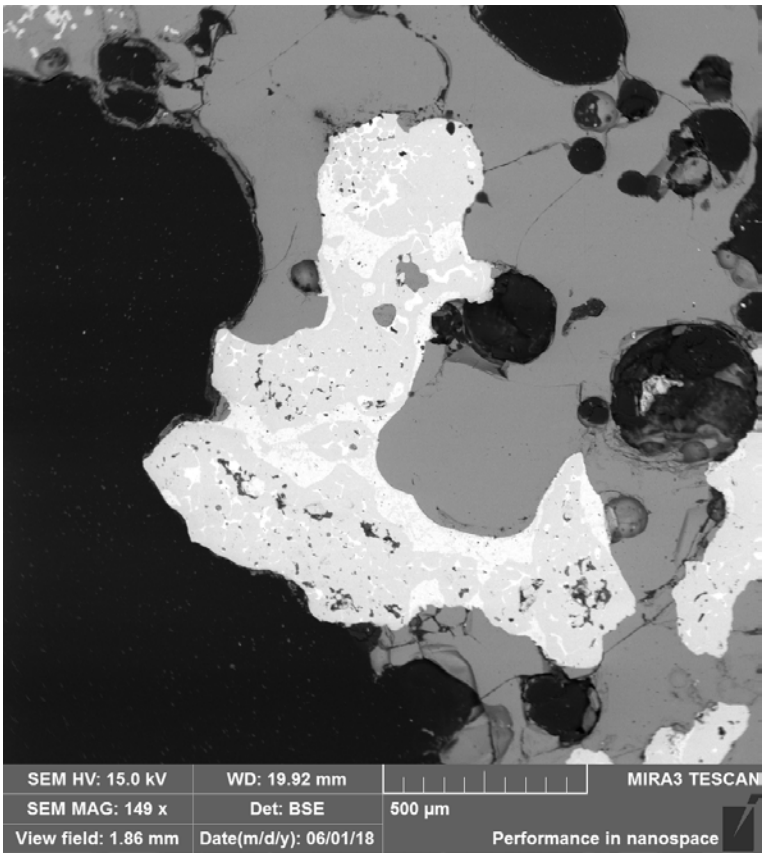

Figure 78. Site D

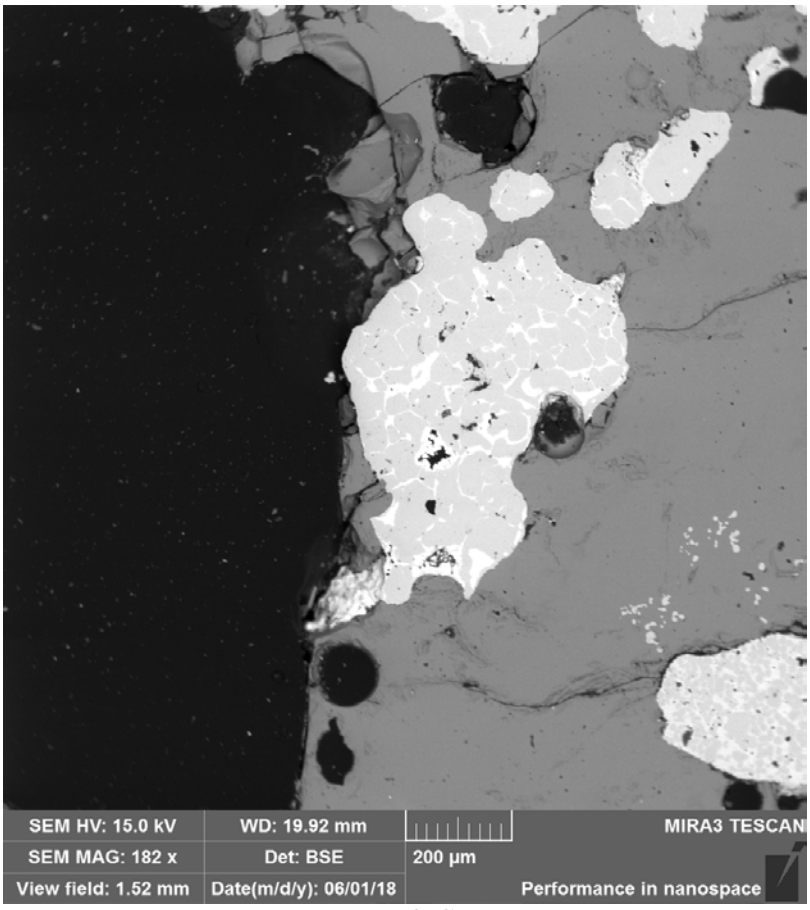

Figure 79. Site E

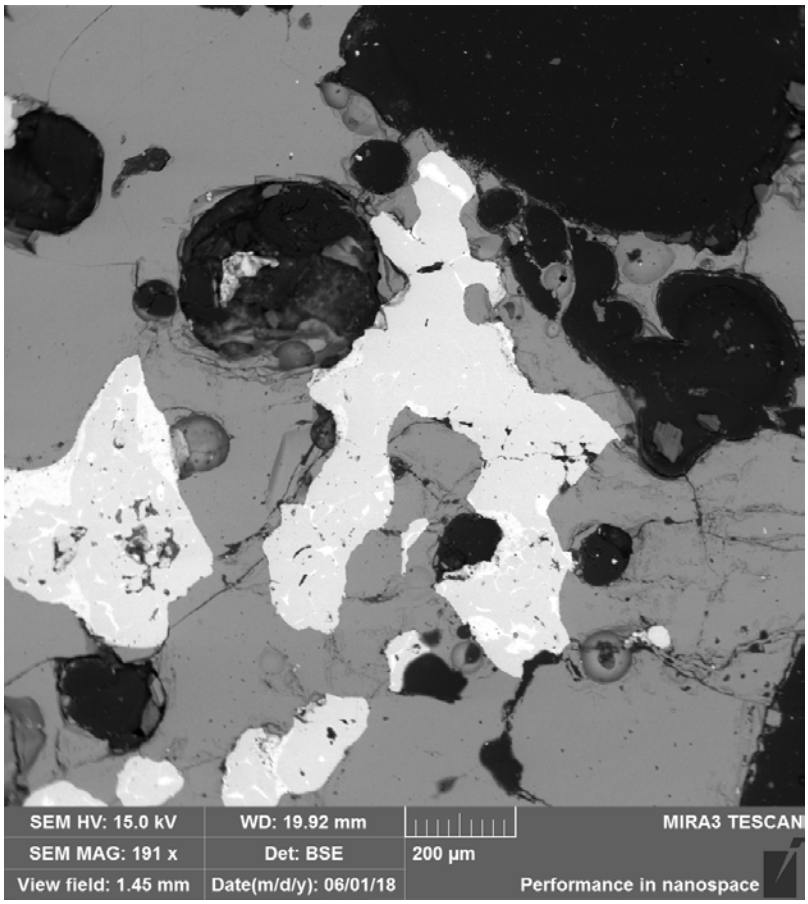

Figure 80. Site F